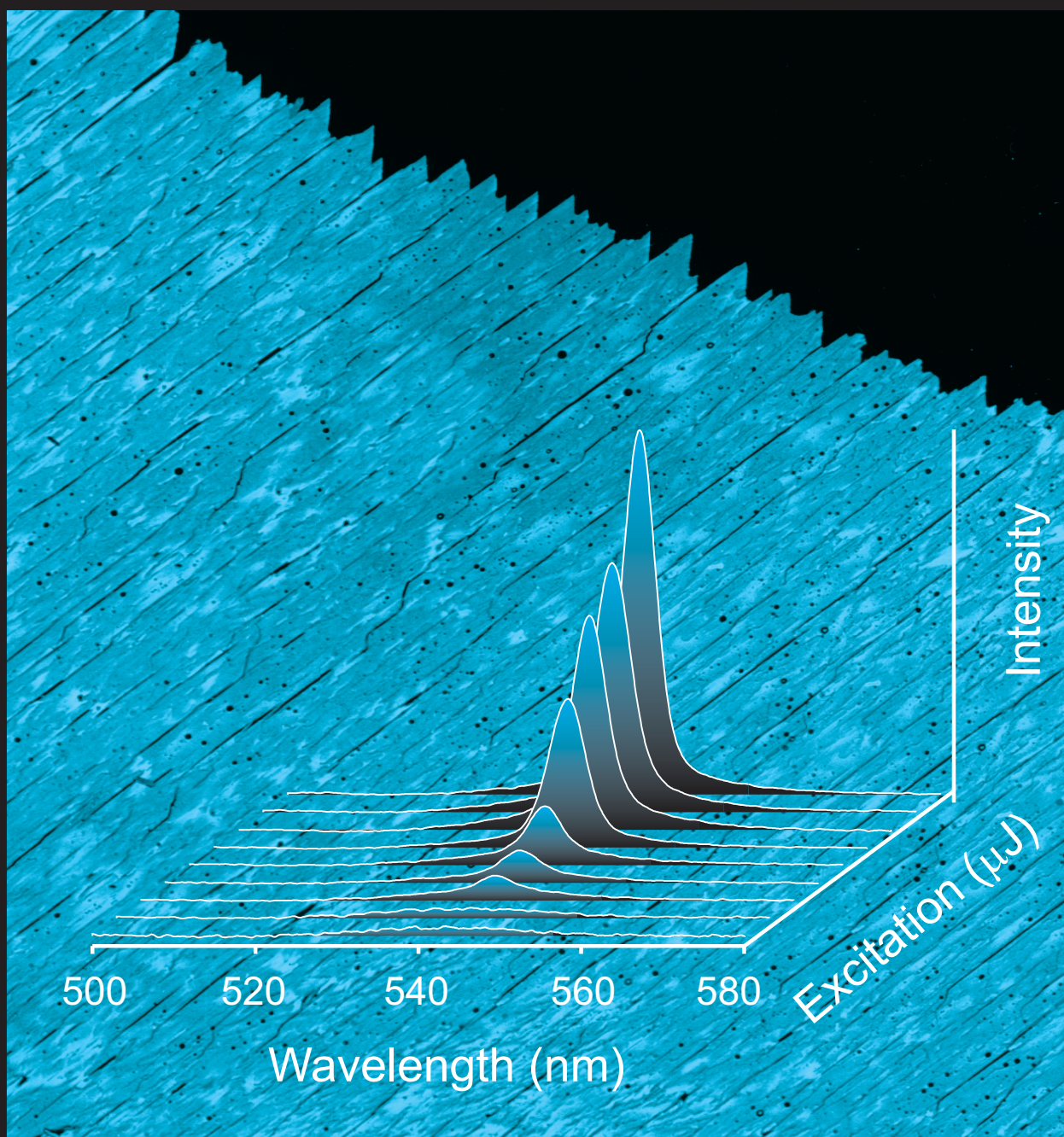


# Semiconducting Polymers for Light-Emitting Diodes and Lasers

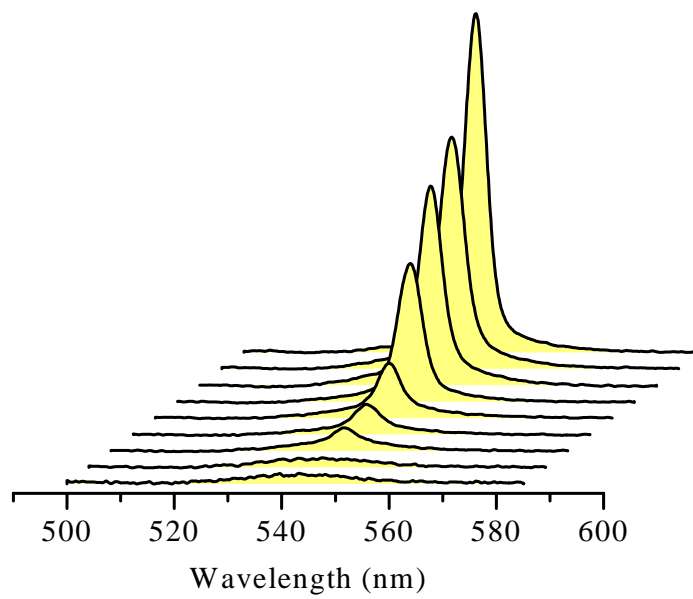
*A structural, photophysical and electrical study of PPV-type alternating copolymers and oligomers*



**Hendrik-Jan Brouwer**

# Semiconducting Polymers for Light-Emitting Diodes and Lasers

*Structural, photophysical and electrical study of alternating PPV copolymers and oligomers*



Reading committee: *Prof. Dr. G.A. Sawatzky*, Department of Solid State Physics,  
University of Groningen, The Netherlands  
*Prof. Dr. D.D.C. Bradley*, Department of Physics, University  
of Sheffield, England  
*Prof. Dr. A.J. Pennings*, Department of Polymer Chemistry,  
University of Groningen, The Netherlands

H.J. Brouwer  
Ph.D. thesis  
University of Groningen, the Netherlands  
March 1998

ISBN-90-367-0878-8

*Cover:* Background: Optical micrograph (crossed polarizers) of an as-deposited Ooct-OPV5 thin film. Inset: Optical micrograph (crossed polarizers) of a recrystallized Ooct-OPV5 thin film after slow cooling from the isotropic melt. Plot: Spectral evolution of the emitted light emerging from a photoexcited MEH-OPV5 thin film.

This research was supported by the Dutch Foundation for Chemical Research (SON) with financial aid of the Dutch Organisation for Scientific Research (NWO).

Drukwerk: Grafisch bedrijf Ponsen & Looijen BV Wageningen

Rijksuniversiteit Groningen

# **Semiconducting Polymers for Light-Emitting Diodes and Lasers**

*Structural, photophysical and electrical study of alternating PPV  
copolymers and oligomers*

Proefschrift

Ter verkrijging van het doctoraat  
In de Wiskunde en Natuurwetenschappen  
aan de Rijksuniversiteit Groningen  
op gezag van de  
Rector Magnificus Dr. F. van der Woude  
In het openbaar te verdedigen op  
Vrijdag 6 maart 1998  
des namiddags te 4.15 uur

door

**Hendrik Jan Brouwer**

geboren op 15 september 1966  
te Biddinghuizen

Promotor: *Prof.Dr. G. Hadziioannou*

Referent: *Dr. V.V. Krasnikov*

# Dankwoord

“Research is teamwork”. Daarom wil ik bij deze alle mensen bedanken die direct en indirect betrokken zijn geweest bij de totstandkoming van dit proefschrift.

Allereerst wil ik natuurlijk mijn promotor *Prof. dr. George Hadziioannou* bedanken voor de mogelijkheid om in zijn onderzoeksgroep te promoveren. Zijn enthousiaste aanpak, emotionele preken/aanmoedigingen en heftige discussies ook over niet-wetenschappelijke zaken heb ik altijd zeer weten te waarderen.

De leescommissie: *Prof. dr. A.J. Pennings*, *Prof. dr. G.A. Sawatzky* en *Prof. dr. D.D.C. Bradley* ben ik erkentelijk voor de snelle en kritische beoordeling van het manuscript.

A special thanks to my russian copilot *Victor Krasnikov*, and roommate at the “smoking cave” (room 18.06). Thanks for the uncountable number of lectures in basic physics, your guidance, expertise and your admirable patience. Our mutual addiction to nicotine and caffeine resulted in numerous discussions at the “coffee corner” on the second floor. Discussions which usually started with the famous words: “In the former Soviet Union .....” and “Give me your tobacco.....” when you ran out of cigarettes again.

Onze “hoofdgeitenbreier” en “administratief-wetenschappelijk grootcoördinator” *Paul van Hutten* wil ik vooral bedanken voor het kritisch lezen en corrigeren van dit proefschrift, artikelen, SON/FOM-jaarverslagen en andere getypte prullaria. Ook ben ik hem erkentelijk voor de X-ray diffractie metingen aan dunne films.

*Alain*, *Richard*, *Jur*, *Geert* en natuurlijk *Michiel “pikkie” Werts* wil ik bedanken voor het synthetiseren van de talloze polymeren en oligomeren die verbruikt en misbruikt zijn tijdens mijn onderzoek. *Alain* en *Richard* wil ik in het bijzonder bedanken voor hun belangrijke bijdragen aan de resultaten. *Joke* voor de vele bruikbare aanwijzingen m.b.t. mijn precursor avontuur. P.s. *Geert* en “*pikkie*”: die mevrouw van het Universitair steunpunt emancipatie zaken wil nog even met jullie van gedachten wisselen m.b.t. valsheid in geschrifte.

Mijn hoofdvakstudenten *Lennart* en *Matthieu* voor de vele emotionele (anti-) climaxen die we samen beleefd hebben. Vooral die explosieve aluminium verdamping in de Edwards (opdamptijd: 2 seconden, schoonmaken van de opdamer: 1 dag) heb ik altijd gezien als het ultieme voorbeeld van “time management”. Ik wens jullie veel plezier en succes tijdens jullie stage bij het CNRS in Strasbourg. Steek er wat van op!

- [1] De “cave”men: *George “Malli”*., *Ahn*, *Gerald*, *Kees*, *Sabri*, *Vasilis*, *Roy*, *Dominique*, *Kostas*, *Yannis*, *Eric v/d V* & *Eric P.*, *Cristine*, *Sjoerd* en *Amalia*.
- [2] De “yellow-light district” AIO’s + Post-Docs: *Jan*, *Henk*, *Theo*, *Erik*, *Marc*, *Laurent*, *Mark*, *Bert*, *Ulf* en alle *studenten* die er de afgelopen jaren rond hebben gelopen.
- [3] De rest van de “Hadzii’s”: *Vagelis*, *Eddy*, *Valerie* en *Andrei*.

a total of [1]+[2]+[3] = eight different nationalities (correct me if I’m wrong)

De mensen aan de “overkant”: *Bart S.*, *Frank G.*, *Edwin S.*, *Hans V.*, *Alex S.* en *Danny W.F.*

De “electronics”: *Nanno Herder*, *Wieger Jonker*, en enkele naamloze stagiaires die geheel vrijblijvend in hun vrijetijd mijn boosterversterker en videorecorder hebben geprobeerd te repareren. Met name *Nanno* die met zijn soms tot kunst neigende soldeer(mis)baksel altijd een snel pasklaar antwoord had voor al onze elektronische problemen. Ook alle uitgefikte (Hitachi spectrometer, home-built thickness monitor, Digikrom 120 monochromator) en doodverklaarde (Parc Scientific AFM head and control-unit) elektronische meetapparatuur zijn door hem doeltreffend gereanimeerd.

*Diny Hissink* en *Betty IJmker*, dat ze mentaal nog in staat zijn om mij bij te staan als paranimpfen, na alle (on)gewenste intimiteiten.

Al het ondersteunend personeel: *Harry Nijland* (sheets & Coreldraw cursussen), *Adams Verweij* (regelneef & veiligheids”neuroot”), *Gert Alberda van Ekenstein* (optische microscopie en DSC), *Minte Mulder* (opdampers), *Simon Bakker* (cleanroom), *Joop Vorenkamp* (IR) *Hans Beekhuis* (portier), *Ulco “wil jij een bib(s)search ?” Kooijstra*, *Henk Knol* (glasblazerij), *Jannes Hommes* (elementenanalyse), *Karel & Anne* (instrumentmakerij) en tot slot *Marjan Ruiters* (secretariaat).

En natuurlijk mijn ouders, familie en vrienden.

# Contents

<b>Chapter 1</b>	<i>Introduction</i>	1
1.1	Conjugated polymers a new class of semiconducting materials ....	1
1.2	Brief historical overview .....	3
1.3	Current understanding of the operating principles of organic Light-emitting Diodes .....	5
1.4	Well-defined PPV copolymers and oligomers .....	8
1.5	Aim and outline of this thesis .....	11
1.6	References .....	13
<b>Chapter 2</b>	<i>Optical properties of alternating PPV copolymers and oligo(<i>p</i>-phenylene vinylene)s</i>	17
2.1	Introduction .....	18
2.2	Experimental .....	21
	2.2.1 Time-correlated single-photon counting .....	21
	2.2.2 Solid-state PL quantum yield measurements .....	22
2.3	Results and discussion .....	24
	2.3.1 Alternating PPV copolymers .....	24
	2.3.2 Oligo( <i>p</i> -phenylene vinylene)s .....	31
2.4	Conclusions .....	45
2.5	References .....	46
<b>Chapter 3</b>	<i>Laser emission from an alternating PPV copolymer in solution</i>	49
3.1	Introduction .....	50
3.2	Experimental .....	51
3.3	Results and discussion .....	52
	3.3.1 Chemical structure and optical properties in solution ..	52
	3.3.2 Dye laser performance .....	54
3.4	Conclusions .....	59
3.5	References .....	60

## Contents

---

<b>Chapter 4</b>	<i>Stimulated emission from neat polymer films</i>	61
4.1	Introduction .....	62
4.2	Experimental .....	63
4.3	Results and discussion .....	65
	4.3.1 Silylene- <i>alt</i> -oligo(phenylene vinylene) copolymer films ..	65
	4.3.2 Poly(2,5-di- <i>n</i> -octyloxy- <i>p</i> -phenylene vinylene) films ..	69
4.4	Conclusions .....	74
4.5	References .....	75
<b>Chapter 5</b>	<i>Stimulated emission from single-crystals and vacuum-deposited thin films of a substituted oligo(<i>p</i>-phenylene vinylene)</i>	77
5.1	Introduction .....	78
5.2	Experimental .....	79
5.3	Results and discussion .....	80
5.4	Conclusions .....	87
5.5	References .....	88
<b>Chapter 6</b>	<i>Light-emitting diodes based on alternating PPV copolymers and oligo(<i>p</i>-phenylene vinylene)s</i>	92
6.1	Introduction .....	92
6.2	Experimental .....	94
6.3	Results and discussion .....	97
	6.3.1 Alternating PPV copolymers .....	97
	6.3.2 Oligo( <i>p</i> -phenylene vinylene)s .....	112
6.4	Conclusions .....	118
6.5	References .....	118
<b>Summary</b>	.....	121
<b>Samenvatting</b>	.....	127
<b>List of publications</b>	.....	135

# Chapter 1

## Introduction

### Abstract

*In this chapter a brief historical overview is presented concerning the progress made in the field of luminescent conjugated polymers in the past decade. The current understanding concerning the device operation of polymeric Light-Emitting Diodes is described, as well as the problems encountered. Furthermore, the synthetic approach towards the development of well-defined highly luminescent copolymers is explained. Finally, the aim and outline of this thesis are presented.*

## 1.1 Conjugated polymers a new class of semiconducting materials

Conjugated polymers attract much interest nowadays for use as active component in electronic, optical and optoelectronic applications, like light-emitting diodes [1,2], light-emitting electrochemical cells [3,4], photodiodes [5,6], photovoltaic cells [7,8], field-effect transistors [9,10], optocouplers [11] and optically pumped lasers in solution [12,13] and solid state [14 -16]. They combine the properties of classical macromolecules, such as low weight, good mechanical behaviour (strength and flexibility) and processability with semiconductor properties, arising from their particular electronic structure. Conjugated polymers have a backbone consisting of alternating single and double bonds (see figure 1.1). The overlap of  $\pi$  bonding and  $\pi^*$  antibonding molecular orbitals forms a continuous system of electron density along the backbone. The extent of this overlap together with the bond alternation (the conjugation length) determines the HOMO-LUMO bandgap. Conjugated polymers have bandgaps in the range of 1 to 4 eV, allowing stable optical excitations and mobile charge carriers.

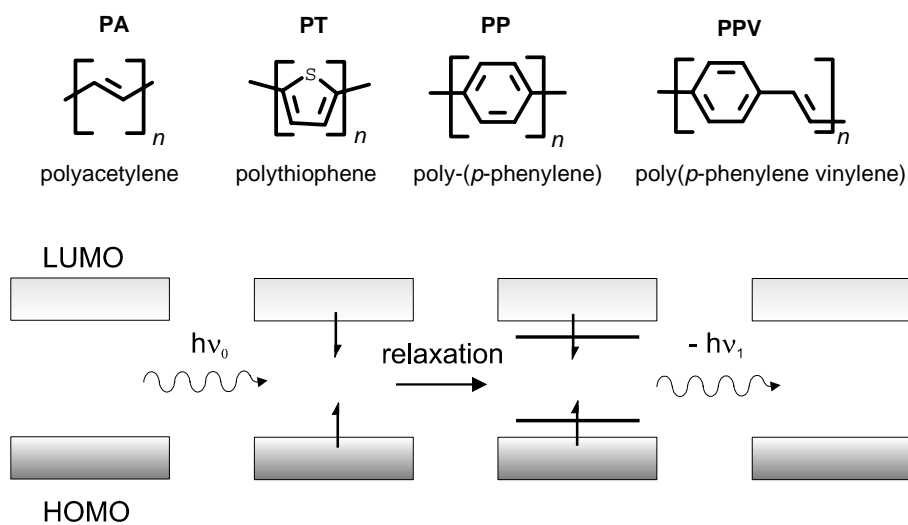


**Figure 1.1** Some examples of conjugated polymers. Below: schematic representation of radiative decay on a polymer chain after photoexcitation.

Excitations can be created by charge injection, light and chemical doping. Excitation (see figure 1.1) results in a local deformation of the molecule around the site of electronic excitation [17,18]. The change of chain geometry (from aromatic to quinoid) has the effect of pulling levels away from the band edges into the gap. The degree of (de)localization is likely to depend on the nature of the conjugated system. Aromatic rings tend to localize the excitation because the alternative electronic

configuration, the quinoid one, is higher in energy. These materials are often strongly fluorescent and emit in the range from near infrared to the ultraviolet. Especially PPV and soluble derivatives thereof, are of great interest, due to the combination of emission in the visible wavelength region and high luminescence quantum yields.

The wavelength of emission depends on the extent of conjugation/delocalization, and can be controlled by modification of the chemical structure. This can be done by the attachment of functional groups, which alter the electronic structure of the conjugated backbone or by making copolymers with non- $\pi$ -conjugated sequences, which interrupt the  $\pi$ -orbital overlap. So, light emission is possible over the entire visible range of the visible spectrum, by “chemical” tuning of the HOMO-LUMO energy gap of the polymer. The tuneable emissive properties are particularly attractive for lighting and display applications, especially in combination with (relatively) low material cost and the possibility of large-area device fabrication by means of simple casting techniques.

## 1.2 Brief historical overview

### *Light-Emitting Diodes*

The first report concerning electroluminescence of an organic semiconductor by Pope *et al.* [19] goes back to 1963. They observed luminescence from single crystals of anthracene (a few tens of microns thick) using silver paste electrodes and bias voltages of a few hundred volts. An extensive and excellent survey of the photophysics, charge injection/transport and electroluminescence in organic crystals can be found in the book “Electronic processes in organic crystals” by Pope and Swenberg [20]. The difficulties with respect to crystal growth and the large voltages required for light emission limited the practical application of organic crystals as LED. Tang *et al.* [21,22] revived the interest in organic EL by using evaporated thin films of  $\approx 100$  nm as emissive layer, which reduced the operating voltages significantly ( $\approx 10$  V). The first publication describing electroluminescence from a polymer (polyvinylcarbazole) by Partridge [23], in 1983, remained largely unnoticed. It lasted until 1990 before a large academic and industrial interest in the field of light-emitting conjugated polymers was established, initiated by a publication from Friend and co-workers [1] describing EL from PPV films. A lot of research in the field has been directed towards the development of new efficient polymeric emitters (for a recent review see [24,25]). A whole range of polymeric LEDs, emitting over the whole visible wavelength region from blue to red, has been reported [26,27]. Furthermore, the LED performance was greatly improved, by means of additional charge-transport layers [28,29]. Double-layer LEDs with high peak brightness and internal electroluminescence efficiencies up to 4% [30] have been reported.

Despite the rapid progress in the field of polymeric light-emitters, no commercial displays based on polymer LEDs have been manufactured yet. The long-

term device stability and device efficiencies of polymer LEDs are rapidly increasing, but improvements are still desired, especially for polymers emitting in the blue wavelength region. The main problem for commercialization of organic LEDs is the device lifetime. Especially oxygen has a detrimental effect on device operation [37]. Oxygen can attack the vinylene bond and result in aldehyde-like chain terminations. These moieties are more electronegative and can act as quenching sites (charge transfer quenching of excitons). Evidence has been reported that even in an inert environment (nitrogen-filled glovebox,  $[O_2] < 1$  ppm) this type of photooxidation reactions can occur due to oxygen diffusion from the ITO contacts [31]. Schlatmann *et al.* [32] already demonstrated that tin, indium and oxygen can diffuse out of the ITO contact into the polymer layer. It has been shown that the LED performance and stability can be significantly enhanced by coating the ITO contact with conducting polyaniline (PAni) [33]. PAni is transparent, has a higher work function than ITO, planarizes the ITO surface (avoiding shorts) and can act as a barrier to avoid diffusion of elements into the polymer layer. Another problem is the interface and contact stability. Low work function metals oxidize in the presence of either water or  $O_2$ . For instance it has been shown that an ITO/PAni/MEH-PPV/Ca device operated in water vapour loses 90% of its efficiency (but only one-third of its current) in 37 seconds! [34]. At that point the electrode is far from being oxidized, and still has its shiny colour, indicating a highly porous morphology. Also water-induced delamination of Mg cathodes in  $Alq_3$  devices, resulting in blackspot formation has been reported. The temperature stability is an important parameter for display applications; displays must withstand extremes in temperature and thermal cycling. It has been shown that for example an ITO/PAni/MEH-PPV/Ca device shows a reduction of lifetime of a factor 20 upon changing the operating temperatures from  $30^\circ C$  to  $60^\circ C$  [34].

#### *Lasing in polymer thin films*

Excited states formed in conjugated polymers by charge injection or photoexcitation have photophysical characteristics similar to those of small organic chromophores such as laser dyes. It was realized that the high photoluminescence (PL) quantum yield and appreciable Stokes shift of conjugated polymers made them promising candidates as laser media in diluted solutions and solid state, the ultimate target being the elaboration of electrically pumped polymer lasers operating in the visible wavelength regime. Soon after the introduction of polymer LEDs, efficient laser action of the semiconducting polymer poly[2-methoxy-5-(2'-ethyl-hexyloxy)-1,4-phenylene-vinylene] (MEH-PPV) in the liquid state [12], operating in the yellow/red wavelength region, was reported. This was followed by blue laser emission from solutions of an alternating PPV copolymer [13]. More recently, laser emission from dilute blends and blends containing titanium dioxide nanocrystals [35,36] has been demonstrated.

However, the prospects for solid-state lasing of neat polymer films seemed less hopeful. In solution and in dilute blends, the individual polymer chains are spatially well separated by the host medium, minimizing interchain interactions, that result in luminescence quenching. Despite the fast sub-nanosecond decay, the substantially decreased PL quantum efficiency (in comparison with solutions) and the photo-induced absorption, stimulated emission was observed in optically pumped neat polymer films in several ultrafast spectroscopy studies [37,38], indicating the possible development of solid-state polymer lasers. This was positively confirmed recently by Tessler *et al.* [14], who reported lasing from spincoated PPV films under pulsed optical excitation in a microcavity construction. Furthermore, gain narrowing in optically pumped neat films of various PPV's without the use of an external feedback system by several groups [15,16,39,40] was reported, including ours.

The observation of lasing in optically pumped neat polymer films with and without external feedback system gives hope for the possible development of an electrically pumped laser diode. The major limiting factor at this moment is the drive-current necessary for electrically pumped lasing to be realized. One can make a rough estimation of the current threshold, based on the excitation density at which spectral narrowing occurs in optically pumped polymer films. It was estimated that current densities in excess of  $10^3 \text{ A.cm}^{-2}$  [15] are needed to establish electrically induced lasing. The highest reported current density achieved in a polymer LED until now is  $\approx 25 \text{ A.cm}^{-2}$  [41] and illustrates the barriers which have to be overcome concerning the development of a polymer laser diode. However, electroluminescence (EL) of a 3 nm thick PPV film by tunnelling injection from a scanning tunnelling microscope (STM) tip with current densities of the order of  $10^4 \text{ A.cm}^{-2}$  has been reported recently by Bradley *et al.* [42]. It indicates, be it under extreme circumstances, an ultra thin film (3 nm) in combination with a nanometer-sized cathode (end of the STM tip, area  $\approx 1 \text{ nm}^2$ ), light emission at high current densities is possible in polymer films.

### 1.3 Current understanding of the operating principles of organic Light-emitting diodes

In a simple LED device, a conjugated polymer film is sandwiched between two metal electrodes and by applying a bias voltage charge injection is established. This is schematically depicted in figure 1.2. The contacts facilitate charge-injection of electrons and holes into the LUMO and HOMO levels of the polymer, which migrate through the bulk under the influence of the applied electric field. This is followed by recombination of the charge carriers on a chain segment resulting in the formation of relatively localized excited states (excitons) which decay radiatively.

*Charge injection.* Indium-tin-oxide (ITO) is the most commonly used hole-injection contact, it has a high work function ( $\phi_{\text{ITO}} = 4.5\text{-}5.3 \text{ eV}$ ) close to the HOMO-level of conjugated polymers and is transparent, which allows the escape of the

generated light out of the device. As electron-injecting contact, low work function metals such as Ca ( $\phi_{Ca}=2.9$  eV), Mg ( $\phi_{Mg}=3.7$  eV) or Al ( $\phi_{Al}=4.3$  eV) are used. The exact charge-injection mechanism is still controversial. It is generally believed that injection of holes at the ITO anode into the polymer is controlled by a superposition of field-emission tunneling and thermionic emission, the important parameter being the magnitude of the injection barrier [43,44]. Parker [43] showed that the I-V characteristics at high fields in a polymer LED can be described reasonably well with a Fowler-Nordheim tunnelling injection model of tunneling through a triangular potential barrier. A recent analysis by Davids *et al.* [45] suggests that tunneling dominates only for barriers higher than several tenths of an electronvolt, with a strong contribution of charge flowback, due to the low mobility of conjugated polymers. For smaller barriers, space-charge-limited thermionic injection is dominant. The influence and importance of an interfacial layer, formed between the polymer and electrode metal, on the injection barrier is still under investigation. It is known that Al forms covalent bonds with PPV [46] and Ca undergoes charge transfer, forming cationic Ca and bipolarons (doubly charged anions) in PPV [47]. A recent study with the inert transition metal ZrC ( $\phi_{ZrC}=3.6$  eV) as cathode metal, revealed that the efficiency in Au/MEH-PPV/ZrC devices is well below that obtained with Al as cathode material [48]. This gives a strong indication that the work function of the injecting contact probably cannot alone account for the charge injection barrier.

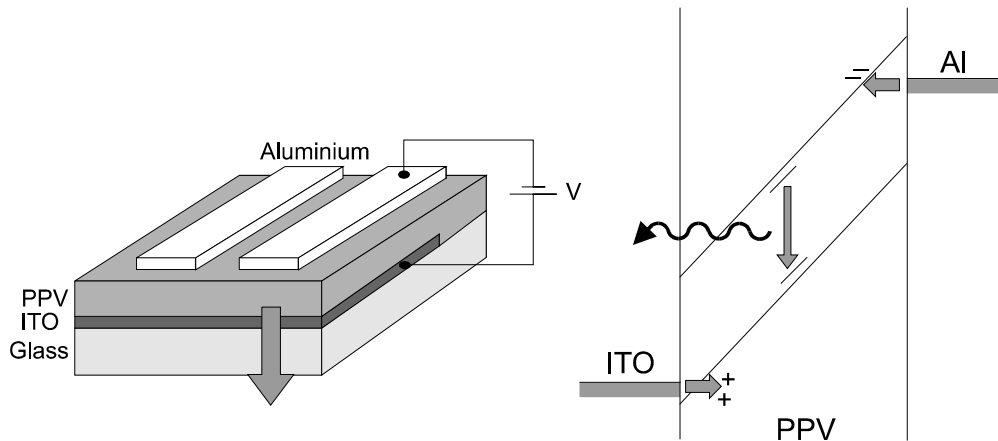


**Figure 1.2** Left: schematic representation of a polymer LED. Right: simple energy level diagram of a polymer LED operating in forward bias.

The injection barrier for electrons is often significantly higher, which limits the injection rate for electrons severely. So, the emissive performance of a single-layer device is usually governed by field-driven electron injection. This has as a consequence that in single-layer devices the injection of opposite charges is

unbalanced resulting in large loss (hole) currents and low efficiencies. Low work function metals like Ca [49] improve the injection rates but have the disadvantage of being highly reactive (oxidation).

*Charge transport.* The charge mobility is an important parameter, which has a significant impact on the device performance (brightness and EL efficiency). Charges move by electron transfer reactions or hopping between polymer chains [50]. Interchain transport is expected to be slower than intrachain transport, because electrical transport through a polymer chain is far more efficient than through space [51]. Conformational disorder and chemical defects can reduce intrachain transport significantly, however. The electron and hole mobilities in conjugated polymers are in general low, in the range of  $10^{-4}$ - $10^{-8}$   $\text{cm}^2\text{V}^{-1}\text{s}^{-1}$  [52]. This puts a constraint on the maximum amount of charges which can be injected into the bulk (so limiting the brightness of the device). In addition, there is good evidence that holes are considerably more mobile than electrons in conjugated polymers due to deep trapping of electrons [53], which makes them preferentially hole transporters. The lower electron mobility results in unbalanced transport and recombination close to the interface of the electron-injecting metal electrode, which has the effect of quenching the emission.

*Balanced injection and transport.* So, for efficient LED operation balanced injection and transport are required. It has been shown that this requirement can be fulfilled in a polymer LED by using additional transport layers [28,30]. A concept which has proven its success in LEDs based on evaporated thin films of small organic emitters [21]. For example the introduction of an appropriate electron transport layer (ETL) can lower the electron-injection barrier, and create an energy offset for holes at the emissive layer/transport layer interface. This energy offset effectively blocks the hole current at the interface and results in a positive space-charge interfacial zone in the emissive layer. The space-charge zone will increase the field over the ETL layer resulting in enhanced electron-injection from the cathode. In addition, recombination will take place in a region (near the hetero-junction) away from the metal cathode. This concept poses some challenges for polymers, because the upper layer of the device must be cast without redissolving the lower one.

*Recombination and decay.* It is obvious that the EL efficiency of a polymer LED is for a large part determined by the efficiency of radiative decay of the excitations formed upon recombination. Charge recombination produces excitons, but generates both singlets and triplets. According to spin statistics, only approximately one quarter of the initially formed excitons will be singlets [28,54]. In PPV a variety of evidence, including the vibronic structure on the emission spectrum, strongly suggests that the luminescence is from an intrachain singlet exciton [55,56]. This is also reflected in the EL spectrum of PPV, which is identical to its PL spectrum. The importance of this is that the estimated upper limit of the EL-efficiency is set to 25 % of the PL efficiency for which the dominant photoexcitation is an intrachain singlet

exciton. In fact the situation is far more complicated as described above, because interchain interactions have a large influence on the decay pathways in the condensed state. Time-resolved photoluminescence studies give valuable information about the nature of the excited states, their lifetime, energy migration and decay pathways [57,58] and therefore helps to understand the photophysics of luminescent polymers. Yan *et al.* [37] reported a photoluminescence study of PPV films, and claimed that intrachain singlet excitons are not the primary photoexcitations generated. They proposed that the majority excitations are interchain excitations (modelled as interchain polaron pairs [59]) which decay non-radiatively, and speculated that they may be formed upon charge recombination to a lesser extent. However, Friend *et al.* [25] claimed that PPV films with 80% PL-efficiency can be prepared, which implies the generation of singlet excitons with unit quantum yield upon photoexcitation. This illustrates the importance of the way of preparation of PPV (amount of chemical and conformational defects as a result of the synthesis), film morphology, intermolecular organization (“packing”), the influence of impurities and oxidation products, etc. The importance of chain packing was also elegantly demonstrated in cyano-substituted PPV derivatives. In this type of polymers the backbones are closely packed, due to strong coulombic interactions. A photoluminescence study by Samuels *et al.* [60] of thin films of cyano-substituted PPV, has shown that in this case interchain excitations are the dominant species, which can give rise to highly efficient luminescence. They based their conclusion on the large Stokes shift, the broad structureless spectrum and the long luminescence lifetime of  $\approx 6$  ns found upon photoexcitation. The exact origin of this emission, whether it originates from dimers/aggregates or excimers is not clear at present. The above-mentioned PL studies illustrate that the design of highly luminescent polymers for light-emission applications is not only a question of choosing a suitable chromophore, but also of controlling their interactions in the condensed state.

## 1.4 Well-defined alternating semiconducting copolymers and oligomers

### *Alternating PPV copolymers*

In conjugated homopolymers the actual conjugation length is an average value determined by random conformational or chemical defects in the polymer backbone and is difficult to control. Our approach to controlling the conjugation length and make the link between the luminescence properties of oligomers and those of polymers, is through multiblock copolymers containing well-defined conjugated sequences (Fig. 1.3). Luminescent chromophores (A: typically  $\pi$ -conjugated oligomers) are either separated by higher band gap blocks (B), or directly linked to

each other in a non-coplanar way. In both molecular structures the conjugation of the polymer main chain is regularly interrupted, giving well-defined tunable optical properties [61,62]. This approach is particularly suitable for blue-light emission, since this demands a short conjugation length. This molecular design can also enhance the luminescence efficiency through confinement of the excitons to the conjugated blocks, hindering their migration to quenching sites [63].

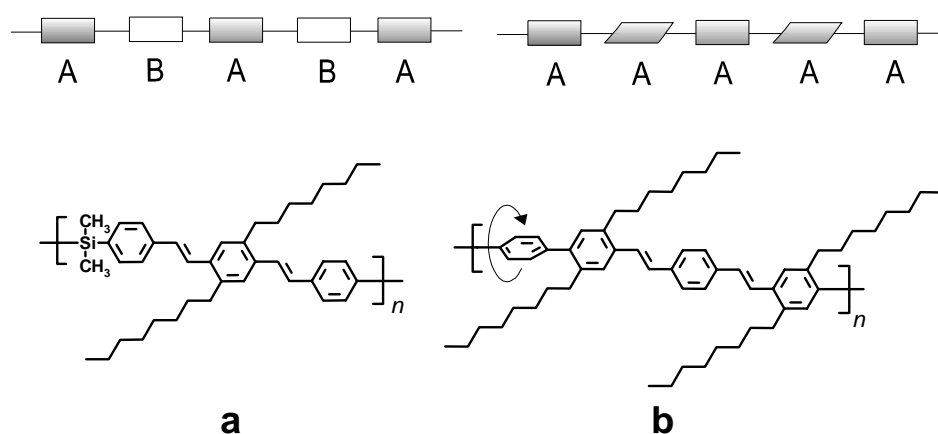


**Figure 1.3** Schematic representation of alternating copolymers; A is the conjugated chromophore, B is the interruption unit. For both approaches an example is given.

Two examples of blue-light-emitting alternating PPV copolymers made following this approach are shown in figure 1.3a and b. In structure (a), abbreviated as SiPPV, PPV oligomers (distyrylbenzene) are linked through dimethylsilylene units. The dimethylsilylene units provide flexibility to the polymer backbone. The choice of this interrupting block is based on previous studies carried out in our group on poly[(silanylene)thiophene]s [64]. In this study it has been shown that the presence of only one silicon atom in the backbone effectively interrupts the conjugation. Structure (b), abbreviated as TOP-PPV, can be regarded as a copolymer of PPV and PP. Actually the PPV blocks are linked through an aromatic phenyl ring within a fully rigid-rod chain. The desired control of the conjugation length is achieved through steric interactions between the side chains and the rings within the terphenylene parts of the copolymer. As can be seen from figure 1.3b (arrow) the middle ring in the terphenylene unit is twisted out of coplanarity, effectively interrupting the  $\pi$ -orbital overlap along the backbone. Also in this copolymer the active chromophore is a distyrylbenzene unit. The wavelength of emission of the copolymers can be tuned by

increasing the size of the oligomeric blocks or by the introduction of substituents, which alter the electronic structure of the chromophore. For instance, by introducing electron-accepting cyano-substituents on the vinylene linkage or by changing the side-chains from alkyl to alkoxy (an electron-donating moiety), the emission can be considerably shifted to the red part of the spectrum.

### *PPV oligomers*

From the preceding section (1.3) it became clear that the efficiency of radiative decay of photoexcited species (photoluminescence) is strongly dependent on the actual chemical structure of the polymer and on its state of aggregation (solid or solution). Since the processes of intramolecular exciton diffusion, intermolecular exciton stabilization, hopping, and exciton trapping at conformational defects, chemical defects or impurities are considered important factors in the competition between radiative and nonradiative decay, the conformation of the polymer molecule and the intermolecular organization (“packing”) are of utmost relevance. These factors however, are hardly controllable if at all, especially in amorphous polymers. The study of small model compounds, which can be obtained in ultra pure form and with controllable molecular structure and organization (single crystals or polycrystalline films), can help in understanding the influence of those factors. With this in mind, a series of soluble 3 and 5-ring oligo(*p*-phenylene vinylene)s representing the PPV blocks of the copolymers have been synthesized and their single-crystal structure has been determined [65,66]. Furthermore, PPV oligomers gained considerable interest, not only as model compounds [67,68], but also for application as active layer in LEDs [69,70]. They are highly fluorescent, and they can be processed by vacuum-deposition from the vapour phase into high-purity thin films. The morphology of the thin films can be controlled by means of adjustment of the substrate temperature during deposition [70], or by annealing after deposition [71]. The optical properties of PPV oligomers (wavelength of absorbance, luminescence and photoconductivity maxima) as a function of the number of repeat units ( $n-1$ , where  $n$  is the number of phenyl rings in the backbone) are converging to that of the corresponding fully conjugated PPV polymer at the five-ring level ( $n = 5$ ) [68,72].

### *Alternating copolymer versus model oligomer*

The effective interruption of  $\pi$ -orbital overlap in our copolymers is illustrated in figure 1.4, where the UV-vis absorption and fluorescence spectra of TOP-PPV and its corresponding PPV model oligomer (tetraoctyl-substituted distyrylbenzene, abbreviated as Oct-OPV3) are shown. The shape and the width of the emission

spectrum of the copolymer are very similar to that of the model oligomer, confirming that the distyrylbenzene units are the active chromophores. In addition, the quantum yield and luminescence lifetimes of the copolymer and model oligomer are comparable. The small red-shift of the copolymer spectra is probably due to a slight electronic contribution of the non-coplanar phenyl rings. The high luminescence quantum yield of these well-defined alternating PPV copolymers indicates their potential as emissive component in light emission applications like LEDs or lasers.

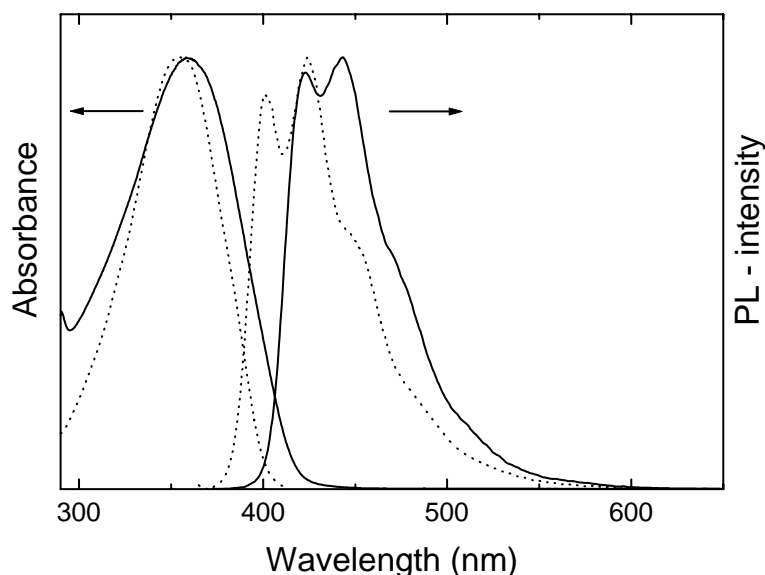


**Figure 1.4** UV-vis absorption and fluorescence spectra in tetrahydrofuran solution of TOP-PPV (solid lines) and Oct-OPV3 (dotted lines).

### 1.5 Aim and outline of this thesis

The primary interest of this study has been the solid-state photophysical characterization of a series of novel well-defined alternating PPV copolymers and crystalline 5-ring oligo(*p*-phenylene vinylene)s, and their application as emissive medium in light-emitting diodes and photopumped lasers.

In *chapter 2* the optical properties in solution and solid state of a series of alternating PPV copolymers and all-*trans* 5-ring oligo(*p*-phenylene vinylene)s are evaluated [73]. The influence of different substitution patterns on the optical properties as well as the differences between the optical properties in dilute solution and thin films are discussed. The spectroscopic properties of the copolymers in dilute

solution are compared with those of distyrylbenzene model oligomers representing the chromophores in the backbone. The optical properties of solution-grown oligo(*p*-phenylene vinylene) single crystals are discussed in terms of molecular conformation and packing based on the X-ray diffraction data of the single crystals. Furthermore, the optical properties of oligomer thin films prepared by vacuum-deposition from the vapour phase are described. The influence of the thin-film morphology of the oligomers on the optical properties was investigated by means of annealing.

*Chapter 3* deals with the application of alternating PPV copolymers as laser dyes in solution. Laser action of an efficient blue-light-emitting copolymer poly[(2, 5, 2'', 5''-tetraoctyl)-*p*-terphenyl-4,4''-ylene vinylene-*p*-phenylene vinylene] is demonstrated [13]. Three different solvents (*n*-hexane, *p*-xylene and tetrahydrofuran) were used to investigate the influence of the molecular environment on the lasing properties. The commercially available laser dyes, Coumarin 47 and 120, were used as a reference to compare the lasing efficiency and wavelength tunability of the copolymer with that of conventional laser dyes.

*Chapter 4* describes the emission properties of spincoated neat films of the blue-light-emitting silylene-*alt*-oligo(phenylene vinylene) copolymer (SiPPV) under pulsed laser excitation [16,74]. Spectral narrowing was observed above a well-defined excitation energy threshold. The influence of film thickness and the size of the excitation area on the threshold of spectral narrowing are discussed, as well as the angular dependence of the emission. Furthermore, laser action in films of a red-light-emitting homopolymer, poly(2,5-di-*n*-octyloxy-*p*-phenylene vinylene) (Ooct-PPV) in a microcavity configuration is demonstrated.

*Chapter 5* describes the emission properties of both solution-grown single crystals and vacuum-deposited thin films of an octyloxy-substituted oligo(*p*-phenylene vinylene) under intense laser excitation. The morphology of the thin films was varied by annealing and by recrystallization from the isotropic melt. In this way, the crystalline domain size could be varied from a few microns up to several millimeters in the latter case. In both single crystals and thin films mirrorless lasing was observed. Stimulated emission in the polycrystalline thin films was only observed after the crystal domain size was increased by a thermal treatment [73,75].

In *chapter 6* the electrical and optical characteristics of light-emitting diodes based on alternating PPV copolymers [61,76] and 5-ring oligo(*p*-phenylene vinylene)s are evaluated. The influence of thin-film morphology on LED performance is discussed for an octyloxy-substituted 5-ring OPV. Device optimization by means of additional charge-transport layers and blending has been applied to enhance the electroluminescence efficiency. A novel polymer with oxadiazole-based side-chains has been used as an electron-transport/hole-blocking layer.

## 1.6 References

- [1] J.H. Burroughes, D.D.C. Bradley, A.R. Brown, R.N. Marks, K. Mackay, R.H. Friend, P.L. Burn, A.B. Holmes, *Nature*, **347**, 539 (1990)
- [2] D. Braun, A.J. Heeger, *Appl. Phys. Lett.*, **58**, 1982 (1991)
- [3] Q. Pei, G. Yu, C. Zhang, Y. Yang, A.J. Heeger, *Science*, **269**, 1086 (1995)
- [4] Q. Pei, Y. Yang, *Synth. Met.*, **80**, 131 (1996)
- [5] G. Yu, C. Zhang, A.J. Heeger, *Appl. Phys. Lett.*, **64**, 1540 (1994)
- [6] G. Yu, K. Pakbaz, A.J. Heeger, *Appl. Phys. Lett.*, **64**, 3422 (1994)
- [7] G. Yu, J. Gao, J.C. Hummelen, F. Wudl, A.J. Heeger, *Science*, **270**, 1789 (1995)
- [8] J.J.M. Halls, C.A. Walsh, N.C. Greenham, E.A. Marseglia, R.H. Friend, S.C. Moratti, A.B. Holmes, *Nature*, **376**, 498 (1995)
- [9] H. Koezuka, A. Tsumara, T. Ando, *Synth. Met.*, **18**, 699 (1987)
- [10] A. Assadi, C. Svensson, M. Wilander, O. Inganäs, *Appl. Phys. Lett.*, **53**, 195 (1988)
- [11] G. Yu, K. Pakbaz, C. Zhang, A.J. Heeger, *J. Electron. Mater.*, **23**, 925 (1994)
- [12] D. Moses, *Appl. Phys. Lett.*, **60**, 3215 (1992)
- [13] H.J. Brouwer, V.V. Krasnikov, A. Hilberer, J. Wildeman, G. Hadziioannou, *Appl. Phys. Lett.*, **66**, 3404 (1995)
- [14] N. Tessler, G.J. Denton, R.H. Friend, *Nature*, **382**, 695 (1996)
- [15] F. Hide, M.A. Díaz-García, B.J. Schwartz, M.R. Andersson, Q. Pei, A.J. Heeger, *Science*, **273**, 1833 (1996)
- [16] H.J. Brouwer, V.V. Krasnikov, A. Hilberer, G. Hadziioannou, *Adv. Mater.*, **8**, 935 (1996)
- [17] A.J. Heeger, S. Kivelson, J.R. Schrieffer, W.P. Su, *Rev. Mod. Phys.*, **60**, 781 (1988)
- [18] J.L. Brédas, G.B. Street, *Acc. Chem. Res.*, **18**, 309 (1985); J.L. Brédas, J. Cornil, A.J. Heeger, *Adv. Mater.*, **8**, 5 (1996)
- [19] M. Pope, H. Kallmann, P. Magnante, *J. Phys. Chem.*, **38**, 2042 (1963)
- [20] M. Pope, C.E. Swenberg, *Electronic processes in organic crystals* (Clarendon press, Oxford, 1982)
- [21] C.W. Tang, S.A. VanSlyke, *Appl. Phys. Lett.*, **51**, 913 (1987)
- [22] C.W. Tang, S.A. VanSlyke, C.H. Chen, *Appl. Phys. Lett.*, **65**, 3610 (1989)
- [23] R.H. Partridge, *Polymer*, **24**, 755 (1983)
- [24] L.J. Rothberg, A.J. Lovinger, *J. Mater. Res.*, **11**, 3174 (1996)
- [25] R. H. Friend, G.J. Denton, J.J.M. Halls, N.T. Harrison, A.B. Holmes, A. Köhler, A. Lux, S.C. Moratti, K. Pichler, N. Tessler, K. Towns, H.F. Wittmann, *Solid State Commun.*, **102**, 249 (1997)
- [26] D. Braun and A.J. Heeger, *Appl. Phys. Lett.*, **58**, 1982 (1991)
- [27] C. Zhang, H. von Seggern, K. Pakbaz, B. Kraabel, H.-W. Schmidt, A.J. Heeger, *Synth. Met.*, **62**, 35 (1994); J.K. Herrema, J. Wildeman, R.H. Wieringa, R.E. Gill, G.G. Malliaras, S.S. Lampoura, G. Hadziioannou, *Polym. Preprints*, **34**, 282 (1993)
- [28] A.R. Brown, D.D.C. Bradley, P.L. Burns, J.H. Burroughes, R.H. Friend, N. Greenham, A.B. Holmes, A. Kraft, *Appl. Phys. Lett.*, **61**, 2793 (1992)
- [29] D.D.C. Bradley, *Synth. Met.*, **54**, 401 (1993)

- [30] N.C. Greenham, S.C. Moratti, D.D.C. Bradley, R.H. Friend, A.B. Holmes, *Nature*, **365**, 628 (1993)
- [31] S. Karg, J.C. Scott, J.R. Salem, M. Angelopoulos, *Synth. Met.*, **80**, 119 (1996)
- [32] A.R. Schlattmann, D. Wilms Floet, A. Hilberer, F.J. Esselink, P.J.M. Smulders, T.M. Klapwijk, G. Hadziioannou, *Appl. Phys. Lett.*, **69**, 1764 (1996)
- [33] A.J. Heeger, I.D. Parker, Y. Yang, *Synth. Met.*, **67**, 23 (1994)
- [34] J.R. Sheats, H. Antoniadis, M. Hueschen, W. Leonard, J. Miller, R. Moon, D. Roitman, A. Stocking, *Science*, **273**, 884 (1996)
- [35] F. Hide, B.J. Schwartz, M.A. Díaz-García, A.J. Heeger, *Chem. Phys. Lett.*, **256**, 424 (1996)
- [36] B.J. Schwartz, F. Hide, M.A. Díaz-García, A.J. Heeger, *PMSE Proceedings ACS fall meeting '96 Orlando*, **75**, 451 (1996)
- [37] M. Yan, L.J. Rothberg, F. Papadimitrakopoulos, M.E. Galvin, T.M. Miller, *Phys. Rev. Lett.*, **72**, 1104 (1994); M. Yan, L.J. Rothberg, B.R. Hsieh, R.R. Alfano, *Phys. Rev. B*, **49**, 9419 (1994)
- [38] W. Graupner, G. Leising, G. Lanzani, M. Nisoli, S. de Silvestri, U. Scherf, *Phys. Rev. Lett.*, **76**, 847 (1996); T. Pauck, R. Henning, M. Perner, U. Lemmer, U. Siegner, R.F. Mahrt, U. Scherf, K. Müllen, H. Bässler, E.O. Göbel, *Chem. Phys. Lett.*, **244**, 171 (1995)
- [39] G.H. Gelinck, J.M. Warman, M. Remmers, D. Neher, *Chem. Phys. Lett.*, **265**, 320 (1997)
- [40] S.V. Frolov, W. Gellermann, Z.V. Vardeny, M. Ozaki, K. Yoshino, *Synth. Met.*, **84**, 471 (1997)
- [41] D. Braun, D. Moses, C. Zhang, A.J. Heeger, *Appl. Phys. Lett.*, **61**, 3902 (1992)
- [42] D.G. Lidzey, D.D.C. Bradley, S.F. Alvarado, P.F. Seidler, *Nature*, **386**, 135 (1997)
- [43] I.D. Parker, *J. Appl. Phys.*, **75**, (1994) 1656
- [44] S. Karg, W. Riess, V. Dyakonov, M. Schwoerer, *Synth. Met.*, **54**, 427 (1993)
- [45] P.S. Davids, Sh.M. Kogan, I.D. Parker, D.L. Smith, *Appl. Phys. Lett.*, **69**, 2270 (1996)
- [46] W.R. Salaneck, J.L. Brédas, *Synth. Met.* **67**, 11 (1994)
- [47] E. Ettetdgui, H. Razafitrimo, K.T. Park, Y. Gao, B.R. Hsieh, *J. Appl. Phys.*, **75**, 7526 (1994)
- [48] W.A. Mackie, R.L. Hartman, M.A. Andersson, P.R. Davis, *J. Vac. Sci. Technol.*, **B12**, 722 (1994)
- [49] D. Braun, A.J. Heeger, H. Kroemer, *J. Electron. Mater.*, **20**, 945 (1991)
- [50] A. Nitzam, M.A. Ratner, *J. Phys. Chem.*, **98**, 1765 (1994)
- [51] B. Paulson, K. Pramod, P. Eaton, G. Gloss, J.R. Miller, *J. Phys. Chem.*, **97**, 13042 (1993)
- [52] P.M. Borsenberger, D.S. Weiss, *Organic photoreceptors for imaging systems* (Dekker, New York, 1993)
- [53] H. Antoniadis, M.A. Abkowitz, B.R. Hsieh, *Appl. Phys. Lett.*, **65**, 2030 (1994)
- [54] A.R. Brown, K. Pichler, N.C. Greenham, D.D.C. Bradley, R.H. Friend, *Chem. Phys. Lett.*, **210**, 61 (1993)
- [55] R.H. Friend, D.D.C. Bradley, P.D. Townsend, *J. Phys. D*, **20**, 1367 (1987)

- [56] J.M. Leng, S. Jeglinski, X. Wei, R.E. Brenner, Z.V. Vardeny, F. Guo, S. Mazumdar, *Phys. Rev. Lett.*, **72**, 156 (1994)
- [57] U. Lemmer, R.F. Mahrt, Y. Wada, A. Greinjer, H. Bässler, E.O. Göbel, *Chem. Phys. Lett.*, **209**, 243 (1993)
- [58] I.D.W. Samuels, B. Crystall, G. Rumbles, P.L. Burn, A.B. Holmes, R.H. Friend, *Synth. Met.*, **54**, 281 (1993)
- [59] E.M. Conwell, H.A. Mizes, *Phys. Rev. B*, **51**, 6953 (1995)
- [60] I.D.W. Samuels, G. Rumbles, C.J. Collison, *Phys. Rev. B*, **52**, R11573 (1995)
- [61] A. Hilberer, H.J. Brouwer, B.J. van der Scheer, J. Wildeman, G. Hadziioannou, *Macromolecules*, **28**, 4525 (1995)
- [62] A. Hilberer, P.F. van Hutten, J. Wildeman, G. Hadziioannou, *Macromol. Chem. Phys.*, **198**, 2211 (1997)
- [63] C. Zhang, D. Braun, A.J. Heeger, *J. Appl. Phys.*, **73**, 5177 (1993)
- [64] J.K. Herrema, P.F. van Hutten, R.E. Gill, J. Wildeman, R.H. Wieringa, G. Hadziioannou, *Macromolecules*, **28**, 8102 (1995)
- [65] R.E. Gill, A. Meetsma, G. Hadziioannou, *Adv. Mater.*, **8**, 212 (1996)
- [66] R.E. Gill, P.F. van Hutten, A. Meetsma, G. Hadziioannou, *Chem. Mater.*, **8**, 1341 (1996)
- [67] R. Schenk, H. Gregorius, K. Meerholz, J. Heinze, K. Müllen, *J. Am. Chem. Soc.*, **113**, 2634 (1991)
- [68] A. Ohlemacher, R. Schenk, H.P. Weitzel, N. Tyutyulkov, M. Tasseva, K. Müllen, *Makromol. Chem.*, **193**, 81 (1992); H.S. Woo, O. Lhost, S.C. Graham, D.D.C. Bradley, R.H. Friend, C. Quattrocchi, J.L. Brédas, R. Schenk, K. Müllen, *Synth. Met.*, **59**, 13 (1993)
- [69] C. Adachi, A. Tsutsui, S. Saito, *Appl. Phys. Lett.*, **56**, 799 (1990)
- [70] M.D. Joswick, I.H. Campbell, N.N. Barashkov, J.P. Ferraris, *J. Appl. Phys.*, **80**, 883 (1996); T. Goodson III, L. Wenjie, A. Gharavi, L. Yu, *Adv. Mater.*, **9**, 639 (1997)
- [71] R.E. Gill, Design, synthesis and characterization of luminescent organic semiconductors (Ph.D. thesis, University of Groningen, 1996), chapter 5
- [72] H.E. Katz, S.F. Bent, W.L. Wilson, M.L. Schilling, S.B. Ungashe, *J. Am. Chem. Soc.*, **116**, 6631 (1994)
- [73] H.J. Brouwer, V.V. Krasnikov, T.-A. Pham, R.E. Gill, P.F. van Hutten, G. Hadziioannou, *Chem. Phys.*, in press
- [74] A. Hilberer, M. Moroni, R.E. Gill, H.J. Brouwer, V.V. Krasnikov, T.-A. Pham, G.G. Malliaras, S.C. Veenstra, P.F. van Hutten, G. Hadziioannou, *Macrom. Symp.*, **125**, 99 (1997)
- [75] P.F. van Hutten, H.J. Brouwer, V.V. Krasnikov, T.-A. Pham, R.E. Gill, G. Hadziioannou, *SPIE Proceedings 1348, San Diego 1997*, in press.
- [76] H.J. Brouwer, A. Hilberer, V.V. Krasnikov, M. Werts, J. Wildeman, G. Hadziioannou, *Synth. Met.*, **84**, 881 (1997)



# Chapter 2

## Optical properties of alternating PPV copolymers and oligo(*p*-phenylene vinylene)s<sup>†</sup>

### Abstract

*In this chapter the optical properties in solution and solid state of a series of well-defined alternating PPV copolymers and all-trans 5-ring oligo(*p*-phenylene vinylene)s are evaluated. The optical properties of the copolymers in dilute solution were similar to those of the distyrylbenzene model oligomers representing the chromophores in the polymer backbone, indicating that the conjugation is effectively interrupted in the copolymers. For the blue-light-emitting alternating copolymers, the photoluminescence (PL) efficiency and lifetime did not significantly change going from solution to the solid state, and shows that the contribution from additional non-radiative decay channels due to interchain interactions in the condensed state is negligible, resulting in efficient solid-state PL.*

*For both the cyano-substituted copolymer and Ooct-OPV5-CN1, a fast double exponential PL decay was measured in dilute solution, which is the result of a fast non-radiative channel associated with the cyano substituents on the vinylene linkages. Restricting the molecular motion (twisting/bending) by dispersing the oligomer in a solid polysulfone matrix resulted in an effective inhibition of the non-radiative decay channel and a much longer single-exponential PL decay with a time constant of 1.7 ns. Remarkably, for Ooct-OPV5-CN2 in solution a long PL-decay with a PL lifetime of 1.4 ns was observed, which indicates that the position of the cyano moieties on the vinylene bonds is an important parameter, governing this fast non-radiative decay channel.*

*For the Ooct-OPV5-CN2 single crystals, the PL spectra are broad and featureless and a long PL lifetime of 8 ns was measured. The long-lived luminescence is attributed to emission from excimers rather than singlet excitons. This is positively confirmed by X-ray diffraction data of the single crystal. On the basis of the packing of the molecules in the crystal lattice, significant  $\pi$ - $\pi$  interactions between adjacent (face-to-face) molecules are to be expected. Also in the case of the cyano-substituted copolymer films there is evidence that the luminescence originates from excimers.*

---

<sup>†</sup> H.J. Brouwer, V.V. Krasnikov, T.A. Pham, R.E. Gill, P.F. van Hutten, G. Hadziioannou, *Chem. Phys.*, in press

## 2.1 Introduction

Time-resolved photoluminescence studies on conjugated polymers can give valuable information about the nature of the excited states, their lifetime, energy migration and decay pathways [1-11]. The measurements of luminescence in conjugated polymers are important for both understanding the photophysics involved and the operation of electroluminescent devices. The operation of a light-emitting diode comprises several steps: charge injection, charge transport, charge recombination and decay of the excitation formed via radiative and non-radiative channels. In the majority of cases the same excited states are responsible for both electroluminescence (EL) and photoluminescence (PL). PL measurements enable the last step to be studied directly.

It is generally accepted that the dominant type of (photo)excitations are intrachain singlet excitons, in dilute solutions where interchain interactions are negligible, which can decay by a combination of radiative and nonradiative processes. The relative rates of the decay processes determine the quantum efficiency of luminescence. If the nonradiative decay process is fast then most of the excitons will decay via this route before they have time to emit, resulting in weak luminescence. The measured lifetime,  $\tau$ , is shorter than the natural radiative lifetime  $\tau_R$ , and can be related to the rate constants for radiative and nonradiative decay  $k_R$  and  $k_{NR}$  by:

$$\tau = \frac{1}{k_R + k_{NR}} \quad (2.1)$$

the PL efficiency is then given by:

$$\Phi = \frac{bk_R}{k_R + k_{NR}} = \frac{b\tau}{\tau_R} \quad (2.2)$$

where  $\tau_R = k_R^{-1}$  is the natural radiative lifetime (the lifetime of the luminescence in the absence of competing non-radiative decay processes) and  $b$  is the fraction of absorbed photons leading to singlet excitons ( $0 \leq b \leq 1$ ). The natural radiative lifetime can be estimated from measurements of  $\Phi$  and  $\tau$ , or via the absorbance and emission spectra using the Strickler-Berg relationship [12] given by:

$$\tau_R^{-1} = \frac{8\pi n^2}{c^2} \langle \nu^{-3} \rangle^{-1} \int \frac{\sigma(\nu) d\nu}{\nu} \quad (2.3)$$

$$\langle \nu^{-3} \rangle^{-1} = \frac{\int L(\nu) d\nu}{\int \nu^{-3} L(\nu) d\nu} \quad (2.4)$$

where  $n$  is the refractive index,  $\sigma(\nu)$  is the absorption cross-section per absorbing species at frequency  $\nu$ , and  $L(\nu)$  is the emission spectrum as a function of photon frequency  $\nu$ . Equation 2.4 is derived from the Einstein relations between transition probabilities for absorption, stimulated emission and spontaneous emission [12]. The equation ignores conformational changes going from the ground state to the excited state upon excitation (which alter the probability of radiative decay and hence the lifetime). Secondly, it is not clear how to define the absorbing unit in a polymer chain (number of repeat units defining the chromophore), which is necessary for calculating the molar extinction coefficient  $\epsilon$ . Furthermore, for solid-state samples (thin films) it is difficult to determine the refractive indices accurately. So, because of the above-mentioned difficulties and shortcomings, radiative lifetimes obtained by equation 2.4 should be regarded as rough estimates.

Despite the large number of ultrafast spectroscopy studies on PPV and its soluble derivatives, there is still great controversy regarding the primary photoexcitations in solid-state PPV films. In the solid state, strong intermolecular interactions can lead to the formation of interchain excitations, which can decay non-radiatively [9,13] or radiatively [14]. Yan *et al.* [9,13] claimed that the majority excitations in PPV upon illumination are non-emissive interchain excitations leading to a value of  $b \approx 0.1$ . These interchain excitations were modelled as interchain bound polaron pairs [15]. On the contrary, Friend *et al.* [16,17] claimed solid-state quantum efficiencies of 0.27 up to 0.8! for PPV, depending on the way of preparation, showing that  $b$  can be very close to 1 and that the primary photoexcitations are in fact intrachain singlet excitons.

An example of polymers which can form interchain excitations upon photoexcitation and that can decay radiatively, are cyano-substituted PPV derivatives. In this type of polymers the backbones are closely packed, due to strong coulombic interactions. A photoluminescence study by Samuels *et al.* [14] of thin films of cyano-substituted PPV, has shown that in this case interchain excitations are the dominant species, which can give rise to highly efficient luminescence. They based their conclusion on the large Stokes shift, the broad structureless spectrum and the long luminescence lifetime of  $\approx 6$  ns found upon photoexcitation. The exact origin of this emission, whether it originates from interchain excitons, dimers or eximers is not clear at present. So, as illustrated by these examples, the type of primary photoexcitations and the branching ratio  $b$  is a complex function of the state of aggregation (solid or liquid), extent of oxidation of the pristine material, the packing of the polymer chains on a microscopic scale, type of substituents, number of chemical and conformational defects, impurities etc.

Samuels *et al.* [18] proposed a kinetic scheme to explain the excited state kinetics of conjugated polymers, which is depicted in figure 2.1.  $X^*$  is the initial excited state and the two processes leading to the population of  $A^*$  and  $B^*$  are described by two rate constants  $k_{XA}$  and  $k_{XB}$ . These processes are very efficient and occur on very short timescales (less than 1 ps). If  $X^*$  is assigned to a non-relaxed or “hot” excitation, then  $k_{XA}$  represents the relaxation of this state into longer conjugated sequences,  $A^*$ . This could be energy relaxation along the polymer backbones or relaxation of the polymer chain around the excitation, or a combination of the two.  $k_{XB}$  represents the population of the interchain states by similar processes. If these processes compete efficiently with  $k_{XA}$ , then on the timescale of a PL decay measurement (resolution 30 ps) this will look as an direct excitation of the interchain  $B^*$  state.

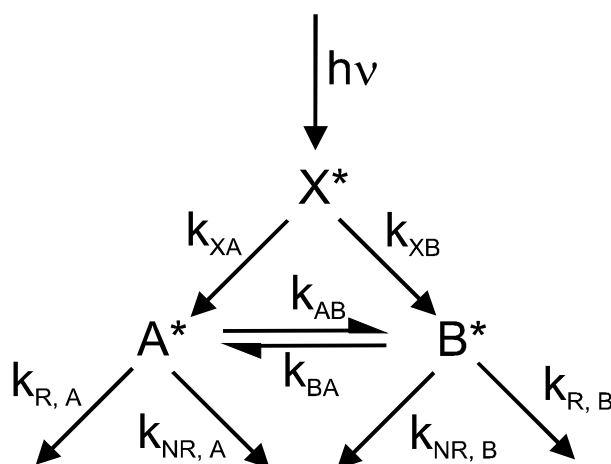


**Figure 2.1** Kinetic scheme for a general model representing the rate processes between an initial excited state ( $X^*$ ), an intrachain ( $A^*$ ) and an interchain ( $B^*$ ) excitation. Taken from reference [18].

Both the  $A^*$  state and  $B^*$  state can decay back to the ground state by radiative and non-radiative channels, with rate constants  $k_{R,A}$ ,  $k_{NR,A}$ ,  $k_{R,B}$  and  $k_{NR,B}$ , respectively.

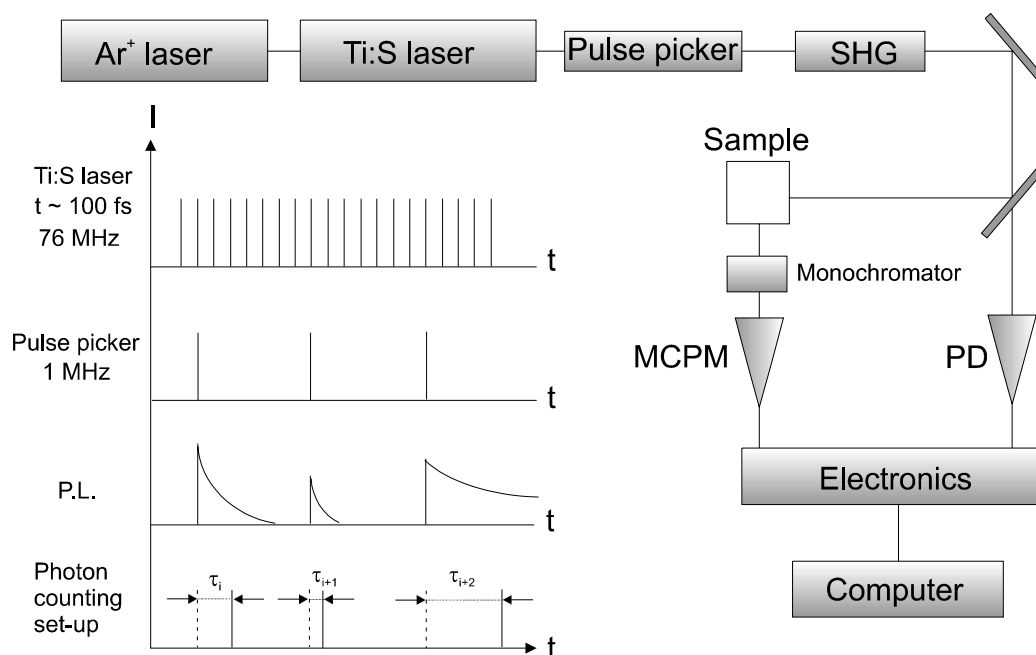
In this chapter, the optical properties in solution and solid state of a series of alternating PPV copolymers and all-*trans* 5-ring oligo(*p*-phenylene vinylene)s are evaluated. The influence of different substitution patterns on the optical properties as well as the differences between the optical properties in dilute solution and thin films are discussed. The spectroscopic properties of the copolymers in dilute solution are compared with those of distyrylbenzene model oligomers representing the chromophores in the backbone. The optical properties of solution-grown oligo(*p*-phenylene vinylene) singlecrystals are discussed in terms of molecular conformation and packing based on the X-ray diffraction data of the single crystals. Furthermore,

the optical properties of oligomer thin films prepared by vacuum deposition from the vapour phase are described.

## 2.2 Experimental

### 2.2.1 Time-correlated single-photon counting

A method to measure the luminescence lifetime of emitting species is via the time-correlated single-photon counting technique [19]. The single-photon counting technique records this distribution by measuring the time delays of individual photons with respect to the excitation pulse. More background information concerning this experimental technique can be found in reference [20].



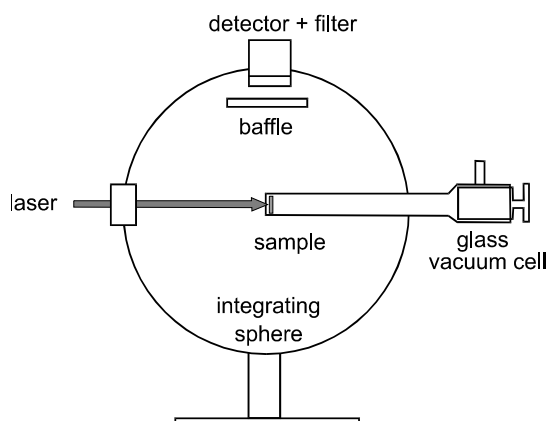
**Figure 2.2** Schematic representation of the time-correlated single-photon counting setup.

Figure 2.2 shows the schematic layout of our time-correlated single-photon counting set-up. Excitation was provided by the frequency-doubled output of a mode-locked Ti:Sapphire laser (Mira 900, Coherent) pumped by an Argon-ion laser (Beamlock 2080 A, Spectra Physics). This system produced  $\approx 100$  fs pulses at a repetition rate of 76 MHz. In order to match the photon counting electronics (Ortec), the laser repetition rate was reduced by an acousto-optical pulse-picker (Bragg cell, CAMAC) to 2 MHz.

The excitation wavelength range was 370-450 nm, and the excitation energy density did not exceed  $1\text{ nJ/cm}^2$  per pulse. The luminescence from the sample was focussed into a monochromator equipped with a microchannel plate photomultiplier detector (MCP-1564-410, Hamamatsu). The instrumental response time, full width at half maximum, was approximately 30 ps. Data analysis was performed by a nonlinear least-squares iterative fitting of the luminescence to a sum of exponentials convoluted with the measured instrumental response function.

### 2.2.2 Solid-state PL quantum yield measurements

The absolute photoluminescence quantum yields of our polymer films were determined using an integrating sphere and an  $\text{Ar}^+$  (488 nm) or frequency-doubled Ti:S (370 nm) laser as excitation source (see figure 2.3) [16,21].



**Figure 2.3** Schematic representation of the PL measurement set-up.

An integrating sphere is a hollow sphere with a diffusely reflecting coating inside. The flux of light measured at any aperture of the sphere is proportional to the total amount of light produced within the sphere, irrespective of its angular distribution. Thin polymer films ( $\approx 1$  mm thickness, optical density preferably  $> 1$ ) were cast on round suprasil glass plates (diameter 10 mm). The films were mounted in a glass cell, which was kept at a static vacuum of  $P < 10^{-4}$  mbar. After evacuation, the cell was mounted in an integrating sphere, with the film centred in the middle. The films were excited under near normal incidence, in such a way that the reflected excitation light did not escape the entrance hole directly. The luminescence was measured with a calibrated optical power meter (Advantest TQ 8210), which was shielded with a diffusely reflecting baffle to avoid direct illumination. A suitable cut-off filter was

placed directly in front of the optical power meter to block the excitation light. The incident power of the excitation beam was measured outside the integrating sphere with the optical power meter and the filter removed. We determined the power efficiency of the integrating sphere by measuring the output power, at the aperture, of a piece of “milky” glass (highly scattering glass) mounted in the vacuum cell illuminated with a HeNe laser ( $\lambda = 633 \text{ nm}$ ). The input power of the HeNe beam was measured outside the sphere with the filter removed. The spectral response of the integrating sphere is flat between 400 nm and 1  $\mu\text{m}$ , thus the power efficiency of the integrated sphere  $\eta_{\text{sphere}}$  is given by:

$$\eta_{\text{sphere}} = \frac{P_{\text{out},633\text{nm}}}{P_{\text{in},633\text{nm}}} \quad (2.5)$$

and the PL quantum efficiency is then given by:

$$\Phi_{\text{PL}} = \frac{P_{\text{out},\text{PL}}}{P_{\text{in},\text{exc}}} \frac{\lambda_{\text{PL}}}{T \eta_{\text{sphere}} \lambda_{\text{exc}}} \quad (2.6)$$

where  $P_{\text{out},\text{PL}}$  is the luminescence output power,  $P_{\text{in},\text{exc}}$  is the incident laser power (measured outside of the integrated sphere),  $T$  the transmittance of the sample at the wavelength of excitation and  $\eta_{\text{sphere}}$  is the power efficiency of the integrating sphere.

A reasonably large experimental error is introduced by the fact that the following contributions were neglected:

- [1] Excitation light which is reflected and diffusely scattered by the sample (a part will be indirectly absorbed by the sample after reflection by the sphere wall).
- [2] Spectral response of the optical power meter (which is assumed constant over the PL wavelength region of the film) and integrating sphere.
- [3] Absorption of luminescence (blue tail) by the cut-off filter.
- [4] Luminescence which escapes via the vacuum cell.
- [5] Luminescence (blue tail) which is reabsorbed by the sample.

The experimental inaccuracies lead to an estimated overall error of about 20 % in the final absolute quantum yields.

## 2.3 Results and discussion

### 2.3.1 Alternating PPV copolymers

The optical properties of a series of four well-defined alternating PPV copolymers containing three-ring oligo(*p*-phenylene vinylene) units as the light-emitting chromophores were studied in solution and solid state (see figure 1.3). The chemical structures of the copolymers are depicted in figure 2.3. In copolymers **I** through **III** the chromophores are directly linked to each other in a non-coplanar way (see paragraph 1.4, page 8 for more detail), while in copolymer **IV** the chromophores are connected by non- $\pi$ -conjugated dimethylsilylene spacer units. The substitution pattern (octyl/octyloxy sidechains and cyano groups on the vinylene linkages) in copolymers **I** to **III** was varied to tune the wavelength of emission. In such a way light emission from the blue to the orange/red wavelength region was established. The synthesis and characterization of the PPV copolymers are described in the references [22,23].

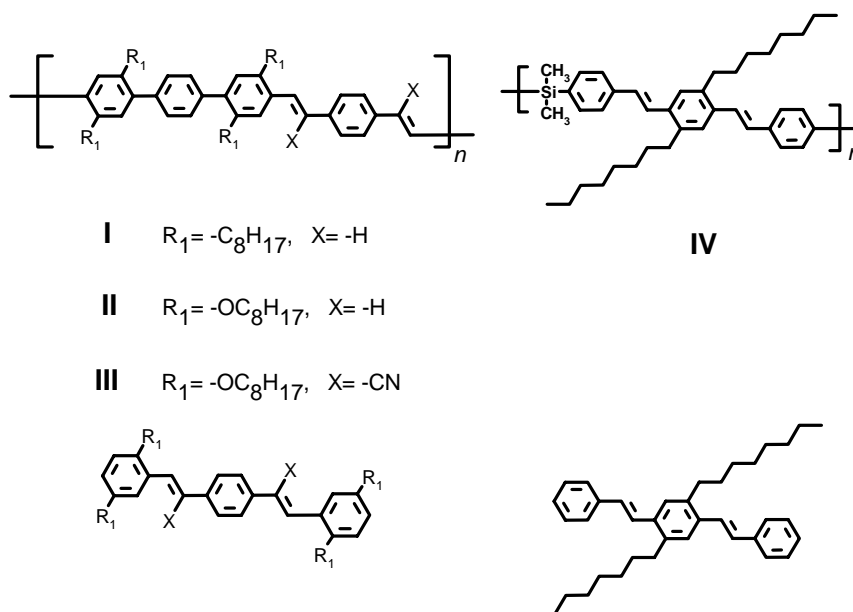


**Figure 2.3** Chemical structure of the alternating copolymers **I - IV** and corresponding oligomers.

All absorption and emission properties of the copolymers in solution (tetrahydrofuran) are summarized in table 2.1 on the next page. In addition, the spectroscopic properties of the corresponding model three-ring oligo(*p*-phenylene vinylene)s were measured for comparison. All copolymers and model oligomers show

**Table 2.1 Absorption and emission properties of copolymers and model compounds in tetrahydrofuran solution.**

Compound	Absorption			Fluorescence					
	$M_w$ (g·mol <sup>-1</sup> )	$M_w/M_n$	$\lambda_{Abs,max}$ (nm) <sup>(a)</sup>	$\epsilon_{max}$ (L·mol <sup>-1</sup> ·cm <sup>-1</sup> )	$\lambda_{Flu,max}$ (nm) <sup>(a,b)</sup>	Shift (cm <sup>-1</sup> ) <sup>(b)</sup>	$\Phi_{Flu}$	$\tau_{Flu,1}$ (ns) <sup>(c)</sup>	$\tau_{Flu,2}$ (ns)
I	5,000	1.7	361	51,600	<u>422</u> , 448	4000, <u>5400</u>	0.80	0.72	
II	39,000	1.8	415	69,800	<u>463</u> , 490	<u>2500</u> , 3700	0.53	0.75	
III <sup>(d)</sup>	7,200	1.1	430	-	540	4700	0.14	0.11	2.3
IV	60,000	2.4	360	28,600	412, <u>438</u>	3500, <u>4900</u>	0.61	0.9	
Mod I			355	52,600	401, <u>423</u>	3200, <u>4500</u>	0.87	1.0	
Mod II			380	48,000	<u>426</u> , 450	<u>2800</u> , 4100	0.88	1.6	
Mod III <sup>(d)</sup>			385	-	425	2400	0.14	-	
Mod IV			351	47,100	400, <u>423</u>	3500, <u>4900</u>	0.80	1.2	

a) taken from reference [22]. b) The shift is defined here as the difference between  $\lambda_{Abs,max}$  and  $\lambda_{Flu,max}$ , the underlined values are the absolute fluorescence maxima. c) PL-decays were measured at the wavelength of the PL maximum. d) Taken from reference [23].

**Table 2.2 Solid-state absorption and emission properties of copolymer thin films.**

Compound	Absorption		Fluorescence			
	$\lambda_{Abs,max}$ (nm)	$\lambda_{Flu,max}$ (nm) <sup>(a)</sup>	Shift (cm <sup>-1</sup> ) <sup>(a)</sup>	$\Phi_{Flu}$	$\tau_{Flu,1}$ (ns) <sup>(b)</sup>	$\tau_{Flu,2}$ (ns)
I	355	434, <u>455</u>	5100, <u>6200</u>	0.5	0.8	
II	418	484, <u>510</u>	3300, <u>4300</u>	0.09	0.2	0.7
III	450	592	5300	0.4	2.6	
IV	352	<u>452</u> , 483	<u>6300</u> , 7700	0.4	0.9	

a) The shift is defined here as the difference between  $\lambda_{Abs,max}$  and  $\lambda_{Flu,max}$ , the underlined values are the absolute fluorescence maxima.

b) PL-decays were measured at the maximum of the PL spectra.

a strong absorption band ( $\epsilon_{\max} \approx 10^4 \text{ L}\cdot\text{mol}^{-1}\cdot\text{cm}^{-1}$ ) in the ultraviolet and/or blue part of the visible spectrum. Blue light emission is observed from copolymer **I** and **IV** in which the chromophores are alkyl-substituted distyrylbenzene units, ( $\lambda_{\text{Flu,max}} = 422/448 \text{ nm}$  and  $412/438 \text{ nm}$ , respectively). The change of the type of side chains from alkyl to alkoxy (copolymer **II**) shifts the emission wavelength to the blue/green ( $\lambda_{\text{Flu,max}} = 463/490 \text{ nm}$ ), due to the increased electron density of the  $\pi$ -system induced by the electron-donating alkoxy group. Alkoxy side chains in combination with cyano substituents (copolymer **III**) results in a red shift to the orange part of the spectrum ( $\lambda_{\text{Flu,max}} = 540 \text{ nm}$ ). It has been demonstrated that cyano groups on the vinylene linkage lower both the HOMO and LUMO level, but that the LUMO level is stabilized more, resulting in a red shift [24,25].

If one compares the polymers and models, it appears for copolymer **IV** that there is a striking similarity with the optical properties of model **IV**. The absorbance and fluorescence maxima are slightly red-shifted in comparison with the model, but the Stokes shifts are identical. The red-shift can be readily explained by the weakly electron-donating character of the silylene interruption units. If we compare the copolymers **I-III** with the corresponding models, we must make a distinction between the different types of side chain (octyl or octyloxy). For the octyl-substituted copolymer **I** also a small red-shift is found with respect to the model (see also figure 1.4, page 11). However, for the octyloxy-substituted copolymers **II** and **III**, the shifts are larger. These results can be explained by the steric interactions in the terphenyl part of those polymers. It is known that isolated non-substituted oligophenylenes are non-planar [26], because steric hindrance between protons on adjacent phenyl rings induces a twist between the rings. Molecular modelling calculations showed that this twist is about  $40^\circ$  [27]. In such a situation some overlap of the  $\pi$ -orbitals is still possible, which allows conjugation. When substituents on the rings are present the twist angle will be larger. Hilberer *et al.* [22] performed supplementary calculations on substituted terphenylenes by means of the AM1 semi-empirical quantum chemical method. They found that alkyl-substituted terphenylenes have twist angles between adjacent rings which are significantly shifted to  $90^\circ$ . In the case of the sterically less demanding alkoxy side-chains the twist angle was smaller ( $\approx 50^\circ$ ). These findings suggest that overlap of  $\pi$ -orbitals is significantly diminished in the case of alkoxy substitution and effectively cancelled for alkyl substituents. This means that in the copolymers **I-III** the conjugation is rather effectively interrupted when octyl sidechains are present and to a lesser extent when octyloxy chains are present, which explains why the octyloxy-substituted copolymers show a larger red-shift in comparison with their model compounds. But for all copolymers the width and shape are still similar to those of the models, indicating well-defined optical properties.

The fluorescence quantum yields  $\Phi_{\text{Flu}}$  were measured relative to quinine sulfate ( $\Phi_{\text{Flu}}=0.55$ ) [28]. The experimental inaccuracies lead to an overall error of about 10 – 15 % in the final quantum yields. The fluorescence quantum yields for all compounds

in solution are high (except for structure **III**), and the yields for the copolymers are only slightly reduced in comparison to the corresponding model compounds. All PL-decay curves of the copolymers and models in solution show a single-exponential dependence, except for the cyano-substituted copolymer and oligomer. The reason for the fast decay and low fluorescence quantum yield for this type of compounds will be explained later on in this chapter. Single-exponential decay is more or less expected in dilute solution due to the absence of strong intermolecular interactions. The fluorescence lifetimes (0.7-0.9 ns) of our copolymers are somewhat shorter than those of the model oligomers, but they are significantly longer than that of fully conjugated PPV homopolymers like poly[2-methoxy,5-(2'-ethyl-hexyloxy)-*p*-phenylene vinylene] (MEH-PPV:  $\tau=270$  ps [29],  $\tau=300$  ps [30] and  $\tau=300$  ps [9]). The reason for the longer lifetimes in our copolymers could be that non-radiative decay channels, like exciton diffusion to quenching sites, are efficiently inhibited by the blocking units [6]. In addition, the number of chemical and conformational defects which could lead to quenching, is expected to be less in this type of copolymers.

#### *Solid-state optical properties*

In table 2.2 the solid-state spectroscopic properties of the copolymers are summarized. The photoluminescence measurements were performed on thin (100–300 nm) spincoated films on quartz substrates, under a static vacuum of  $P < 10^{-4}$  mbar, unless otherwise stated. The absorbance and emission spectra for all copolymers are depicted in figure 2.4. For all compounds the absorbance spectra are red-shifted. The red-shift is probably due to the effect of solid-state packing and the change of dielectric environment. For copolymer **I** and **IV**, comparing the spectral position of the absorbance maximum in table 2.2 is rather misleading (in that case a slight blue-shift would be concluded). In fact the spectra of the thin films are significantly more inhomogeneously broadened (probably due to an increase in conformational disorder upon spin-casting) than solution spectra and also for the copolymers **I** and **IV** a red-shift of the low-energy tail is observed. The lowest-energy absorption peaks of **I** (355 nm) and **IV** (352 nm) are significantly blue-shifted in comparison to thin films of a fully conjugated alkyl-substituted PPV homopolymers ( $\lambda_{\text{Abs,max}} = 405$  nm [31]), demonstrating the effective interruption of the conjugation along the backbone.

The same trend (red-shift) was found for the solid-state luminescence spectra. The shift between absorbance and luminescence is generally in the range of 3300 – 6300  $\text{cm}^{-1}$  (0.3-0.6 eV). A part of this shift is attributed to the stabilization of the excited state through a change in molecular geometry (electron-phonon coupling) and migration of the excitation towards low-energy chain segments. Note that the shifts (in  $\text{cm}^{-1}$ ) summarized in table 2.1 and 2.2 are not the exact Stokes shifts but the differences between absorbance and luminescence maximum. The ill-resolved nature of the spectra precludes the straightforward determination of the Stokes shift.

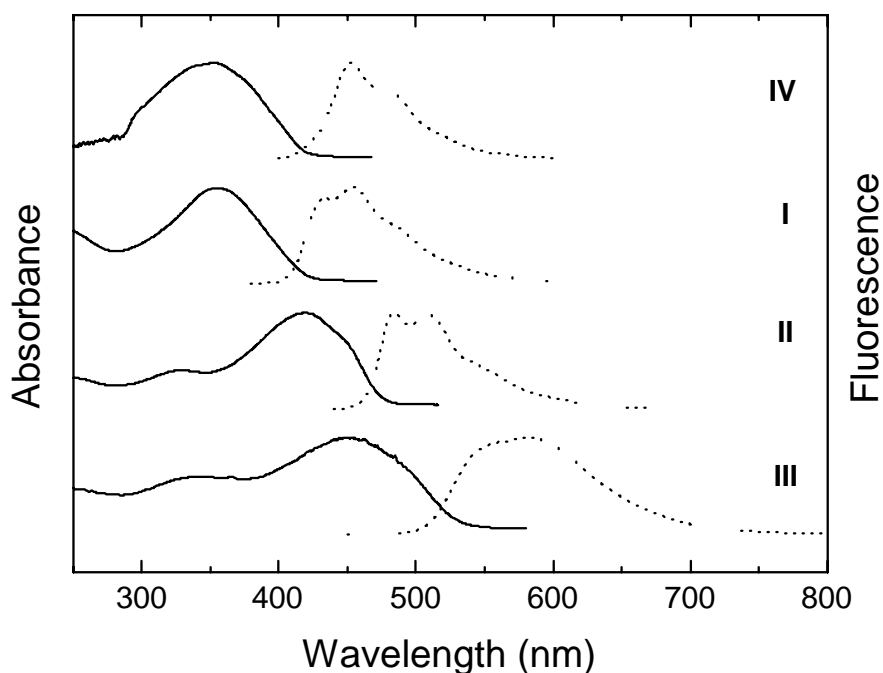


**Figure 2.4** Solid-state absorbance & fluorescence spectra of copolymer I through IV.

The different bands in the luminescence spectra arise from strong coupling of vibrations of the molecular skeleton to the exciton level. The vibronic features are also present in the absorbance spectra but much less pronounced. The enhancement of the vibronic features in the luminescence spectra is usually attributed to the fact that the emission occurs after migration of excitons to chain segments with the lowest energy [32]. So the emission in this case is characterized by the low-energy sites rather than contributions from all chain segments, resulting in a more pronounced spectrum.

If we compare the solid-state PL quantum yields with those obtained from dilute solution we see that the PL efficiencies for the blue-emitting copolymers **I** and **IV** decreased, while the PL lifetimes (both show a single-exponential decay in solution and solid state) are approximately constant, going from solution to solid-state. These observations contradict each other. This apparent difference in PL efficiencies can be attributed to the fact that we compare efficiencies obtained by two different techniques which both have a reasonably large experimental error. Hence, for the blue-light-emitting copolymers we can conclude that the contributions of additional non-radiative decay channels due to interchain interactions in the

condensed state are negligible, resulting in efficient solid-state PL. The situation for copolymers **II** and **III** is totally different. For the cyano-substituted copolymer (**III**) a significant increase in both PL efficiency (0.4) and lifetime ( $\tau_{\text{Flu}}=2.6$  ns) is observed in the solid state. In addition, the luminescence spectrum is significantly broader and the vibronic features are poorly resolved in comparison to the other copolymers. Further on in this chapter we will demonstrate that the PL in copolymer **III** has a different origin, and arises from interchain excitations (excimer/dimer luminescence) rather than intrachain singlet excitons. For copolymer **II** a large decrease in PL efficiency (0.09) and lifetime was observed upon spin-casting. The PL decay showed a double exponential dependence with a fast initial component ( $\tau_{\text{Flu},1} \approx 200$  ps with a pre-exponential weight factor  $a_1 = 0.8$ ) followed by a second component with a lifetime of  $\tau_{\text{Flu},2} \approx 700$  ps. So, in this particular case the contribution from non-radiative decay channels is significant. The exact reason for this is not known. It could be due to a difference in chain packing in comparison to the octyl-substituted copolymers, resulting in interchain interactions, which stimulate efficient non-radiative decay channels. Another possible explanation could be the fact that the conjugation is less effectively broken for the octyloxy-substituted copolymers and exciton migration to quenching sites will be much faster in this case, resulting in a faster PL-decay [33]. Unfortunately, we cannot compare the results with those of copolymer **III**, which also has octyloxy sidechains, due to the different origin of the solid-state luminescence for that polymer.

### Wavelength dependence of the PL decay

The wavelength dependence of photoluminescence decay was measured for our copolymer thin films. In figure 2.5 (right side) a semi-log plot of the luminescence decay curves collected from a copolymer **IV** film at  $\lambda = 420$  nm, 460 nm and 500 nm is depicted. For comparison, the wavelength-dependent PL decay of a converted precursor PPV film is shown on the left side of figure 2.5. It is obvious from the decay curves of the copolymer **IV** film that the PL decay becomes faster at shorter wavelength. However, for the PPV film the PL-decay is independent of the wavelength of emission. The faster PL decay in the blue tail of the emission spectra for copolymer **IV** could arise from exciton diffusion to low energy sites. Bässler *et al.* [32] reported that for fully conjugated PPV, exciton diffusion to lower energy sites (longer conjugated chain segments) takes place at a time-scale of  $< \text{ps}$ . So, exciton diffusion takes place at a time-scale which cannot be resolved with our experimental setup (system response  $\approx 30$  ps). For this reason one would expect that the PL decay is independent on wavelength as displayed in figure 2.5. For the copolymers, the situation could be different due to the fact that we incorporated well-defined potential barriers (the interruption blocks), which can effectively lower the mobility for exciton

migration. The excitons have to pass the barriers by either a tunnelling or hopping process, which can slow down the diffusion process significantly. If diffusion occurs on a time-scale longer than 30 ps, this process acts as a non-radiative decay channel in the blue part of the emission spectrum, resulting in wavelength dependent PL-decay.

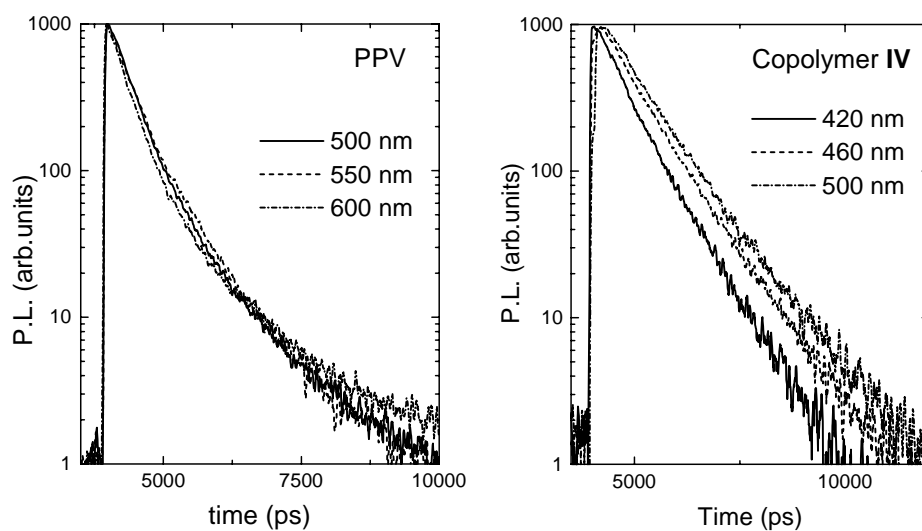


**Figure 2.5** Left: Semi-log plot of the luminescence decay curves collected from a converted precursor PPV film at  $\lambda = 500$  nm, 550 nm and 600 nm. Right: Semi-log plot of the luminescence decay curves collected from a copolymer IV film at  $\lambda = 420$  nm, 460 nm and 500 nm.

### 2.3.2 Oligo(*p*-phenylene vinylene)s

The optical properties of a series of three different five-ring oligo(*p*-phenylene vinylene)s have been studied in solution and solid state. The chemical structures of the OPVs employed for this study are depicted in figure 2.6. The synthesis, characterization and steady-state optical properties of the compounds can be found in reference [34].

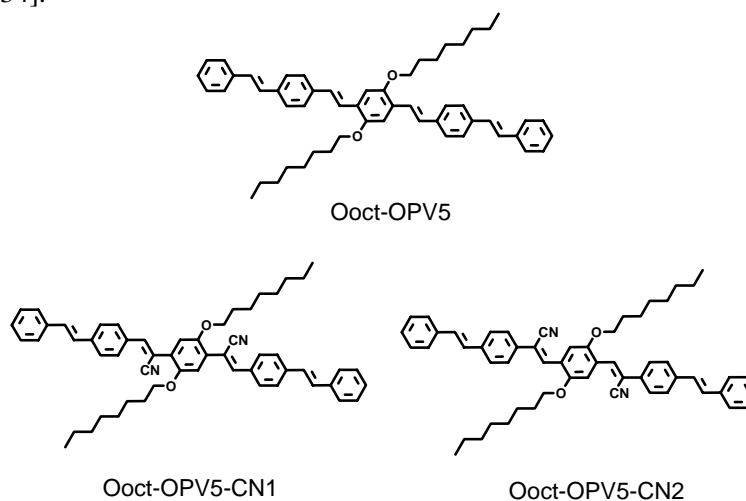


**Figure 2.6** Chemical formulae and abbreviations of the five-ring oligo(*p*-phenylene vinylene)s used in this study.

The series comprises OPVs with octyloxy side chains on the middle ring, which two have cyano substituents on the adjacent central vinylene linkages. Ooct-OPV5-CN1 has the cyano substituents at the *inner* positions of these vinylene linkages, while Ooct-OPV5-CN2 has them on the *outer* positions. All absorption and emission properties of the oligo(*p*-phenylene vinylene)s in solution (chloroform) are summarized in table 2.3 on the next page. For Ooct-OPV5 and Ooct-OPV5-CN2, the spectroscopic properties in solution are similar to those reported for small conjugated molecules. The PL efficiencies are high (0.7-0.9) and the PL time-decay curves are single-exponential corresponding to lifetimes around 1 ns. These values are similar to those reported for other substituted 5-ring PPV oligomers [35]. For both oligomers the emission spectra show pronounced vibronic features. The absorbance and emission spectra for Ooct-OPV5-CN2 are red-shifted with respect to Ooct-OPV5, which can be explained by the influence of the electron-accepting cyano group on the electronic structure of the molecule. However, in the case of Ooct-OPV5-CN1, the fluorescence quantum yield is extremely low (0.04) in combination with a fast double-exponential PL-decay, indicating an efficient non-radiative decay channel.

**Table 2.3 Absorption and emission properties of the five-ring oligo(*p*-phenylene vinylene)s in chloroform solution.**

Compound	Absorption		Fluorescence			
	$\lambda_{\text{Abs,max}}$ (nm) <sup>(a)</sup>	$\lambda_{\text{Flu,max}}$ (nm) <sup>(a)</sup>	Shift (cm <sup>-1</sup> ) <sup>(b)</sup>	$\Phi_{\text{Flu}}$	$\tau_{\text{Flu,1}}$ (ns) <sup>(c)</sup>	$\tau_{\text{Flu,2}}$ (ns)
Ooct-OPV5	422	<u>483</u> , 513	3000, <u>4200</u>	0.9	1.2	
Ooct-OPV5-CN1	<u>360</u> , 400	502	<u>7900</u> , 5100	0.04	0.08	1.3
Ooct-OPV5-CN2	453	<u>536</u> , 568	<u>3400</u> , 4500	0.7	1.4	

a) taken from reference [37]. b) The shift is defined here as the difference between  $\lambda_{\text{Abs,max}}$  and  $\lambda_{\text{Flu,max}}$ , the underlined values are the absolute fluorescence maxima. c) PL-decays were measured at the wavelength of the PL maximum.

**Table 2.4 Solid-state absorption and emission properties of oligo(*p*-phenylene vinylene) thin films and single crystals.**

Compound	Absorption		Fluorescence			
	$\lambda_{\text{Abs,max}}$ (nm)	$\lambda_{\text{Flu,max}}$ (nm)	Shift (cm <sup>-1</sup> ) <sup>(a)</sup>	$\Phi_{\text{Flu}}$	$\tau_{\text{Flu,1}}$ (ns) <sup>(b)</sup>	$\tau_{\text{Flu,2}}$ (ns)
Ooct-OPV5	Single crystal	- <sup>(c)</sup>	-	0.5	1.0	
	As-deposited	442	<u>539</u> , 563	0.5	1.1	
	Annealed	442	539	3700, 4100	0.7	1.7
Ooct-OPV5-CN1	Single crystal	-	560	0.4	2.2	
Ooct-OPV5-CN2	Single crystal	-	630	0.5	8.0	
	As-deposited	468	<u>609</u>	0.4	1.3	7.0
	Annealed	475	615	4800	0.6	3.4

a) The shift is defined here as the difference between  $\lambda_{\text{Abs,max}}$  and  $\lambda_{\text{Flu,max}}$ , the underlined values are the absolute fluorescence maxima. b) PL-decays were measured at the wavelength of the PL maximum. c) No absorption spectra could be measured for the single crystals, O.D. too high.

The absorbance spectrum of Ooct-OPV5-CN1 is blue-shifted with respect to Ooct-OPV5, and its emission spectrum is broad and featureless. The blue-shift of Ooct-OPV5-CN1 in chloroform in comparison to Ooct-OPV5-CN2 suggests that the former is less planar in the ground state, while the broad and featureless PL spectrum likely indicates that a relaxed excited state is not reached upon photoexcitation. To constrain the degree of freedom of the oligomers, dilute blends with polysulfone as transparent host-matrix were prepared. In figure 2.7 the PL decay curves for CN1 and CN2 in both chloroform and polysulfone are depicted and the PL spectra of Ooct-OPV5-CN1 in chloroform and polysulfone.

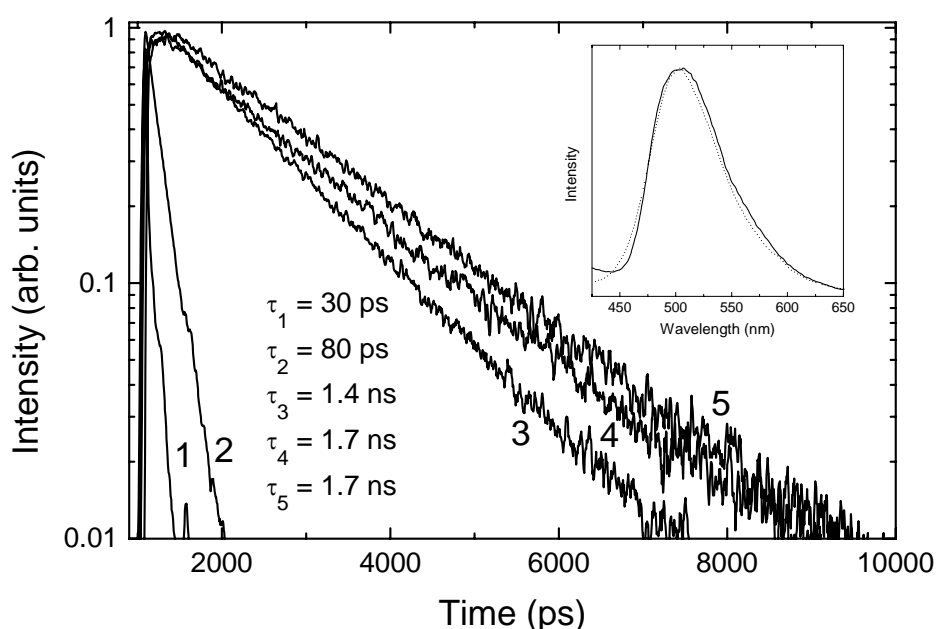


**Figure 2.7** PL decay curves of cyano-substituted PPV oligomers (1) System response (2) Ooct-OPV5-CN1 in  $\text{CHCl}_3$  (3) Ooct-OPV5-CN2 in  $\text{CHCl}_3$  (4) Ooct-OPV5-CN2 in polysulfone (5) Ooct-OPV5-CN1 in polysulfone. Inset right: PL spectra of Ooct-OPV5-CN1 in chloroform (solid line) and polysulfone (dotted line).

From the identical shape and position of the absorbance (not shown) and photoluminescence spectra in chloroform and polysulfone we conclude that the distribution of molecular geometries of the CN1 oligomers is the same in both situations. As can be seen from figure 2.7, a fast decay is observed for CN1 in chloroform ( $\tau=80$  ps). In polysulfone the non-radiative decay channel is effectively inhibited and a normal single exponential decay with a time constant of 1.7 ns is seen

however. From these measurements we can conclude that the efficient non-radiative decay channel observed for CN1 in solution is connected with the extend of conformational freedom it possesses in the surrounding medium. Restriction of the molecular motion reduces the efficiency of the non-radiative decay pathway, severely.

For CN2 the decay curves in solution and the solid polysulfone matrix do not differ much (1.4 and 1.7 ns, respectively). These results indicate that the conformational freedom is somehow associated with the position of the cyano substituents on the oligomer backbone. The slight increase in the PL-lifetime of CN2 going from solution to the solid state may also be attributed to the same effect, which is probably general for all PPVs. It is not possible at this moment to specify the exact degree of freedom responsible for the fast non-radiative decay channel. It could possibly be associated with a twisting or bending motion. An elegant illustration to visualize how the relaxation processes for Oct-OPV-CN1 may look like is depicted in figure 2.8. In this figure the potential energy surfaces of the ground and excited state associated with the *cis-trans* isomerization of *cis*-stilbene are shown [36] as an example.

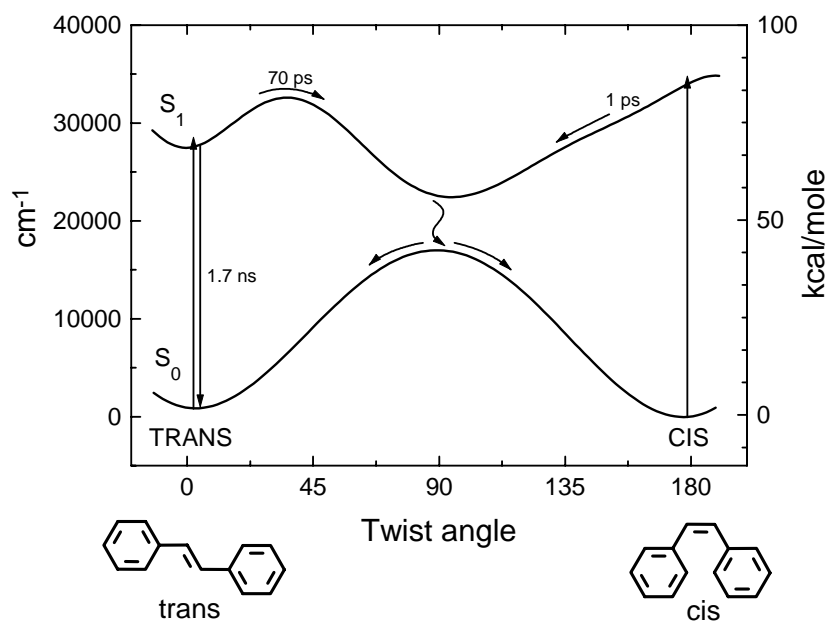


**Figure 2.8** One-dimensional representation of the ground- and excited-state potential surfaces for *trans*- and *cis*-stilbene, from reference [36].

If we adapt this picture to our situation, it is clear that the coordinate (for stilbene: the twisting angle) in our case is not known, it could well be multidimensional. If we now associate the right-hand side of the plot to the situation in solution, we see that after

optical excitation the molecule moves from the Frank-Condon region of the  $S_1$  surface to a twisted geometry along the potential surface with either no or a small barrier. In the twisted region, non-radiative relaxation to the ground-state is very rapid. For the situation where the molecules are dispersed into a solid matrix, the ground and excited state potential surfaces look different from the ones displayed in figure 2.8. The constraint on the twisting motion in this case will favour a normal radiative relaxation process. The emission spectrum (inset figure 2.7) for CN1 remains broad and featureless upon changing the matrix from chloroform to polysulfone; this is probably due to the fact that we excite a large distribution of rotamers with different non-planar geometries.

For copolymer **III** we see a similar behaviour as displayed by Ooct-OPV5-CN1. In solution a fast double-exponential decay was found, while in a polysulfone matrix single-exponential decay with a time-constant of 1.7 ns was observed. We attribute this behaviour to the same phenomena.

#### *Single crystals*

From all three octyloxy-substituted oligo(*p*-phenylene vinylene)s needle-shaped single crystals could be obtained by crystallization from solution. Ooct-OPV5 was crystallized from a THF/methanol mixture and the cyano-substituted derivatives from a chloroform/*n*-hexane mixture.

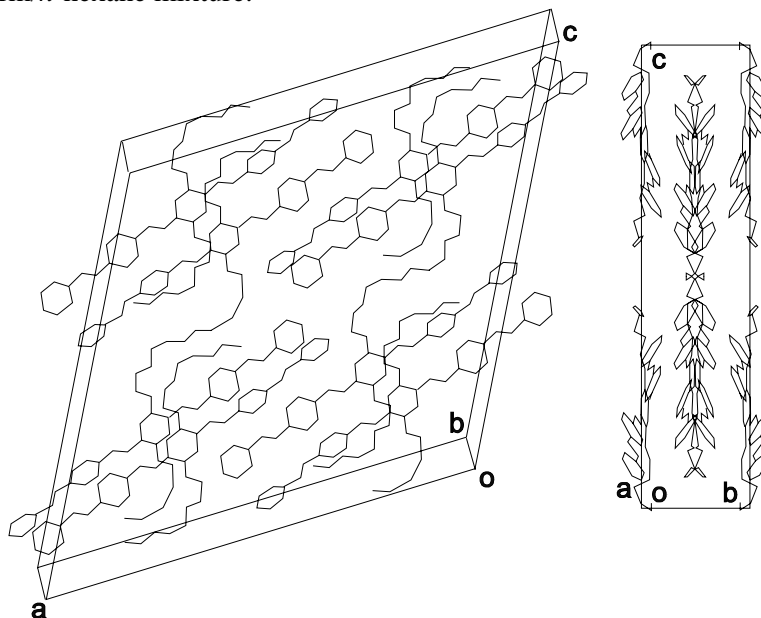


**Figure 2.9** Molecular packing of Ooct-OPV5 in the unit cell. Left: oblique view of the unit cell of Ooct-OPV5 perpendicular to the (*ac*) plane. Right: projection of the unit cell on the (*bc*) plane (*c*-axis vertical). From reference [34].

The structure of all three oligomers has been resolved by X-ray crystallography [34,37,38]. For a detailed description of the experimental procedure and crystallographic data, see reference [34]. For Ooct-OPV5 the unit cell is monoclinic, space group  $I2/a$ , and contains eight discrete molecules separated by normal van der Waals distances. The representation of the unit cell in figure 2.9 shows that the conjugated backbones lie parallel to each other, lined up in strings along the  $a$ -axis and separated along the  $c$ -axis by a layer accommodating the aliphatic side-chains. Although the phenyl rings are not “ $\pi$ -stacked”, the molecules are nonetheless contained in layers parallel to the (010) plane. The interlayer distance is  $b/2 = 3.77 \text{ \AA}$ , which is indeed larger than the typical values for  $\pi$ -stacking, 3.3 - 3.4  $\text{\AA}$  [39].

For both cyano-substituted oligomers, the unit cell was defined as triclinic, space group  $P-1$ , containing one discrete molecule. For Ooct-OPV5-CN1 the molecules have a remarkable, “wave-like” shape, which involves deviations from planarity of the vinylene moieties as well as the rings (see figure 2.10). The bending is the strongest for the vinylene moieties. Such distortions indicate the presence of considerable packing forces. This is corroborated by the value of the crystal density,  $1.210 \text{ g.cm}^{-3}$ , which is almost 10 % higher than that of the monoclinic crystalline phase of Ooct-OPV5 ( $1.107 \text{ g.cm}^{-3}$ ). The introduction of the cyano groups has obviously strongly enhanced the intermolecular interaction, resulting in a dense packing of the molecules (see figure 2.10). However, no  $\pi$ - $\pi$  interactions are expected, since the phenyl rings are both laterally and axially shifted and as a result there is no overlap of the aromatic backbone. The axial shift, approximately half the length of a styryl-unit, is an essential aspect, since it serves to bring the nitrogen atom of the cyano group above the center of the middle phenyl ring of the neighbor molecule. This is attributed to a strong Coulombic interaction between the two: the cyano group bears a negative charge while the central phenyl ring is positively charged due to its octyloxy substituents (from AM1 quantum-chemical calculations: -0.15 and +0.07 electron units, respectively [34]). There is a distinct out-of-plane bending of the cyano group, which brings the nitrogen atom at a distance of only 3.3  $\text{\AA}$  above the ring. Remarkably, Conwell *et al.* [40,41] found the same distance for the nitrogen atom in a cyano-PPV polymer. They determine the lowest energy configuration by a Monte Carlo simulation for a layer of cyano-PPV homopolymer, consisting of 5 face-to-face segments, each with three phenyl rings ( $1/2$  repeat unit). In the lowest-energy configuration, the cyano group in one chain overlapped the edge of a phenyl ring in the nearest-neighbor chain.

For Ooct-OPV5-CN2, which has its cyano substituents at the *outer*-position of the central vinylene linkages, the situation is different and significant  $\pi$ - $\pi$  interactions

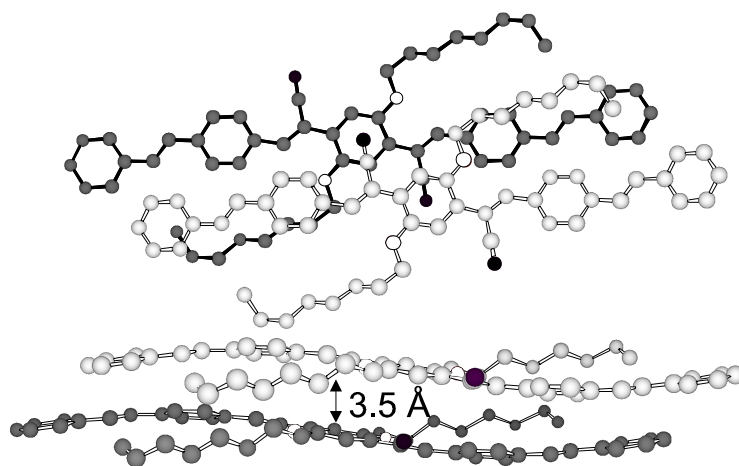


**Figure 2.10** Top-view (top) and side-view (bottom) of two nearest-neighbour Ooct-OPV-CN1 molecules in the unit cell. Atom colors: light and dark gray: carbon atoms of the front and rear molecule respectively; white: oxygen atoms; black: nitrogen atoms. The distance corresponds to the shortest distance measured between the atoms of two neighbour molecules in perpendicular direction.

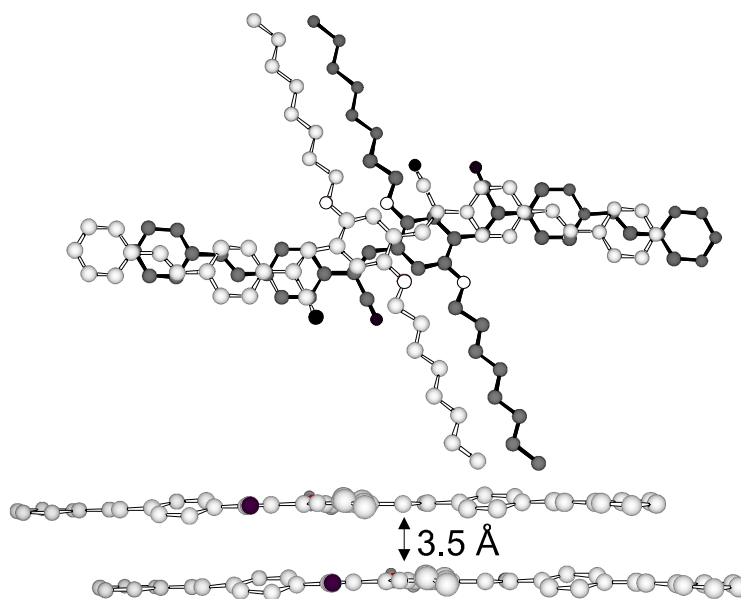


**Figure 2.11** Top-view (top) and side-view (bottom) of two nearest-neighbour Ooct-OPV-CN2 molecules in the unit cell. Atom colors: light and dark gray: carbon atoms of the front and rear molecule respectively; white: oxygen atoms; black: nitrogen atoms.

are possible between neighbouring molecules. As can be seen from figure 2.11, the nearest neighbour molecules, which are separated by a distance of approximately 3.5 Å, exhibit only an axial displacement of approximately one phenyl ring (half a repeat unit), resulting in strong overlap of the aromatic backbones. The CN2 molecules do not display the “wave-like” shape as observed for the CN1 molecules, and appear to be almost flat with the octyloxy chains extended nearly perpendicular to the molecular axis, in the plane of the aromatic backbone.

For the three octyloxy-substituted oligomers the normalized photoluminescence spectra are depicted in figure 2.12. Ooct-OPV5 and Ooct-OPV5-CN1 the optical properties of the single crystal. Due to the large absorption coefficient (more than  $10^5 \text{ cm}^{-1}$  in maximum) we were not able to measure the absorbance spectra of relatively thick (20 - 30  $\mu\text{m}$ ) single crystals.

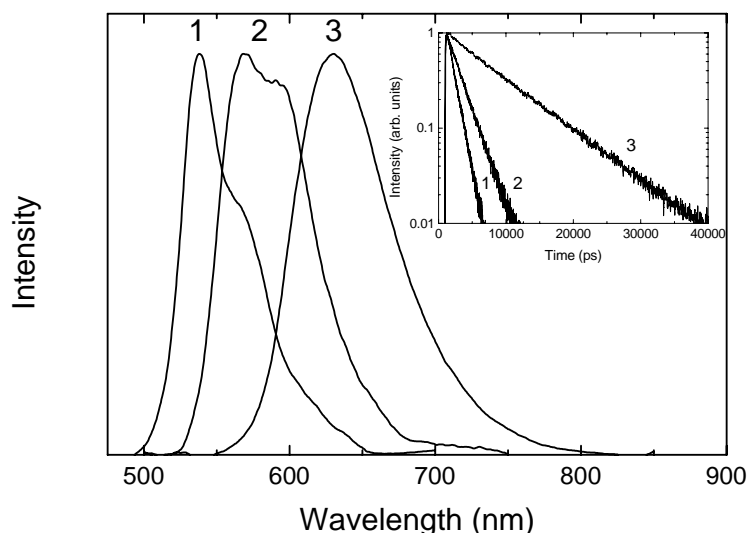


**Figure 2.12** Normalized photoluminescence spectra of (1) Ooct-OPV5, (2) Ooct-OPV5-CN1 and (3) Ooct-OPV5-CN2 single crystals. Inset top-right: corresponding PL decay curves (semi-log plot).

For Ooct-OPV5 and Ooct-OPV5-CN1 the PL spectra (figure 2.12) show reasonably pronounced vibrational structure similar to that of a free single molecule. In addition, the estimated natural radiative lifetimes (based on  $\Phi_{\text{Flu}}$  and  $\tau_{\text{Flu}}$ , table 2.4) for the oligomer single crystals, 2 and 5.5 ns respectively, are typical values reported for small organic dyes. The observation of luminescence originating from an intramolecular excitation for both oligomers, agrees with the conclusions drawn on the

basis of the molecular packing of the single crystal. For both oligomers no significant  $\pi$ - $\pi$  interactions were expected on the basis of the crystal structure.

From the molecular organization within the Ooct-OPV5-CN2 single-crystals it became clear that significant  $\pi$ - $\pi$  interactions can be expected between neighboring molecules in the crystal lattice. This is reflected in the emission properties of the Ooct-OPV5-CN2 single crystals, which differ significantly from those of the two others. The CN2 single-crystal luminescence spectrum is broad and featureless and red-shifted in comparison to that of its chemical isomer Ooct-OPV5-CN1. Secondly, the estimated natural radiative lifetime,  $\approx 16$  ns, is significantly longer. The behaviour is similar to that reported by Samuels et al. [14] for cyano-PPV films, which they attributed to either excimer or dimer luminescence originating from interchain excitations. An excimer is a pair of identical planar molecules in a cofacial arrangement whose interaction is repulsive in the ground state but attractive if one of the molecules is excited. A situation which occurs when the molecules are separated between roughly 3 and 4 Å [39,42]. In this situation the  $\pi$ -orbitals of the molecules can overlap, allowing delocalization of the electrons over more than one molecule. In the case of polymers, the excimer is thought to be formed by coplanar conjugated chain segments of two or more polymer chains, which are parallel to each other separated by a distance of presumably less than 4 Å to allow  $\pi$ -orbital overlap. To illustrate the excimer formation, a sketch of the potential energy surfaces as function of intermolecular separation is given in figure 2.13.

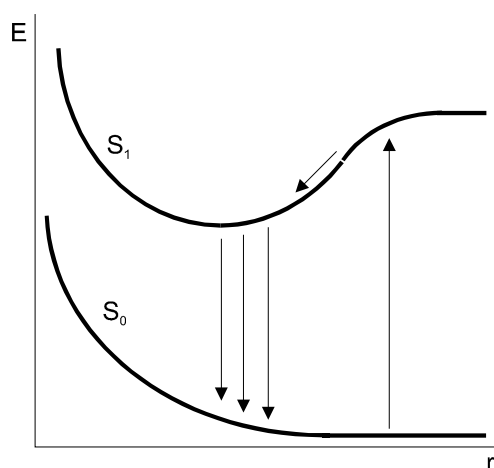


**Figure 2.13** Potential energy surface as a function of intermolecular separation. From reference [42].

From this sketch the red-shift and the absence of vibronic features for an excimer is obvious. Another characteristic of an excimer is a long radiative lifetime, because the transition is usually forbidden by symmetry.

Sometimes it is difficult to distinguish between an excimer and a physical dimer/aggregate, because both can give rise to the above-mentioned emission behaviour. Only in the latter case the interacting molecules also have a stable ground state. This should result in the appearance of an additional absorption band. It is difficult to identify this additional absorption band, because it is usually fully masked by the inhomogeneously broadened absorbance spectra.

For copolymer **III** we have found similar behaviour as displayed by the Oct-OPV5-CN2 single crystals and the cyano-PPV reported by Samuels *et al.* [14]. An appreciable red-shift of the absorbance (20 nm) and luminescence spectra (50 nm) going from solution to the solid state, a broad and featureless luminescence spectrum and a relatively long PL lifetime of 2.6 ns in comparison with the other copolymers. The estimated natural radiative lifetime of 6.5 ns, for the copolymer, is relatively short in comparison to the 16 ns reported for cyano-PPV [14]. The possible reasons for the difference in PL lifetime could be the intermolecular distance or displacement (axial or lateral displacement of the chain segments), which determine the magnitude of  $\pi$ -orbital overlap, or the degree of symmetry of the interacting chain segments. For instance, the symmetry of the ensemble of interacting molecules or chain segments can be lower if the molecules are not parallel to each other but slightly tilted. This will influence the emission probability and can result in a faster PL decay.

#### *Vacuum-deposited oligomer thin films*

As already mentioned in chapter 1 it is also possible to process the oligomers into high-purity thin films via vacuum deposition. Oligo(*p*-phenylene vinylene) thin films were prepared by slow evaporation (pressure  $\approx 10^{-6}$  mbar, evaporation rate 2-4 Å/s) of the compounds from a molybdenum boat just above their melting point, with the quartz substrates positioned about 10 cm above the boat. A Dektak 3030ST surface profiler was used to determine the layer thickness. All oligomers gave pin-hole free polycrystalline layers, showing a granular structure when observed under the optical microscope (crossed polarizers), indicating the films to be at least to some extent crystalline. All oligomers showed liquid-crystalline behaviour, which is attributed to the combination of long aliphatic side-chains and the rigid-rod *trans p*-phenylene vinylene backbone, which can act as a mesogenic unit. Similar behaviour has been observed for side-chain-substituted PPV homopolymers [43]. Gill [34] showed that annealing the oligomer thin films below the first melting point (crystal-mesophase transition) resulted in a recrystallization of the films. X-ray diffraction studies of the films clearly indicated an enhanced molecular orientation upon annealing.

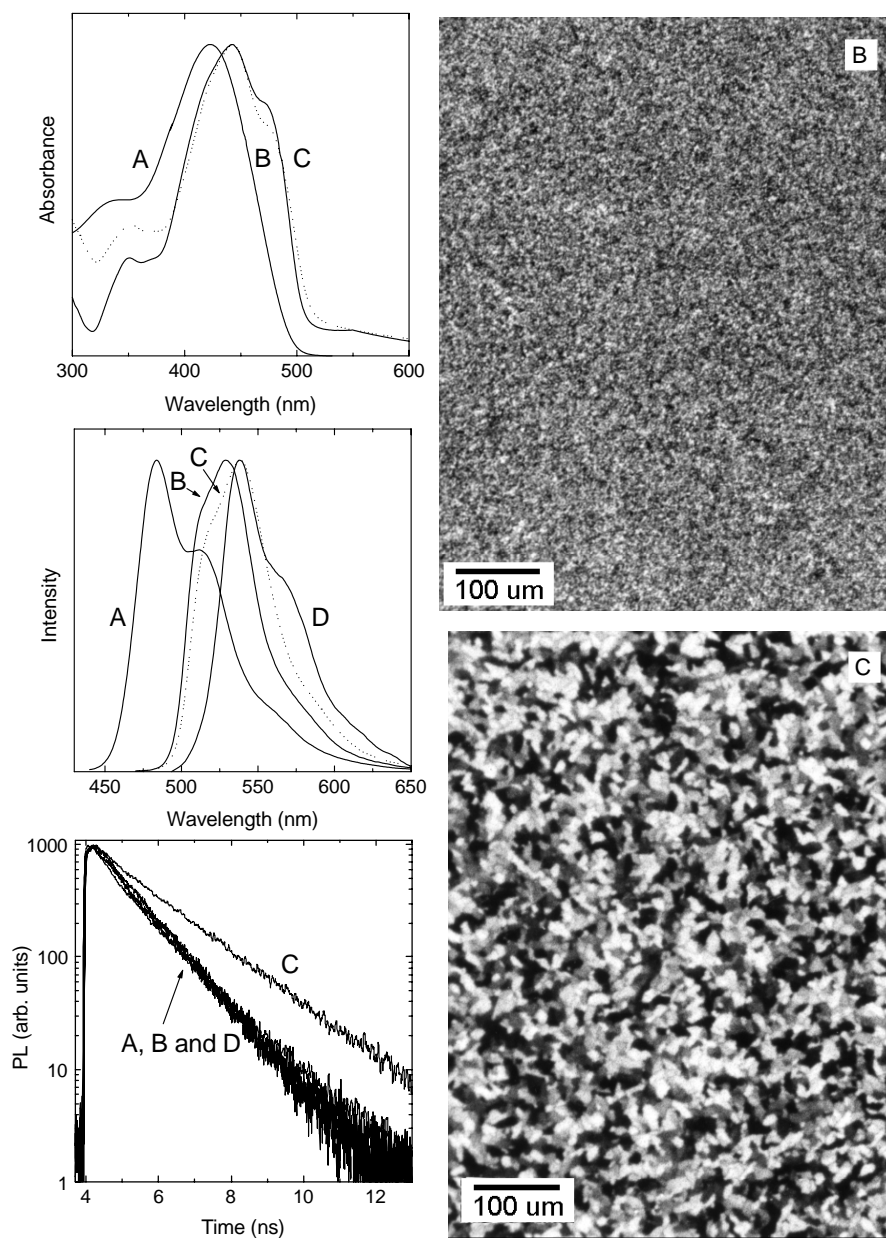


**Figure 2.14** Absorbance and emission spectra and PL-decay of Ooct-OPV5 in (A) solution, (B) as-deposited film, (C) annealed film (120 °C, 5 min) and (D) single crystal. Right: polarized light micrographs of the two thin-film morphologies.

For Ooct-OPV5 and Ooct-OPV5-CN2 we will discuss the optical properties of the as-deposited and annealed films in more detail and compare them with the optical properties of solutions and the single crystals.

### *Ooct-OPV5*

The absorbance and emission spectra and PL-decay of Ooct-OPV5 in (A) solution, (B) as-deposited film, (C) annealed film and (D) single crystal are shown in figure 2.14, as are optical micrographs of the as-deposited and annealed Ooct-OPV5 films. Heating the film at 120 °C for 5 minutes resulted in an increase of the domain size from a few  $\mu\text{m}$  to approximately 20  $\mu\text{m}$ . The individual domains of the annealed films appeared to be highly birefringent when observed under crossed polarizers. An X-ray diffraction study of the films showed that the lattice period changed upon annealing and is in any case smaller than that of the single crystal (16.34 Å): as-deposited film 14.9 Å, annealed film 15.05 Å. The existence of various crystalline forms can be explained by the compressibility of the aliphatic layer between the conjugated backbones, resulting in a deformability of the unit cell. This deformation is reflected in an adjustment of the *c*-axis and/or monoclinic angle. In figure 2.15 a schematic representation of the molecular orientation of the annealed film of Ooct-OPV5 on glass is shown, as proposed by Gill [34].

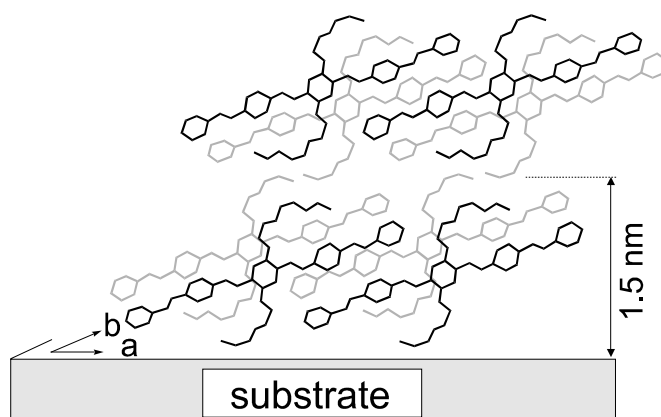


**Figure 2.15** Schematic representation of one unit cell of Ooct-OPV5 on a glass substrate, showing two adjacent rows of oligomers. From ref [34].

All PL spectra show reasonably pronounced vibrational structure similar to that of free single molecule. The apparent absence of a band in luminescence spectrum from the single crystal around 500 nm is likely due to self-absorption. Unlike the luminescence from evaporated films the luminescence from the single crystals was strongly

polarized along the molecule's long axis with a dichroic ratio around 12, corresponding to that of an oriented Ooct-OPV5 thin film [44]. The red shift in both luminescence and absorbance spectra with the increase in crystallinity size and crystalline fraction is evident. The increase in the intramolecular order (transition from the as-deposited film to single crystal) may result in two effects. First, oligomers are almost planar in the crystalline phase, while they may be twisted in the disordered phase resulting in a shorter effective conjugation length [45]. Secondly, the coupling between the molecular transition dipoles in the close-packed organization of the crystal leads to splitting of the energy levels. In the simplest case of a dimer with coplanar inclined transition dipoles, a decrease in the shift angle results in a red shift of the lowest dipole-allowed electron transition with respect to that in a monomer [46]. According to X-ray data, the shift angle of the single crystal is approximately 45 degrees, indicating that such a mechanism of transition energy lowering is possible. Both these effects contribute to the red shift, but their relative importance is not clear.

It is obvious from figure 2.14 that for Ooct-OPV5 in solution, the as-deposited film and the single crystal, the PL lifetimes are approximately the same, around 1–1.2 ns. However, for the annealed film a significantly longer PL lifetime of 1.7 ns was observed. The PL quantum yield of the films increased from 0.5 to approximately 0.7 upon annealing, which agrees with the observed longer PL lifetime. The exact reason for the longer lifetime is currently not known.

#### *Ooct-OPV5-CN2*

The absorbance and emission spectra and PL-decay of Ooct-OPV5-CN2 in (A) solution, (B) as deposited film, (C) annealed film and (D) single crystal, are shown in figure 2.16, along with optical micrographs of the as-deposited and annealed Ooct-OPV5-CN2 films. Heating an as-deposited film at 160 °C for 5 minutes resulted in the formation of small needle-like crystallites, suggesting an enhanced molecular orientation and increase of the crystalline fraction upon annealing. X-ray diffraction (XRD) studies to get more insight in the molecular structure of the different thin-film morphologies are currently in progress. The first preliminary XRD result showed that the as-deposited films are poorly crystalline, while annealing the film indeed results in an increase of the number of reflections in the XRD-pattern, which shows that a higher degree of orientation is obtained.

In the emission spectra we see an apparent gradual transition from single molecule luminescence to excimer luminescence associated with the Ooct-OPV5-CN2 crystal lattice going from solution to the single crystal. Apparently, the as-deposited and annealed films represent an intermediate state, with contributions from both a disordered (amorphous) and an ordered (crystalline) morphology.

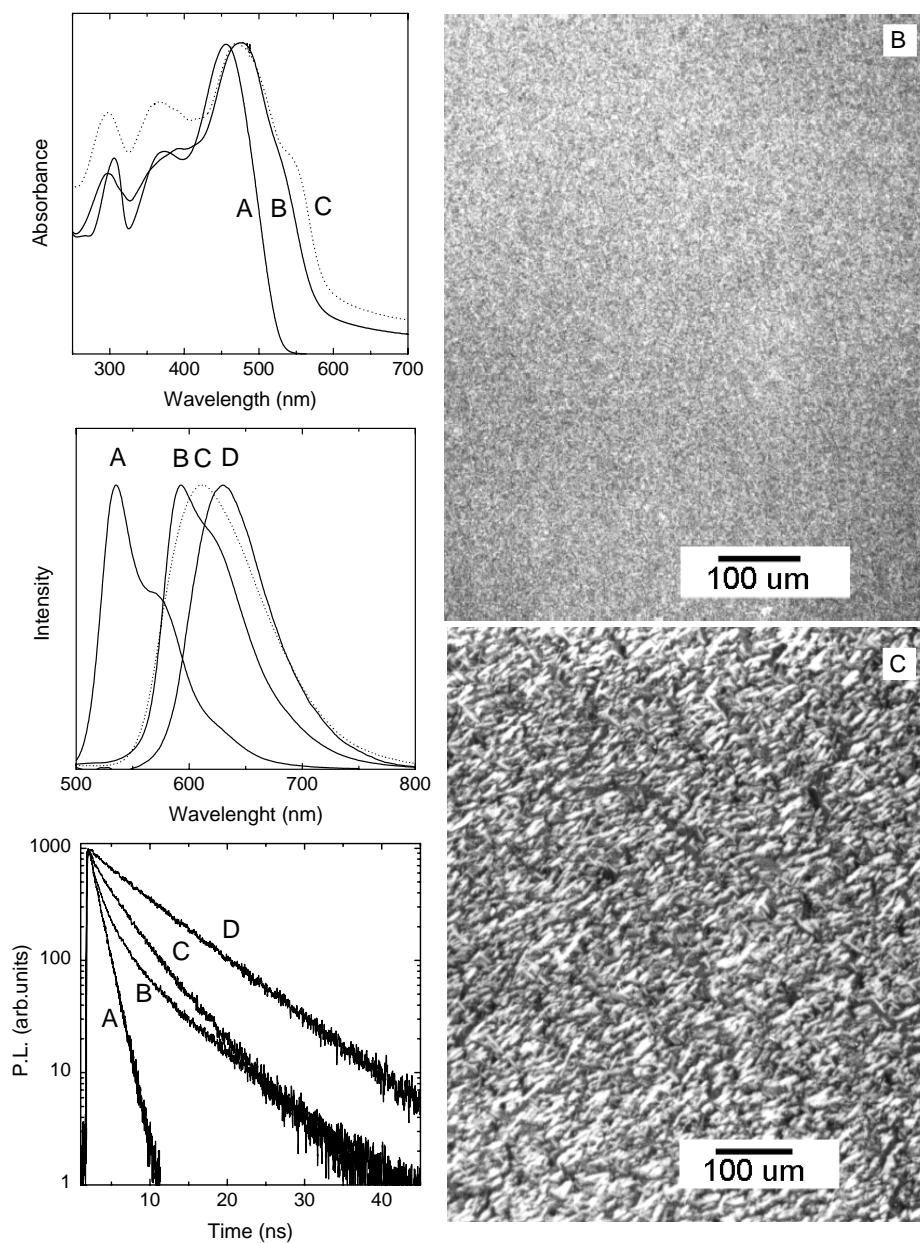


**Figure 2.16** Absorbance and emission spectra and PL-decay of Ooct-OPV5-CN2 in (A) solution, (B) as-deposited film, (C) annealed film (160 °C, 5 min) and (D) single crystal. Right: polarized light micrographs of the two thin-film morphologies.

The PL spectrum of the as-deposited film (B) shows pronounced vibrational features, common for single-molecule luminescence, indicating that the contribution from the amorphous fraction is more dominant. For the annealed film (C), a broad and featureless composite spectrum is observed, due to a larger contribution from the crystalline fraction. From the absorbance spectra of the thin films it is obvious that the low-energy shoulder is red-shifted and slightly more pronounced for the annealed film. The absorbance from the crystalline phase is less inhomogeneous broadened and the molecules have a more coplanar geometry, resulting in a red-shift. Note that the absorbance spectrum of the solution-grown single crystal is absent, due to the high absorption coefficient we were not able to measure the absorbance spectrum for the relatively thick single crystals.

The disorder-to-order transition is also clearly reflected in the time-resolved PL decay curves. For Ooct-OPV5-CN2 in solution and the single crystal, single-exponential decay curves were observed corresponding to PL lifetimes of 1.4 and 8 ns, respectively. They are representing the two extremes: single-molecule and excimer luminescence. However, the PL-decay curves for the as-deposited and annealed films show double-exponential dependencies with lifetimes of 1.5/7.0 ns ( $\tau_1/\tau_2$ ) and 3.4/8.0 ns, respectively. This shows that the contribution of the fast decay associated with single-molecule luminescence decreases upon annealing, which is in agreement with the observed increase of the crystalline fraction upon annealing.

## 2.4 Conclusions

In this chapter, the optical properties in solution and solid state for a series of well-defined alternating PPV copolymers and all-*trans* 5-ring oligo(*p*-phenylene vinylene)s were evaluated. The optical properties of the copolymers in dilute solution were similar to those of the distyrylbenzene model oligomers representing the chromophores in the polymer backbone, indicating that the conjugation is effectively interrupted in the copolymers. For the blue-light-emitting alternating copolymers the photoluminescence (PL) efficiency and lifetime did not significantly change going from solution to the solid-state, indicating that the contribution from additional non-radiative decay channels due to interchain interactions in the condensed state is negligible, resulting in efficient solid-state PL.

For both the cyano-substituted copolymer and Ooct-OPV5-CN1, a fast double exponential PL decay was measured in dilute solution, which is the result of a fast non-radiative relaxation pathway associated with the cyano substituents on the vinylene linkages. Restricting the molecular motion by dispersing the oligomer in a solid polysulfone matrix resulted in an effective inhibition of the non-radiative decay channel and a much longer single-exponential PL decay with a time constant of 1.7 ns. Remarkably, for Ooct-OPV5-CN2 in solution this effect was not so strong.

A reasonably long PL-decay with a PL lifetime of 1.4 ns was measured, which indicates that the position of the cyano moieties on the vinylene bonds is an important parameter, governing this fast non-radiative decay pathway.

For the Oct-OPV5-CN2 single crystals, the PL spectrum was broad and featureless and a long PL lifetime of 8 ns was measured. The long-lived luminescence is attributed to excimer emission. This is positively confirmed by X-ray diffraction data of the single crystal. On the basis of the packing of the molecules in the crystal lattice, significant  $\pi$ - $\pi$  interactions between adjacent (face-to-face) molecules are to be expected. Also in the case of the cyano-substituted copolymer there is evidence that the luminescence originates from eximers, but though the characteristic features are less pronounced as observed for Oct-OPV5-CN2 and cyano-PPV homopolymers [14].

## 2.5 References

- [1] R.H. Friend, D.D.C. Bradley, P.D. Townsend, *J. Phys. D.*, **20**, 1367 (1987)
- [2] N.F. Colaneri, D.D.C. Bradley, R.H. Friend, P.L. Burn, A.B. Holmes, C.W. Spangler, *Phys. Rev. B*, **42**, 11670 (1990)
- [3] U. Rauscher, H. Bässler, D.D.C. Bradley, M. Hennecke, *Phys. Rev. B*, 9830 (1990)
- [4] R. Kersting, U. Lemmer, R.F. Mahrt, K. Leo, H. Kurz, H. Bässler, E.O. Göbel, *Phys. Rev. Lett.*, **70**, 3820 (1993)
- [5] U. Lemmer, R.F. Mahrt, Y. Wada, A. Greiner, H. Bässler, E.O. Göbel, *Chem. Phys. Lett.*, **209**, 243 (1993)
- [6] I.D.W. Samuels, B. Crystall, G. Rumbles, P.L. Burn, A.B. Holmes, R.H. Friend, *Synth. Met.*, **54**, 281 (1993)
- [7] A.R. Brown, K. Pichler, N.C. Greenham, D.D.C. Bradley, R.H. Friend, A.B. Holmes, *Chem. Phys. Lett.*, **210**, 61 (1993)
- [8] J. Leng, S. Jeglinski, X. Wei, R. Benner, Z.V. Vardeny, *Phys. Rev. Lett.*, **72**, 156 (1994)
- [9] M. Yan, L.J. Rothberg, E.W. Knock, T.M. Miller, *Phys. Rev. Lett.*, **75**, 1992 (1995)
- [10] W. Graupner, G. Leising, G. Lanzani, M. Nisoli, S de Silvestri, U. Scherf, *Phys. Rev. Lett.*, **76**, 847 (1996)
- [11] N.T. Harrison, G.R. Hayes, R.T. Phillips, R.H. Friend, *Phys. Rev. Lett.*, **77**, 1881 (1996)
- [12] S.J. Strickler, R.A. Berg, *J. Phys. Chem.*, **37**, 814 (1962)
- [13] M. Yan, L.J. Rothberg, F. Papadimitrakopoulos, M.E. Galvin, T.M. Miller, *Phys. Rev. Lett.*, **72**, 1104 (1994)
- [14] I.D.W. Samuels, G. Rumbles, C.J. Collison, *Phys. Rev. B Rapid Comm.*, **52**, R11573 (1995)
- [15] E.M. Conwell, H.A. Mizes, *Phys. Rev. B*, **51**, 6953 (1995)
- [16] N.C. Greenham, I.D.W. Samuel, G.R. Hayes, R.T. Phillips, Y.A.R.R. Kessener, S.C. Moratti, A.B. Holmes, R.H. Friend, *Chem. Phys. Lett.*, **241**, 89 (1995)

- [17] R.H. Friend, G.J. Denton, J.J.M. Halls, N.T. Harrison, A.B. Holmes, A. Köhler, A. Lux, S.C. Moratti, K. Pichler, N. Tessler, K. Towns, H.F. Wittmann, *Solid State Commun.*, **102**, 249 (1997)
- [18] I.D.W. Samuels, G. Rumbles, C.J. Collison, R.H. Friend, S.C. Moratti, A.B. Holmes, *Synth. Met.*, **84**, 497 (1997)
- [19] L.M. Bollinger, G.E. Thomas, *Rev. Sci. Instrum.*, **32**, 1044 (1961)
- [20] J.R. Lakowicz, Topics in fluorescence spectroscopy, volume 1: techniques (Plenum press, New York, 1991), chapter 1
- [21] J.C. de Mello, H.F. Wittmann, R.H. Friend, *Adv. Mater.*, **9**, 230 (1997)
- [22] A. Hilberer, P.F. van Hutten, J. Wildeman, G. Hadziioannou, *Macromol. Chem. Phys.*, **198**, 2211 (1997)
- [23] M.P.L. Werts, Synthesis of cyano-substituted PPV-polymers for LEDs (undergraduate report, University of Groningen, 1996)
- [24] N.C. Greenham, S.C. Moratti, D.D.C. Bradley, R.H. Friend and A.B. Holmes, *Nature*, **365**, 628 (1993)
- [25] J.L. Brédas, *Adv. Mater.*, **7**, 264 (1995)
- [26] K.N. Backer, A.V. Vratini, T. Resch, H.C. Knachel, W.W. Adams, E.P. Socci, B.L. Farmer, *Polymer*, **34**, 1571 (1993)
- [27] B. Champagne, D.H. Mosley, J.G. Fripiat, J.-M. André, *Phys. Rev. B*, **54**, 2381 (1996)
- [28] J.N. Demas, G.A. Crosby, *J. Phys. Chem.*, **75**, 991 (1971)
- [29] L. Smilowitz, A. Hays, A.J. Heeger, G. Wang, J.E. Bowers, *J. Chem. Phys.*, **98**, 6504 (1993)
- [30] V.V. Krasnikov, H.J. Brouwer, *unpublished results*
- [31] B.J. Schwartz, F. Hide, M.R. Andersson, A.J. Heeger, *Synth. Met.*, **84**, 663 (1997)
- [32] S. Heun, R.F. Mahrt, A. Greiner, U. Lemmer, H. Bässler, D.A. Halliday, D.D.C. Bradley, P.L. Burns, A.B. Holmes, *J. Phys.: Condens. Matter*, **5**, 247 (1995)
- [33] I.D.W. Samuel, B. Crystall, G. Rumbles, P.L. Burns, A.B. Holmes, R.H. Friend, *Chem. Phys. Lett.*, **213**, 472 (1993)
- [34] R.E. Gill, Design, synthesis and characterization of luminescent organic semiconductors (Ph.D. thesis, University of Groningen, 1996), chapter 3 to 5
- [35] C.M. Heller, I.H. Campbell, B.K. Laurich, D.L. Smith, D.D.C. Bradley, P.L. Burn, J.P. Ferraris, K. Müllen, *Phys. Rev.*, **54**, 5516 (1996)
- [36] D.C. Todd, J.M. Jean, S.J. Rosenthal, A.J. Ruggiero, D. Yang, G.R. Fleming, *J. Chem. Phys.*, **93**, 8658 (1990)
- [37] R.E. Gill, A. Meetsma, G. Hadziioannou, *Adv. Mater.*, **8**, 212 (1996)
- [38] R.E. Gill, P.F. van Hutten, A. Meetsma, G. Hadziioannou, *Chem. Mater.*, **8**, 1341 (1996)
- [39] M.S. Dresselhaus, G. Dresselhaus, *Adv. Phys.*, **30**, 139 (1981)
- [40] E.M. Conwell, J. Perlstein, S. Shaik, *Phys. Rev. B*, **54**, R2308
- [41] E.M. Conwell, *TRIP*, **5**, 218 (1997)
- [42] M. Pope, C.E. Swenberg, Electronic processes in organic crystals (Clarendon press, Oxford, 1982)
- [43] L. Yu, Z. Bao, *Adv. Mater.*, **6**, 156 (1994)

- [44] R.E. Gill, G. Hadziioannou, P. Lang, F. Garnier, J.C. Wittmann, *Adv. Mater.*, **9**, 331 (1997)
- [45] B. Tian, G. Zerbi, R. Schenk, K. Müllen, *J. Chem. Phys.*, **95**, 3191 (1991)
- [46] M. Kasha, H.R. Rawls, M.A. El-Bayoumi, *Pure. Appl. Chem.*, **11**, 371(1965)

## Chapter 3

# Laser emission from an alternating PPV copolymer in solution<sup>†</sup>

### Abstract

*The lasing efficiency and wavelength tunability of a novel blue-light-emitting copolymer, poly[(2, 5, 2'', 5''-tetraoctyl)-p-terphenyl-4,4''-ylene vinylene-p-phenylene vinylene], TOP-PPV, was studied in various organic solvents. Laser generation was established using the third harmonic radiation of a Nd:YAG laser as pump source. The results were compared with the conventional laser dyes Coumarin 120 and Coumarin 47 in ethanol under identical experimental conditions. The energy conversion efficiency of TOP-PPV in hexane exceeds that of both coumarin dyes with more than 50%. The laser emission of the copolymer dye in hexane is tuneable in the wavelength region between 414 and 456 nm ( $\Delta\lambda=38$  nm).*

---

<sup>†</sup> H.J. Brouwer, V.V. Krasnikov, A. Hilberer, J. Wildeman, G. Hadziioannou, *Appl. Phys. Lett.*, **66**, 3404 (1995)

### 3.1 Introduction

It was realized that the large absorption cross-section and high photoluminescence (PL) quantum yield of substituted PPV's make them promising candidates as active laser media in dilute solution and blends (i.e. the active polymer dispersed in a transparent solid host matrix) in analogy with conventional laser dyes [1]. Under these conditions the individual polymer chains are spatially well-separated by the host medium so that interchain interactions which result in fast non-radiative decay and luminescence quenching are neglectable. In conventional solid-state dye lasers the transparent host matrices are either organically modified sol-gel glasses (Ormosils) [2,3] or amorphous polymers like polyurethanes [4], or poly(methylmethacrylate) (PMMA) [5] and copolymers [6,7] thereof. The poor compatibility of the laser dyes with the host matrix and the small dimensions of the dye molecules leads to fast phase separation (recrystallization) during operation and subsequent formation of aggregates, which usually exhibit weak fluorescence [1]. PPV-based homo- and copolymers can be considered as attractive materials for the possible application as active gain media in solid-state dye lasers, since they combine high PL-quantum yields and tuneable optical properties with good processability and excellent mechanical properties.

Laser action of a soluble conjugated polymer, poly(2-methoxy-5-(2'-ethyl-hexyloxy)-*p*-phenylenevinylene) (MEH-PPV) in the liquid state [8,9] was achieved for the first time in 1992. Lasing of the polymer solution in a transverse cavity configuration was observed at 596 nm using second harmonic radiation of a Nd:YAG laser ( $\lambda = 532$  nm, pulse width 6 ns, repetition rate 10 Hz) as excitation source. The reported lasing performance of MEH-PPV was comparable to that of the most efficient laser dye in the yellow/red wavelength region, Rhodamine 6G. Holzer *et al.* [10] reported on laser emission from a PPV copolymer solution in the blue wavelength region by pumping with 35 ps pulses from a frequency-doubled ruby laser. Recently, laser emission from blend films containing MEH-PPV and TiO<sub>2</sub> nanoparticles in a polystyrene (PS) matrix [11] has been reported. The TiO<sub>2</sub> nanoparticles in these films strongly scatter the emitted photons and provide the feedback necessary for lasing [12]. Both observations in liquid and solid state are consistent with the reported stimulated emission (SE) in an ultrafast spectroscopy study by Yan *et al.* [13] of solutions and blends of MEH-PPV in PS.

In this chapter, laser action of an efficient blue-light-emitting PPV-based copolymer, poly[(2, 5, 2'', 5''-tetraoctyl)-*p*-terphenyl-4,4''-ylene vinylene-*p*-phenylene vinylene] (abbreviated as TOP-PPV) [14 - 16] in solution is demonstrated. The lasing performance of TOP-PPV is quantified in terms of energy conversion efficiency and wavelength tuneability for the specific dispersive resonator configuration used in this study. Three different solvents (*n*-hexane, *p*-xylene and tetrahydrofuran) were used to investigate the influence of the molecular environment on the lasing properties of the TOP-PPV copolymer in solution. The blue-light-

emitting laser dyes, Coumarine 47 and 120, were used as reference to compare the lasing efficiency and wavelength tuneability of the PPV-copolymer with that of conventional laser dyes.

### 3.2 Experimental

The energy conversion efficiency measurements were performed using a linear non-dispersive cavity in a quasi-longitudinal pumping arrangement. The experimental set-up is schematically depicted in figure 3.1. The cavity is defined by a concave metallic rear mirror and a flat dielectric output coupler (transmittance  $T = 81\%$ ,  $\lambda = 360 - 460$  nm) separated by a distance of 95 mm.

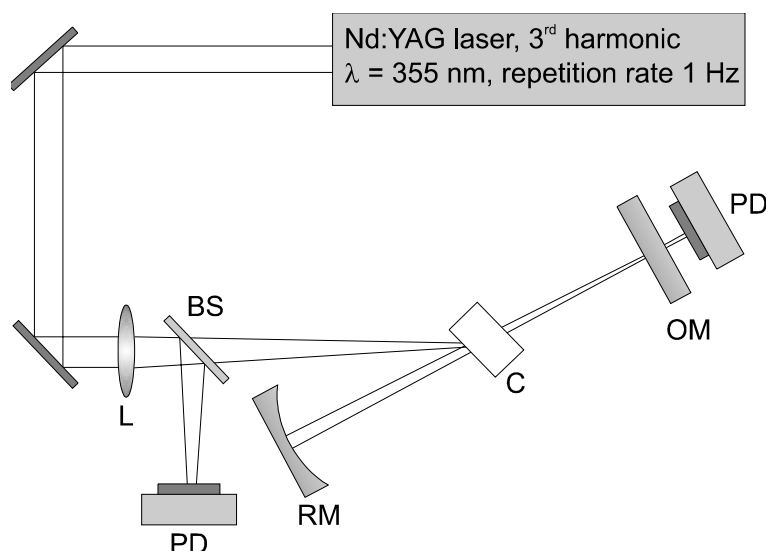


**Figure 3.1** Experimental set-up: L: lens, BS: beam splitter, PD: pyroelectric detector, RM: concave rear mirror, C: flow cell and OM: dielectric output mirror.

The pump source was a Nd:YAG laser, Quanta-Ray GCR 130-50, operating at tripled frequency ( $\lambda = 355$  nm,  $p$ -polarized, pulse width = 8 ns) with a repetition rate of 1 Hz. In order to prevent laser generation from the cell walls and to minimize Fresnel losses, the dye cell (pathlength 10-mm) was tilted with respect to the pumping beam. The angle between the pumping and generated beam was approximately  $7^\circ$ . The input and output pulse energy was monitored with two calibrated pyroelectric detectors (Coherent LMP 5 and Molectron J3-02, respectively). The spectral characteristics of the laser output were measured with an Optical Multichannel Analyzer (Princeton Instruments). In the case of the tuning-range measurements, a quartz prism was

incorporated between the rear mirror and the dye cell as a dispersive element. Wavelength tuning was achieved by rotation of the rear mirror.

The lasing performance of TOP-PPV was studied in three solvents: tetrahydrofuran (THF), *n*-hexane and *p*-xylene (Merck, spectroscopic grade). The solubility of TOP-PPV in the non-polar solvent hexane was low, which made it difficult to determine the concentration accurately in this case. All solutions were filtered over a 0.2  $\mu\text{m}$  filter, to remove dust and, in the case of hexane, undissolved compound. The reference laser dyes Coumarin 120 and 47 (Lambdachrome LC 4400 and LC 4700) [17] were used in ethanol solution (Merck, spectroscopic grade). Absorbance and fluorescence spectra were recorded on an SLM Aminco 3000 diode array spectrometer and a SLM Aminco SPF-500 fluoro-spectrometer, respectively. Luminescence quantum yields in solution were obtained using quinine sulphate in sulphuric acid ( $\Phi_F=0.55$ ) as the fluorescence standard. Luminescence lifetime measurements were made using the time-correlated single-photon counting technique, described in chapter 2.

### 3.3 Results and discussion

#### 3.3.1 Chemical structure and optical properties in solution

In figure 3.2 (A) the structure of the repeat unit of the TOP-PPV copolymer is given. The rigid-rod copolymer ( $M_w = 4.5 \times 10^3$ ,  $M_w/M_n=1.7$ ) has a well defined conjugated backbone, consisting of regularly alternating tetraoctylterphenylene (TOP) and *p*-phenylenebisvinylene blocks. The copolymer was synthesized via a Heck-coupling reaction and a detailed description of the synthesis is given in reference [14]. The copolymer is thermally stable, up to 420°C under nitrogen and has a glass transition temperature of  $-20^\circ\text{C}$ . The presence of four octyl side chains on the terphenylene unit provides solubility of the rigid copolymer in common organic solvents such as THF, chloroform and toluene.

The TOP-PPV copolymer consists of well-defined chromophores, which are the direct result of steric interactions in the backbone. The middle rings in the terphenylene units are twisted out of coplanarity due to steric hindrance induced by the bulky side chains and the  $\pi$ -conjugation is effectively interrupted [14]. Hence, the actual chromophores in the copolymer backbone are 1,4-bis(2,5-dioctylstyryl)benzene units connected to each other by non-coplanar phenylene groups. These well-defined conjugated PPV segments give to the copolymer the optical properties similar to those observed in small dye molecules, in particular exceptionally efficient blue fluorescence. The number of chromophores per polymer chain in TOP-PPV is equal to the number of repeat units, which in this case are 5 to 6 chromophores. Figure 3.2A shows the absorbance ( $\lambda_{\text{Abs, max}} = 352 \text{ nm}$ ) and emission ( $\lambda_{\text{Flu, max}} = 440 \text{ nm}$ ) spectra of a dilute solution of the TOP-PPV copolymer in *n*-hexane. The absorbance and luminescence of TOP-PPV in both THF and *p*-xylene are approximately 7 nm red-

shifted. The photoluminescence (PL) quantum yields of TOP-PPV in THF and *p*-xylene were measured as  $\Phi_F = 0.8$  ( $\tau_{Flu} = 0.7$  ns); a value of  $\Phi_{Flu} = 0.9$  ( $\tau_{Flu} = 0.8$  ns) was found in hexane.

Coumarins are known as a class of efficient laser dyes in the blue-green wavelength region [1] and were chosen as a reference for this reason. The chemical structure and optical spectra in ethanol of the two coumarin derivatives used in this study, 7-amino-4-methylcoumarin (Coumarin 120) and 7-diethylamino-4-methylcoumarin (Coumarin 47), are depicted in figure 3.2B and C, respectively.

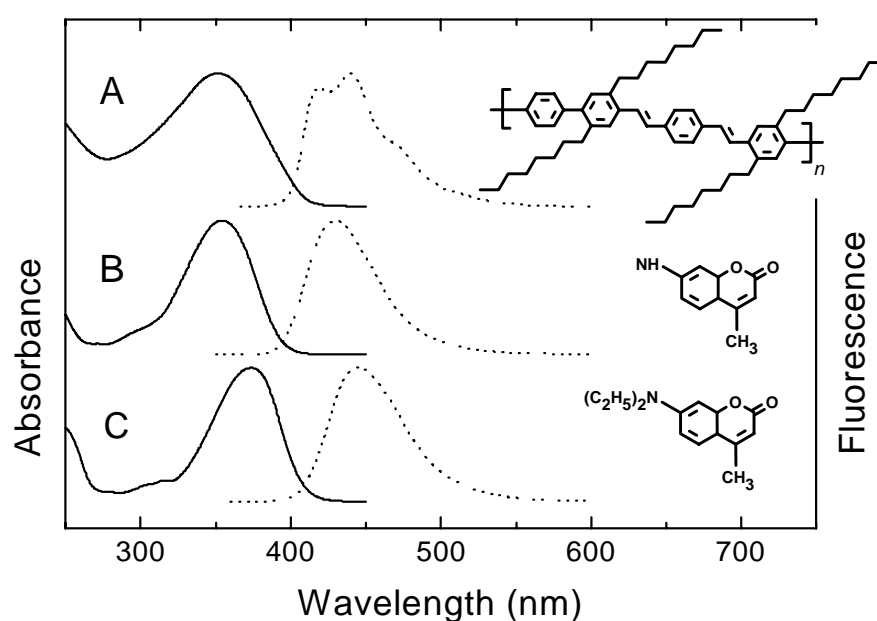


**Figure 3.2** Absorbance (solid line) and emission spectra (dotted line) at low solute concentration (*O.D.* at  $\lambda_{Abs, max} \approx 0.1$ ) of (A) TOP-PPV in hexane, (B) Coumarin 120 in ethanol and (C) Coumarin 47 in ethanol. Inset (right): the chemical structure of the TOP-PPV repeat unit, Coumarin 120 and Coumarin 47.

The absorbance ( $\lambda_{Abs, max} = 354$  nm) and fluorescence ( $\lambda_{Flu, max} = 432$  nm) of Coumarin 120 in ethanol are in the same spectral region as that of the copolymer in hexane and the absorbance maxima of both compounds are in close proximity of the wavelength of our Nd:YAG pump source. In the case of Coumarin 47 in ethanol, the absorbance ( $\lambda_{Abs, max} = 373$  nm) and fluorescence ( $\lambda_{Flu, max} = 446$  nm) are red-shifted with respect to Coumarin 120 due to the electron-donating character of the ethyl group, and the

spectral region of emission coincides with that of TOP-PPV in THF or *p*-xylene. The measured PL quantum yields of Coumarin 120 and Coumarin 47 are  $\Phi_F = 0.5$  ( $\tau_F = 3.6$  ns) and  $\Phi_F = 0.6$  ( $\tau_F = 3.1$  ns), respectively.

### 3.3.2 Dye laser performance

All dye solutions used in this study had a transmittance of  $T=1\%$  (quartz cuvette, 10 mm path length) at the wavelength of the pump source ( $\lambda = 355$  nm), which was in the region of optimum lasing efficiency.

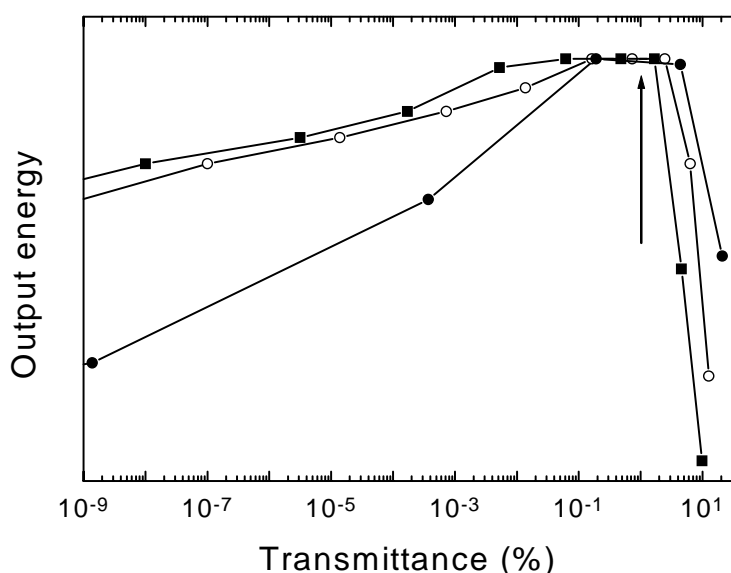


**Figure 3.3** Normalized dye laser output energy (at fixed pumped energy) as a function of transmittance of the dye solution at  $\lambda = 355$  nm (quartz cuvette, 10 mm path length): ■: TOP-PPV in THF, ○: TOP-PPV in *p*-xylene and ●: Coumarin 120 in ethanol. Arrow:  $T = 1\%$ .

Concentration-dependent measurements at a fixed pump energy of 10 mJ showed that the maximum achievable output energy in our linear resonator was constant between a dye cell transmittance of  $T=0.1$  and 6% for all compounds, which can be seen in figure 3.3. A transmittance of  $T=1\%$  corresponded with a TOP-PPV chromophore concentration in THF of  $5.9 \times 10^{-5}$  M and a chromophore density of  $3.6 \times 10^{16}$  cm<sup>-3</sup>.

Clear evidence of laser action of the TOP-PPV copolymer is shown in figure 3.4. When the pump energy exceed the threshold energy for lasing, intense blue light with a narrow spectral bandwidth (7 nm, FWHM) was emerging from the output coupler. The spectrum of the spontaneous emission was obtained after blocking the rear mirror of the resonator to interrupt the feedback system. The wavelength of laser generation of TOP-PPV coincided with the maximum of the spontaneous emission spectrum (the wavelength of maximum gain to a first approximation) as expected for a free-running (self-tuning) resonator.

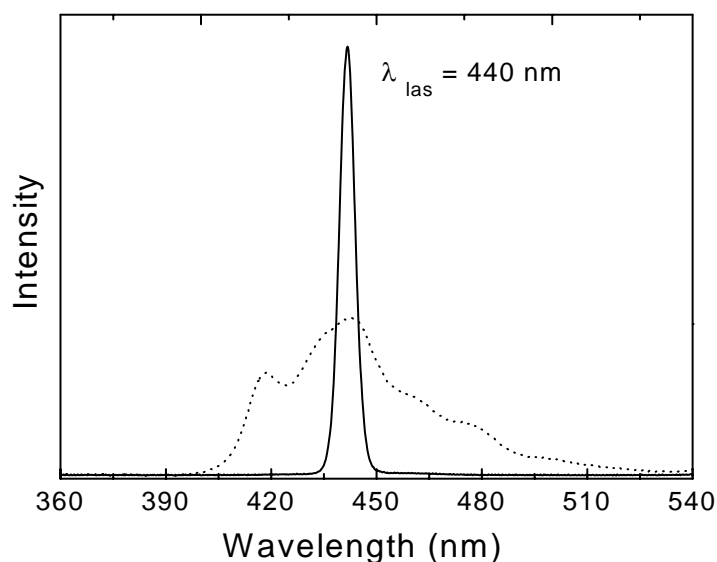


**Figure 3.4** Spontaneous (dotted line) and stimulated (solid line) emission spectra of TOP-PPV in hexane as measured with the linear non-dispersive cavity.

Figure 3.5 shows the ordinary linear dependence of the output pulse energy of the dyes as function on the input pulse energy of the Nd:YAG laser. The slope of the lines represents the energy conversion efficiency (or slope efficiency) and the intercept of the lines with the abscissa corresponds to the threshold energy for lasing. The conversion efficiency of TOP-PPV was dependent on the solvent used. The conversion efficiency (7%) of TOP-PPV in *n*-hexane is significantly higher than in all other cases. The conversion efficiencies and lasing wavelengths for all dyes are given in table 3.1.

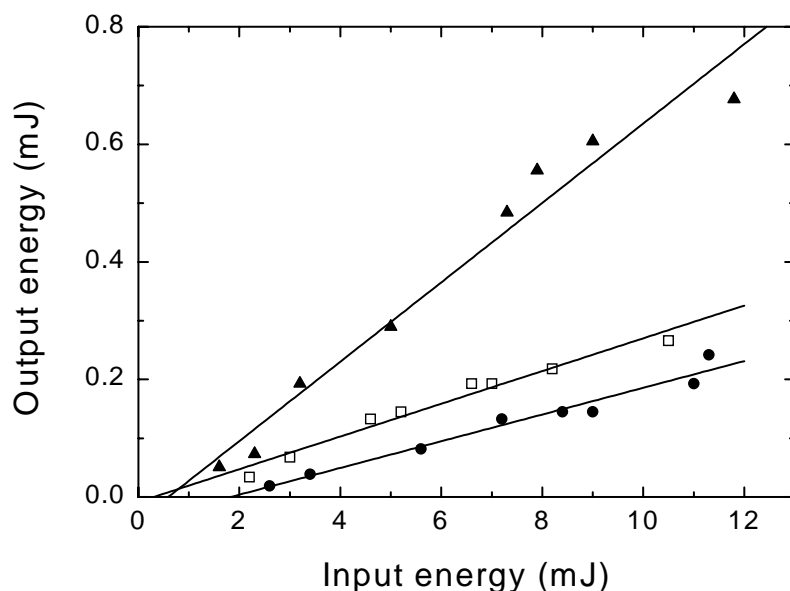


**Figure 3.5:** Plot of the output pulse energy of the dye laser as a function of the input pulse energy of the Nd:YAG pump beam in the case of : TOP-PPV copolymer in hexane, ◻ : TOP-PPV copolymer in *p*-xylene and ● : Coumarin 120 in ethanol.

**Table 3.1:** The lasing characteristics of coumarin 47, coumarin 120 and TOP-PPV.

Dye	Solvent	$\lambda_{\text{las}}^{(a)}$ (nm)	$E_{\text{threshold}}^{(a)}$ (mJ)	Eff <sup>a</sup> (%)	tuning range <sup>(b)</sup> (nm)	$\Delta\lambda^{(b)}$ (nm)
TOP-PPV	THF	449	0.8	1.8	438 – 456	18
	<i>p</i> -xylene	449	0.5	2.8	436 – 456	20
	Hexane	440	0.6	6.8	414 – 452	38
Coumarin 47	Ethanol	451	1.3	2.8	444 - 470	26
Coumarin 120	Ethanol	439	1.8	2.3	424 - 450	26

a) Linear non-dispersive resonator, b) Dispersive resonator

The efficiencies of TOP-PPV in THF and *p*-xylene (1.8 and 2.8%, respectively) are comparable to those of both coumarin dyes, but their lasing threshold energies are a factor two lower. As expected, the lasing wavelength, for TOP-PPV in THF and *p*-xylene are red-shifted with respect to hexane due to increasing solvent polarity/dielectric constant. The lasing bandwidth of the TOP-PPV polymer was

approximately 7 nm in all solvents. The bandwidth of both coumarin dyes was almost twice as large, 12 nm. During all measurements no signs of photodegradation were observed.

The wavelength tuneability of the copolymer and dye solutions has been determined in the same resonator; a prism was incorporated between the rear mirror and the dye cell as wavelength-selective element. The results of the wavelength tuneability measurements are shown in table 3.1.

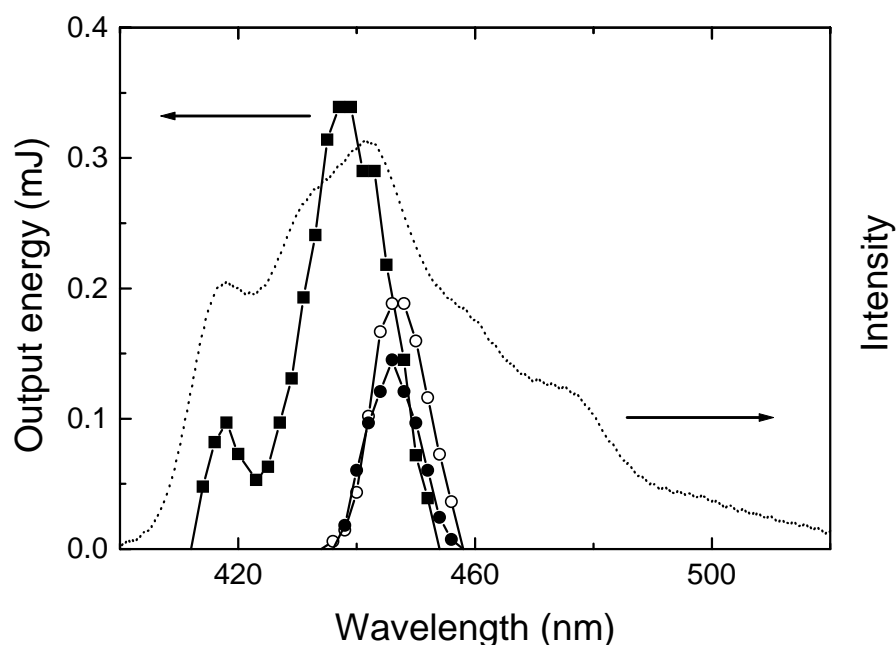


**Figure 3.6** Tuning curve (■) and luminescence spectrum (dashed line) of the TOP-PPV copolymer in hexane (pump energy 10 mJ) and the tuning curves of TOP-PPV in *p*-xylene (○) and tetrahydrofuran (●).

The tuning curves for the TOP-PPV copolymer in *n*-hexane, THF and *p*-xylene are plotted in figure 3.6. The curves were recorded at a pump energy of 10 mJ. The luminescence spectrum of TOP-PPV in hexane is shown in the same figure for comparison. From this plot it can be seen that the tuning curve for TOP-PPV in *n*-hexane follows the shape of the emission spectrum in the region between 414 and 452 nm. The cross-section for stimulated emission as a function of wavelength  $\sigma_{em}(\lambda)$  to a

first approximation coincides with the spontaneous emission spectrum, which is expressed in the following relationship [1]:

$$\sigma_{em}(\lambda) = \frac{\lambda^4 E(\lambda)}{8\pi n^2 c_0 \tau_F} \quad (3.1)$$

where  $n$ ,  $c_0$  and  $\tau_F$  are the refractive index, velocity of light and luminescence lifetime, respectively  $E(\lambda)$  is the normalized spontaneous emission lineshape function such that  $\int E(\lambda) d\lambda = \Phi_F$ , the fluorescence quantum yield. If we assume that the losses due to intersystem crossing,  $S_1 \rightarrow T_1$  (based on the high fluorescence quantum yield), and excited state absorption,  $S_1 \rightarrow S_n$ , are small, then the gain as function of wavelength is  $G(\lambda) \approx \sigma_{em}(\lambda) - \sigma_{abs}(\lambda)$ . The latter term represents the cross-section of residual ground-state absorption at the wavelength of interest; its contribution should also be reasonably small, considering the small overlap between absorption and emission. The magnitude of the laser power output is determined by the combination of cavity losses and gain. The power output efficiency  $\eta$  in the case of optimum output coupling for a standing-wave laser oscillator is given by [18]:

$$\eta_{opt} = \left[ 1 - \sqrt{\frac{\delta_0}{2\alpha_{m0} p_m}} \right]^2 \quad (3.2)$$

where  $\delta_0$  represents the internal cavity losses and  $2\alpha_{m0} p_m$  the unsaturated round-trip laser gain. From equation 3.2 it is obvious that the output power efficiency rapidly decreases as the ratio of internal cavity losses to unsaturated gain increases. Since the reflectivities of the resonator mirrors and other cavity losses are approximately constant in the wavelength region of luminescence, the laser output power as a function of wavelength should reflect the fluorescence spectrum, as shown for TOP-PPV in hexane in figure 3.6. The tuning curve looks rather peculiar if one compares it with that of conventional laser dyes, which are usually featureless due to the lack of pronounced vibrational coupling.

The wavelength tuning range of TOP-PPV in hexane ( $\Delta\lambda = 38$  nm) was the widest among all dye/solvent systems measured, which demonstrated the superior efficiency of this polymer solution. It should be mentioned that the bandwidth of laser generation was 3 nm (FWHM) in all cases and was mainly determined by the dispersion of the cavity.

The reason for the higher conversion efficiency of TOP-PPV in hexane is unclear at this moment. Gel Permeation Chromatography (GPC) was used to investigate which molecular weight fraction of the copolymer dissolved in hexane. The molecular

weight distribution of the copolymer in hexane indeed differed from that in THF and *p*-xylene. Due to the poor solubility in hexane, only the lower molecular weight species dissolved and as a result the polydispersity ( $M_w / M_n$ ) decreased from 1.7 (in THF) to 1.17 ( $M_n = 3.1 \times 10^3$ ,  $M_w = 3.6 \times 10^3$ ). Hence, in hexane the average number of chromophores is 4 per polymer chain. It is unlikely that this difference in molecular weight distribution is the main reason for the higher conversion efficiency in hexane. The luminescence quantum efficiency (in solution) of the copolymer,  $\Phi_F = 0.9$ , is the same as that of the model compound 1,4-bis(2,5-dioctylstyryl)benzene (the chromophore in TOP-PPV) [14], which indicates that the efficiency does not change drastically as a function of chain length.

### 3.4 Conclusions

In conclusion, we have demonstrated efficient laser action of a novel blue-light-emitting PPV copolymer in solution, photoexcited by ns pulses from the frequency-tripled output of a Nd:YAG laser. The energy conversion efficiency and wavelength tuning range of TOP-PPV in *n*-hexane exceeded that of both reference coumarin dyes. This study clearly demonstrates the potential of conjugated PPV polymers for dye laser applications. Further comprehensive studies concerning photostability, conversion efficiencies, wavelength tunability, and the effect of solvent environment on the photophysical parameters are necessary however in view of possible future applications.

The prospects for PPV polymers as active lasing medium in optically pumped solid state dye lasers and amplifiers based on dilute blends seem good, based on the above mentioned observations in solution. The superior mechanical properties and thermal stability of conjugated polymers over conventional laser dyes in combination with efficient emission will likely result in an overall improvement of the performance of such solid-state dye lasers.

Moreover, lasing from neat PPV (and derivatives thereof) films under pulsed optical excitation has been reported recently [19,20], which demonstrates that polymers exhibit considerable net gain in the solid state even under extreme conditions were the chains are in close contact. The possibility to generate laser light in pure PPV films with a typical thickness of 100 – 300 nm, prepared by the simple spincoating technique, can be considered as an important development. Our efforts with respect to studies of neat homo- and copolymer films under intense optical excitation are described in the next chapter.

### 3.5 References

- [1] F.P. Schäfer, Dye lasers (Springer-Verlag, Berlin, 1973)
- [2] E.T. Knobbe, B. Dunn, P.D. Fuqua, F. Nishida, *Appl. Optics*, **29**, 2729 (1990)
- [3] D. Lo, J.E. Parris, J.L. Lawless, *Appl. Phys. B*, **56**, 385 (1993)
- [4] H.P. Weber, R. Ulrich, *Appl. Phys. Lett.*, **19**, 38 (1971)
- [5] O.G. Peterson, B.B. Snively, *Appl. Phys. Lett.*, **12**, 238 (1968)
- [6] R.E. Hermes, T.H. Allik, S. Chandra, J.A. Hutchinson, *Appl. Phys. Lett.*, **63**, 877 (1993)
- [7] F. Amat, A. Costela, J.M. Figuera, F. Florido, I. Garcia-Moreno, R. Duchowicz, R. Sastre, *Opt. Commun.*, **114**, 442 (1995)
- [8] D. Moses, *Appl. Phys. Lett.*, **60**, 3215 (1992)
- [9] D. Moses, U.S. Patent No. 5,237,582 A (1992)
- [10] W. Holzer, A. Penzkofer, S-H. Gong, A. Bleyer, D.D.C. Bradley, *Adv. Mater.*, **8**, 974 (1996)
- [11] F. Hide, B.J. Schwartz, M.A. Díaz-García, A.J. Heeger, *Chem. Phys. Lett.*, **256**, 424 (1996)
- [12] N.W. Lawandy, R.M. Balachandran, A.S.L. Gomez, E. Sauvain, *Nature*, **368**, 436 (1994)
- [13] M. Yan, L.J. Rothberg, E.W. Kwock, T.M. Miller, *Phys. Rev. Lett.*, **75**, 1992 (1995)
- [14] A. Hilberer, H.J. Brouwer, B.J. van der Scheer, J. Wildeman, G. Hadziioannou, *Macromolecules*, **28**, 4525 (1995)
- [15] A. Hilberer, H.J. Brouwer, F. Garten, J. Wildeman, G. Hadziioannou, *SPIE Proceedings San Diego*, **2528**, 74 (1995)
- [16] H.J. Brouwer, V.V. Krasnikov, A. Hilberer, J. Wildeman, G. Hadziioannou, *Appl. Phys. Lett.*, **66**, 3404 (1995)
- [17] U. Brackmann, Lambda-dachrome<sup>R</sup> Laser-grade Dyes (Lambda Physik GmbH, Göttingen, 1986), III-59 and III-67
- [18] A.E. Siegman, Lasers (University Science Books, Mill Valley CA, 1986), chapter 12
- [19] N. Tessler, G.J. Denton, R.H. Friend, *Nature*, **382**, 695 (1996)
- [20] F. Hide, M.A. Díaz-García, B.J. Schwartz, M.R. Andersson, Q. Pei, A.J. Heeger, *Science*, **273**, 1833 (1996)

# Chapter 4

## Stimulated emission from neat polymer films<sup>†</sup>

### Abstract

*We have observed mirrorless lasing in optically-pumped, neat films of a PPV based alternating copolymer and a PPV homopolymer with octyloxy side chains. This mirrorless laser emission is the result of Amplification of Spontaneous Emission (ASE) due to optically induced net gain. Propagation of the emitted photons by waveguiding, inside the polymer film, is important, because it provides the necessary length of interaction of the emitted light to build up sufficient net gain. A threshold for spectral narrowing was observed above which superradiant emission appeared with a narrow spectral bandwidth of 6 – 7 nm (FWHM). The observed narrow emission band was located near the maximum of the low-intensity fluorescence spectrum ( $\approx$ gain maximum) for both polymers. Additionally, laser action from an Ooct-PPV film in a planar cavity configuration, consisting of two dielectric mirrors, was demonstrated. The cavity construction enabled us to tune the wavelength of the laser emission. A wavelength tuning range of approximately 20 nm was observed for the laser emission from Ooct-PPV, centred at the gain maximum located at 631 nm.*

---

<sup>†</sup> H.J. Brouwer, V.V. Krasnikov, A. Hilberer, G. Hadziioannou, *Adv. Mater.*, **8**, 935 (1997)

## 4.1 Introduction

The introduction of Light Emitting Diodes (LEDs) based on a semiconducting polymer, poly(*p*-phenylene vinylene) (PPV) [1,2], seven years ago triggered intensive research in the field of conjugated polymers. This led to the elaboration of various other conjugated polymer LEDs with impressive efficiencies [3] and light emission over the entire range of the visible spectrum [4-10]. The use of microcavities (i.e., an optical resonator consisting of two coplanar reflectors separated by a distance of 1  $\mu\text{m}$  or less) in polymer LEDs [11-13] made it possible to alter the emission properties significantly through coupling of the generated electroluminescence (EL) to resonant cavity modes. It results in substantially narrowed emission, increased directionality of the emitted light and wavelength tuneability of the emission (in the region of EL) by varying the cavity path length. The combination of efficient photoluminescence, the possibility to establish light emission by current injection and the successful application of microcavities in polymer LEDs, indicates that the development of polymer diode lasers operating in the visible can possibly be achieved on the long run. Recently, lasing in optically pumped neat (undiluted) polymer films was reported by several groups, which is an important development supporting such a possibility.

In chapter three, lasing from PPV copolymer in the dilute solutions has been discussed. Under these conditions, the chromophores are spatially well separated and interchain interactions are negligible. As anticipated, laser action in direct analogy with conventional laser dyes was observed, consistent with other similar studies [14,15] reported in literature. Correspondingly, lasing from solid-state films based on a dilute blend of poly(2-methoxy-5-(2'-ethyl-hexyloxy)-*p*-phenylene vinylene) (MEH-PPV) in polystyrene was reported by Hide *et al.* [16]. However, the prospects for neat MEH-PPV films as active laser medium seemed less hopeful because of the large contribution of photoinduced absorption resulting from interchain interactions, which cancelled out the stimulated emission (SE) in such films [17]. Despite the fast sub-nanosecond decay, the substantially decreased PL quantum efficiency and the photoinduced absorption, SE was observed in optically pumped neat polymer films in several ultrafast spectroscopy studies [18-21], indicating the possibility of lasing. This was positively confirmed recently by Tessler *et al.* [22] whom reported lasing from spincast PPV films under pulsed optical excitation in a microcavity construction. Furthermore, gain narrowing in optically pumped neat films of various PPV's was reported without the use of an external feedback system by several groups [23-27], including ours.

This chapter describes the emission properties of spincasted neat films of the blue-light-emitting silylene-*alt*-oligo(phenylene vinylene) copolymer (abbreviated as SiPPV) under pulsed laser excitation. This copolymer differs from its fully conjugated counterparts, due to the broken conjugation induced by the dimethylsilylene interruption units and can be seen as a long flexible chain of separate oligomers (di-*n*-octyl distyrylbenzene) connected by small spacer units. Spectral narrowing of the emission from the SiPPV films was observed with increasing excitation energy. The

intensity of the narrow band scaled super-linear with excitation energy. The influence of film thickness and the size of the excitation area on the threshold of spectral narrowing are discussed as well as the angular dependence of the emission. Furthermore, the emission properties of drop-cast films of a red-light-emitting homopolymer poly (2,5-di-*n*-octyloxy-*p*-phenylene vinylene) (Ooct-PPV) under pulsed laser excitation are described. In this case optical feedback was established using a planar cavity configuration consisting of two dielectric mirrors.

## 4.2 Experimental

Thin SiPPV films were fabricated by spincoating the copolymer from a toluene solution (5% w/w) onto glass slides ( $20 \times 20 \text{ mm}^2$ ). The solution was filtered ( $0.2 \mu\text{m}$ -filters, Spartan 13/30) prior to spincoating to ensure good optical quality films. After spincoating the films were dried under vacuum at  $50 \text{ }^\circ\text{C}$  to remove all residual toluene. The Ooct-PPV films were made by dropcasting the chlorine-precursor polymer from a filtered chloroform solution onto glass slides or dielectric mirror in the case of the cavity experiments. The precursor-PPV films were converted under vacuum at  $100 \text{ }^\circ\text{C}$  for 2 hours.

A Dektak 3030 ST surface profiler was used to determine the layer thickness. The absorbance spectra of the films were recorded on an SLM-Aminco 3000 array spectrophotometer. Fluorescence spectra were recorded on a Perkin-Elmer LS50-B fluorospectrometer. Luminescence lifetimes were determined using the time-correlated single-photon counting technique and absolute PL quantum yields of the films were measured in an integrated sphere as described in chapter 2.

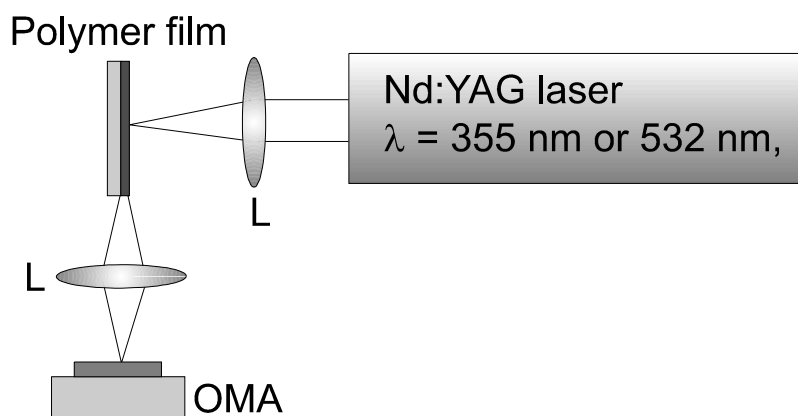


**Figure 4.1** *The experimental geometry for excitation and detection.*

The third harmonic radiation of a Nd:YAG laser (Quanta-Ray GRC 130-50,  $\lambda = 355$  nm, pulse width = 15 ns) operating at a repetition rate of 1 Hz, was used for photoexcitation of the SiPPV films. The beam was focused to an elliptical spot size of 5.0 by 2.5 mm<sup>2</sup> with a cylindrical lens (see figure 4.1). The energy of the excitation beam was varied using neutral density filters. The copolymer films were excited under normal incidence. The emitted light emerging from the edge of the films along the long axis of the beam spot was collected with a lens and focused into a multimode optical fiber input of an Optical Multichannel Analyzer (Chromex 250 SI polychromator with Chromcam I CCD detector). The acceptance cone (full angle) was approximately 10°. The Ooct-PPV films were photoexcited (diameter of the excited area  $\approx 2$  mm) under normal incidence by the frequency-doubled output of the Nd:YAG laser ( $\lambda = 532$  nm), and the total emission from the films was measured using an integrating sphere.

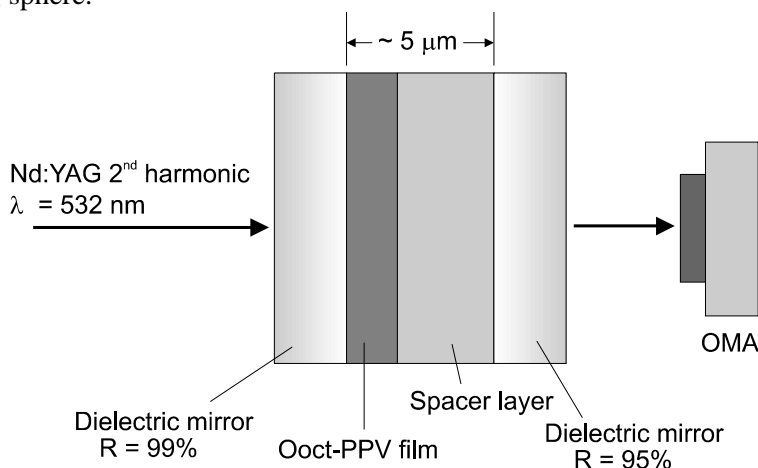


**Figure 4.2** *Ooct-PPV cavity structure.*

The emission properties of Ooct-PPV films were measured in a planar cavity structure as depicted in figure 4.2. The cavity consisted of two flat dielectric mirrors with reflectivities of  $R = 95$  and  $R = 99\%$  in the red wavelength region. The polymer was cast on top of the high-reflectance dielectric mirror ( $R=99\%$ ) as described above, and the second dielectric mirror was mounted on the polymer film using a small amount of transparent silicone grease (Dow-Corning) forming a thin compressible spacer film. The cavity structure was clamped into a mechanical holder, and by varying the applied force onto the mirrors, it was possible to adjust the cavity length and so tune the wavelength of emission. The layer thickness of the Ooct-PPV films was approximately 1.5  $\mu\text{m}$  and the total cavity path length in the experiments described was estimated to be roughly 5  $\mu\text{m}$ . It should be explicitly stated that all above-mentioned photoexcitation experiments were performed under ambient conditions.

## 4.3 Results and discussion

### 4.3.1 Silylene-*alt*-oligo(phenylene vinylene) copolymer films

In figure 4.3 (inset) the structure of the repeat unit of the copolymer poly[dimethyl silylene-*p*-phenylene-vinylene-(2,5-di-*n*-octyl-*p*-phenylene)-vinylene-*p*-phenylene] is given. The synthesis, full characterization and optical properties in solution are described in reference [28]. The Si-PPV copolymer ( $M_w = 25.000$ ,  $M_n/M_w = 2.4$ ) has a well-defined backbone consisting of regularly alternating di-*n*-octyl-distyrylbenzene and fully saturated dimethylsilylene units.

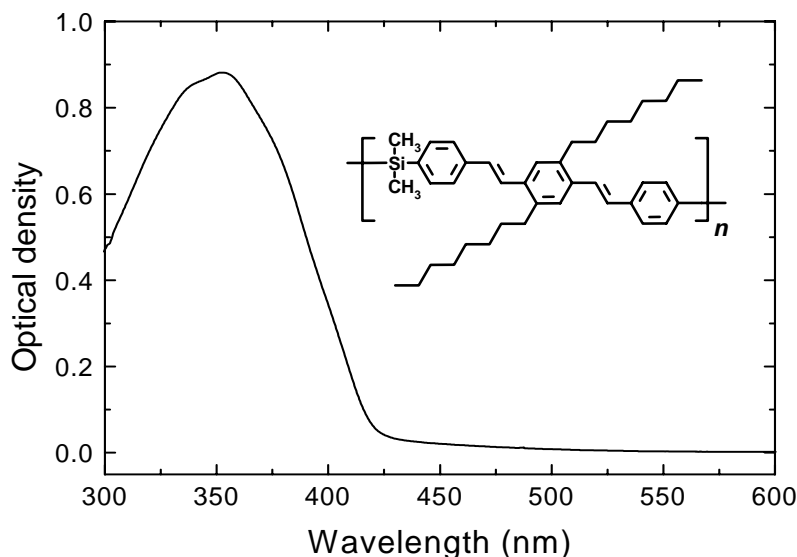


**Figure 4.3** Absorbance spectrum of a spincoated SiPPV copolymer film (150 nm). Inset: the chemical structure of the SiPPV repeat unit and luminescence decay curve of the film.

The average number of chromophores per SiPPV chain is equal to the number of repeat units, which in this case is 45 chromophores/chain. Figure 4.3 shows the absorbance spectrum ( $\lambda_{\text{Abs, max}} = 352$  nm) of a spincoated SiPPV film, with a thickness of 150 nm. The copolymer exhibits a large absorption coefficient ( $\alpha_{352 \text{ nm}} = 1.3 \cdot 10^5 \text{ cm}^{-1}$ ) due to the high density of chromophores. In solution, PL-quantum yields of  $\Phi_F \approx 0.6$  ( $\tau_F = 0.9$  ns) have been measured [29]. The solid-state quantum yield of a SiPPV film determined in an integrated sphere was  $\Phi_F = 0.4$  ( $\lambda_{\text{Flu, max}} = 452 / 483$  nm), with a luminescence decay showing a single-exponential dependence with a time constant of

$\tau_F = 0.9$  ns. Based on these observations, it can be concluded that the PL quantum yield does not drop significant going from solution to solid state. The apparent difference in PL efficiencies can be attributed to the fact that we compare efficiencies obtained by two different techniques which both have a reasonably large experimental error.

We have measured light emission spectra from a series of SiPPV copolymer films with different film thickness. The typical spectral evolution as a function of excitation energy is shown in figure 4.4 (spectra 2,3 and 4) for a 150 nm thick sample. The spectra represent the emission emerging from the edge of the film; they are normalized on excitation energy. For comparison, a photoluminescence spectrum (1) collected at an angle of  $30^\circ$  with respect to the film is also included.

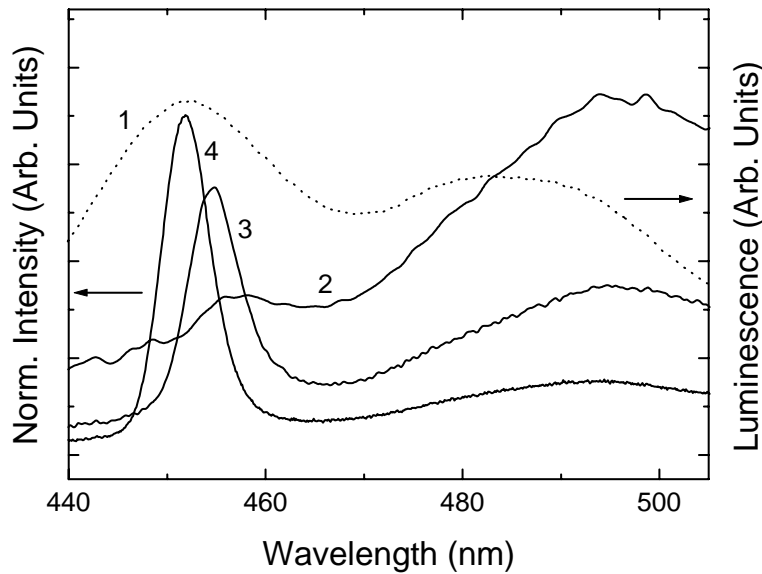


**Figure 4.4** Fluorescence spectrum (1) and emission spectra normalized on excitation energy of an SiPPV copolymer film (thickness 150 nm): (2) emission spectrum below lasing threshold,  $E_{ex} = 7.5 \cdot 10^{-2}$  mJ and emission spectra above threshold (3)  $E_{ex} = 0.25$  mJ and (4)  $E_{ex} = 1$  mJ.

An increase in pump energy resulted in spectral narrowing and the appearance of a sharp peak surrounded by a broad luminescence tail. The super-linear increase in amplitude of the sharp peak, as well as the sub-linear growth of the broad tail, are evident. As a result, the higher the excitation energy, the more dominant the spectrally

narrow emission becomes. The ratio of the spectrally narrow emission to the background luminescence increases with excitation energy, which is shown in figure 4.5.

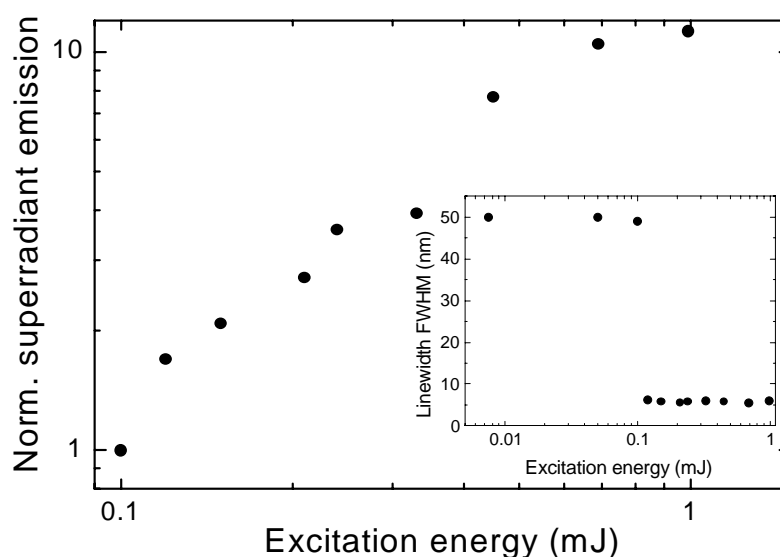


**Figure 4.5** Normalized intensity ratio of superradiant emission and luminescence background as a function of excitation energy. Inset (bottom right): emission linewidth as a function of excitation energy.

Above an energy threshold of approximately 0.1 mJ, narrow blue emission with a full width at half maximum (FWHM) of 6 nm was emerging from the edge of the film (inset, figure 4.5). The main features of the spectral behaviour of our system remained the same at any light collection angle. Only the relative amplitude of the sharp maximum with respect to the amplitude of the broad tails and the shape of the emission spectrum below threshold depended on the angle of observation. It should be mentioned that the threshold of breakdown lies at approximately 1.5 - 2 mJ, depending on the film quality, allowing measurements at pump energy levels well above the threshold of spectral narrowing to be made. We have measured the spectral characteristics as a function of pump energy for several samples of the same thickness and under the same conditions with a good sample-to-sample reproducibility.

The behaviour observed, *viz.* the appearance of a spectrally narrow peak above a well-defined energy threshold and the relative suppression of the broad luminescence tails, indicating the redistribution of spectral energy within the emitted light, is a clear signature of light-induced net gain due to stimulated emission. This

radiation, which appears regardless of whether there is any input radiation, is called Amplified Spontaneous Emission (ASE). ASE has at least some properties resembling laser radiation. For this reason systems emitting ASE are often referred to as mirrorless lasers or superradiant lasers and such mirrorless lasing is sometimes called superradiance [30,31].

Mirrorless lasing requires light-induced amplification with a sufficient length of interaction for the generated light to build up considerable net gain. We believe that, in our case, the emission propagates through a waveguide formed by the thin polymer film, based on the following four observations. 1) The spectral shape of emission below threshold of lasing differs from the luminescence spectrum collected under an angle of  $30^\circ$  (figure 4.4, spectra 1 and 4). This difference can be explained as being due to waveguiding of the light collected at the edge of the film and is caused by the dispersions of both the absorption tail and waveguiding; 2) We observed a dramatic increase in lasing threshold with decreasing excitation spot size, while keeping the light intensity the same; 3) No change in spectral behaviour of the thin films was observed when varying the thickness of the glass slide; 4) A decrease of film thickness from 150 to 50 nm resulted in the absence of laser generation at any pump energy up to the damage threshold, which indicates the existence of a cut-off thickness. The cut-off thickness  $h_{\text{cut-off}}$  for asymmetric planar waveguides, below which radiation of  $\lambda = 452$  nm (maximum of the narrow emission band) cannot propagate, can be calculated using the following expression [32]:

$$h_{\text{cut-off}} = \frac{\lambda}{2\pi\sqrt{n_f^2 - n_s^2}} \tan^{-1} \left( \sqrt{\frac{n_s^2 - n_c^2}{n_f^2 - n_s^2}} \right) \quad (3.1)$$

where  $n_f$ ,  $n_s$  and  $n_c$  are the refractive indices of the film, substrate and cladding, respectively. We calculated a  $h_{\text{cut-off}} \approx 85$  nm, using  $n_s(\text{glass}) = 1.5$ ,  $n_f(\text{SiPPV}) = 1.7$  and  $n_c(\text{air}) = 1$ . This value is in good agreement with our experimental observations.

The wavelength of the superradiant peak ( $\lambda_{\text{max}} = 452$  nm) at high pump energies coincides with the maximum of the fluorescence emission spectrum (figure 4.4). The exact reason of the recorded blue shift (of approximately 5 nm) of the laser emission with increasing excitation energy is not entirely clear. Most likely it is caused by (I) light-induced depopulation of the ground state of the photoactive chromophores (ground-state bleaching) and (II) light-induced excited-state absorption, which is usually red-shifted. A possible role of light-induced absorption due to interchain interaction and the influence of singlet-triplet intersystem crossing cannot be excluded either.

### 4.3.2 Poly(2,5-di-*n*-octyloxy-*p*-phenylene vinylene) films

We also studied the spectral behaviour of a red-light-emitting PPV homopolymer. In figure 4.6 (inset) the structure of the repeat unit of the homopolymer poly(2,5-di-*n*-octyloxy-*p*-phenylene vinylene) is given. The polymer was synthesized via the chlorine precursor route (CPR-route) [33,34], which gave a precursor polymer with a molecular weight of  $M_w \approx 1.10^6$  g/mol determined by gel permeation chromatography. The drop-cast precursor Ooct-PPV films were heated at 100 °C under vacuum for 2 hours, which gave partially converted PPV films with PL-efficiencies between 10-15%.

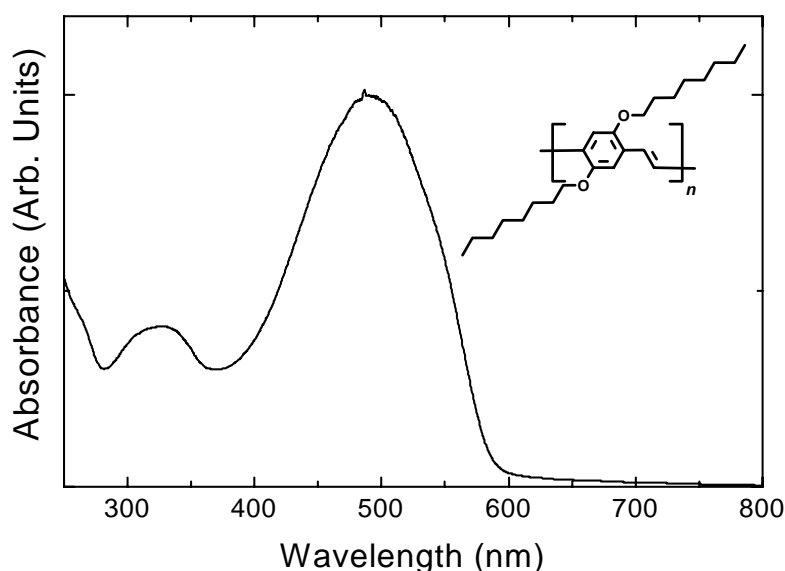


**Figure 4.6** Absorbance spectrum of a partially converted Ooct-PPV film. Inset: the structure of the Ooct-PPV repeat unit.

The absorbance and emission spectra corresponded to those of fully converted Ooct-PPV [35], which indicated that our polymer had converted sequences longer than the average effective conjugation length and that the density of non-converted chain segments was reasonably low. A typical absorbance spectrum of a partially converted Ooct-PPV film on glass is shown in figure 4.6 which exhibits an absorbance maximum at  $\lambda_{\text{Abs, max}}=492$  nm. The emission spectra of an Ooct-PPV film as a function of excitation energy are shown in figure 4.7. The polymer was photoexcited ( $\lambda_{\text{Excitation}} = 532$  nm) at the red absorption edge. The same trend in emission behaviour as displayed by SiPPV is observed with increasing excitation energy, which we attribute to ASE. The spectral narrowing of Ooct-PPV occurs at a lower energy threshold

( $\approx 30 \mu\text{J}$ ) and the suppression of the broad luminescence tail is more pronounced. The narrow emission band is slightly red-shifted with respect to the maximum of the 0-1 vibronic peak and its wavelength ( $\lambda_{\text{max}} = 637 \text{ nm}$ ,  $\text{FWHM} = 7 \text{ nm}$ ) position did not shift with increasing excitation energy as in the case of SiPPV. However, it should be stated that the absolute value of the excitation threshold, wavelength position and the absolute magnitude of gain narrowing, differed from (polymerization) batch-to-batch and even from sample-to-sample, which makes a quantitative analysis of the process for Ooct-PPV difficult.

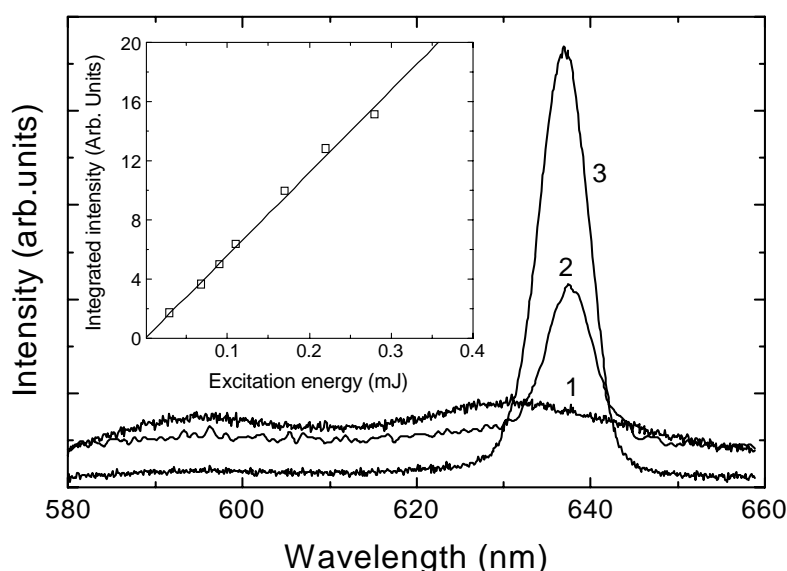


**Figure 4.7** Emission spectra from a 1.5 mm thick Ooct-PPV film on glass at different excitation energies: (1)  $E_{\text{ex}} = 20 \mu\text{J}$  (below threshold); (2)  $E_{\text{ex}} = 90 \mu\text{J}$ ; (3)  $E_{\text{ex}} = 280 \mu\text{J}$ . Inset (left): the integrated emission intensity as a function of excitation energy of the same film measured in an integrated sphere. The solid line is a linear fit through the data points. Beam diameter  $\approx 2 \text{ mm}$ .

The (polymerization) batch-to-batch variations are caused by the differences in obtained molecular weight (distributions), the extent of chemical and conformational defects and amount of chemical impurities present. Sample-to-sample variations are likely the result of differences in microscopic structure of the film, the extent of precursor conversion and amount of defects introduced by thermal and photochemical oxidation. Hide *et al.* [23] already showed the importance of microscopic morphology on the gain-narrowing process by varying the solvent from which the polymer was

spincast, resulting in a significant difference in the energy threshold of emission narrowing.

The integrated emission intensity of the above-mentioned Ooct-PPV film as a function of excitation energy was measured in an integrated sphere (shown in the inset of figure 4.7). In this way we were able to collect all light emerging from the sample. The maximum excitation energy (0.3 mJ) displayed lies well beyond the threshold for emission narrowing ( $\approx 30 \mu\text{J}$ ). No discontinuity in output energy was observed and the integrated emission output showed a linear dependence up to excitation energies of 0.3 mJ (corresponding to a pump fluence  $\approx 2.4 \text{ mJ}\cdot\text{cm}^{-2}$  and an exciton density of  $n \approx 10^{19} \text{ cm}^{-3}$ ). The absence of a threshold in output energy, is a clear indication that the spectral narrowing in the Ooct-PPV film is due to a single-pass amplification process like ASE rather than multiple-pass amplification established by resonant feedback [22,40]. Above 0.3 mJ (not shown in figure 4.7) the dependence became sub-linear, but we were unable to measure the emission reproducibly at much higher excitation energies due to degradation of the sample. Ground-state bleaching as a possible cause for this sub-linear behaviour is unlikely, because of the relative thick ( $1.5 \mu\text{m}$ ) polymer film used and the absence of a significant increase in pump transmission at high excitation energies. It has been reported for PPV that at high excitation densities, bimolecular exciton annihilation [38,39] starts playing a role, resulting in a decreased emission quantum yield. We cannot exclude that this mechanism is operative at high exciton concentrations ( $n > 10^{19} \text{ cm}^{-3}$ ) in Ooct-PPV.

Frolov *et al.* [26,35,36] also studied the emission properties of Ooct-PPV but under intense ps laser excitation. The reported time-integrated spectral behaviour is roughly similar to that observed by us. They attributed the spectral narrowing to super fluorescence (SF), which is a co-operative emission process [31,37] in which an initially uncorrelated ensemble of  $N$  inverted emitters develop a coherent macroscopic dipole moment followed by simultaneous radiative decay resulting in a short burst of emission. This co-operative state is built up by the initial spontaneous emission noise (from a small fraction of emitters) which ‘capture’ or rephase the oscillations in all other inverted emitters. The distinct features of this emission process are: an initial short time delay associated with the development of the macroscopic dipole moment; a shortened emission decay time proportional to  $N^{-1}$  (smaller than the normal fluorescence lifetime  $\tau_F$ , which is independent of the number of emitters involved) and an emission intensity proportional to  $N^2$ . Despite the subtle difference with ordinary ASE, it is extremely difficult to separate ASE and SF experimentally and there are only a few well-documented studies, one of them concerning two-level atoms in the gas phase [37]. It is even questionable if in complicated systems like organic molecules and polymers, SF will have the ideal characteristics as described above. We do not have the facility to perform time-resolved experiments at high excitation

energies in our laboratory, which could give some further insight concerning the origin of the process responsible for spectral narrowing in polymers. Nevertheless we cannot find any objections towards the possible involvement of SF.

In order to study whether or not it was possible to achieve 'true' resonant lasing, a Ooct-PPV thin-film cavity was prepared, consisting of two dielectric mirrors as described in the experimental section. The thin-film cavity was constructed in such a way that it was possible to change the cavity path length and thus the wavelength position of the resonant modes inside the cavity. This in turn gave us control over the lasing wavelength and the possibility to study the wavelength tuneability of the laser emission within the same film. Additionally, by using dielectric mirrors instead of evaporated metal mirrors we avoid PL quenching at the polymer/metal interface [41,42] and we assure a high Q of the cavity.

In figure 4.8 A to C, three sets of emission spectra at low (dotted lines) and high (solid lines) excitation energy are shown. In figure 4.8 A, the emission spectra of an Ooct-PPV film on glass are given for comparison. This film was spincoated from the same Ooct-PPV solution used for the fabrication of the cavity (note that the Ooct-PPV was from a different polymerization batch as the one used in the preceding paragraph). At high excitation energies, ASE with a bandwidth of approximately 7 nm (FWHM) was observed at  $\lambda_{\text{max}} = 631$  nm (note that the ASE in this case coincides with the maximum of the 0-1 transition). In Figure 4.8 B the emission characteristics of an Ooct-PPV film in the planar cavity configuration are shown. At low excitation energy, three cavity modes at 598, 618 and 642 nm are visible, which do not differ significantly in intensity. At high excitation energy, the emission was strongly coupled into the cavity mode located at 642 nm, with a peak area ratio of  $\approx 10$  with respect to the mode at 618 nm. Additionally, the peak width (FWHM) decreased from 5.5 nm to 2.6 nm and the directionality of the emitted light was enhanced at high energy. All observations confirm that 'true' lasing is established in the thin-film cavity, in agreement with the study reported by Tessler *et al.* [22]. A set of emission spectra from the same cavity is shown in figure 4.8 C for a different cavity path length. In this case the wavelength of laser emission is located at 623 nm, demonstrating that wavelength tuning was possible over a range of roughly 20 nm. It should be mentioned that although this particular cavity construction allowed us to tune the lasing wavelength, it was difficult to obtain reproducible results due to the difficulty of aligning the two mirrors exactly parallel to each other, which is necessary for good resonant feedback. A slight misalignment of the mirrors from parallel resulted immediately in the observation of ASE instead of 'true' resonant lasing. Although we did not quantify the threshold for cavity lasing, it is significantly higher than the threshold for gain narrowing without optical feedback. This is probably partly caused by the shorter amplification path length for the thin film cavity (path length is equal to

the film thickness  $\approx 1.5 \mu\text{m}$  in this case). Secondly, the quality of the cavity was far from optimal, which results in high optical losses.

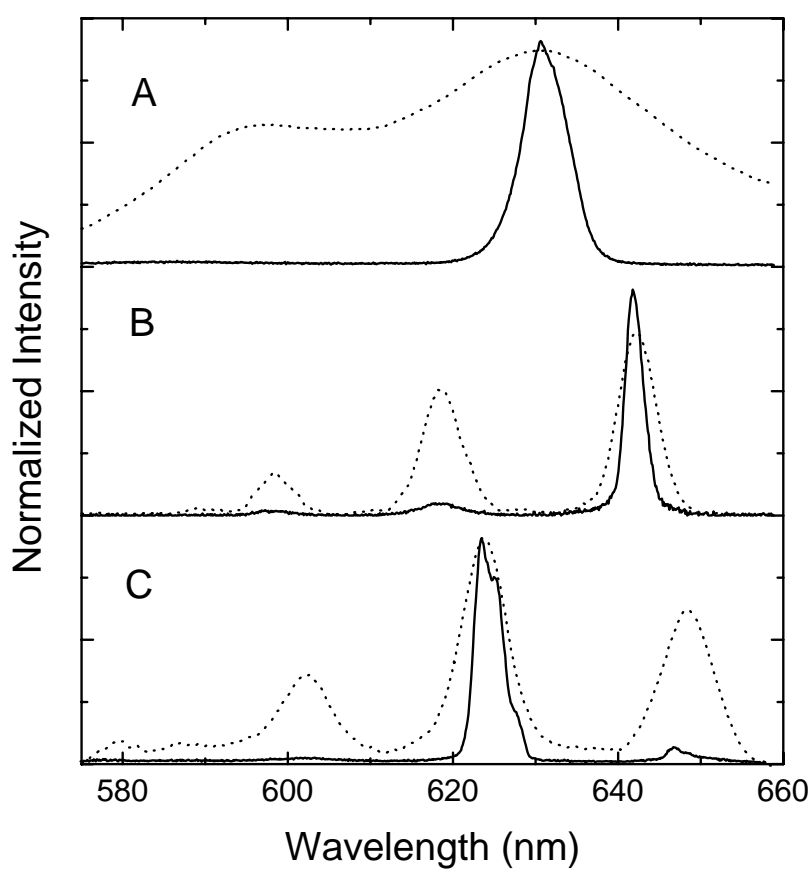


**Figure 4.8** (A) Emission spectra of a  $1.5 \mu\text{m}$  thick Ooct-PPV film on glass. (B) and (C) are two sets of emission spectra of an Ooct-PPV film in a planar optical cavity with different cavity path length. The dotted lines represent the emission spectra at low excitation energy and the solid lines those at high excitation energy. The low-energy spectra are scaled up for the sake of clarity.

We were not able to achieve laser emission in the wavelength region beyond 623 to 642 nm. This indicates that the spectral region of gain (sufficiently large for lasing to occur) is rather narrow and located roughly within 10 nm of the PL maximum ( $\approx$ gain maximum) at  $\lambda = 631$  nm. This observation is in agreement with the small wavelength tuning ranges of 10 – 20 nm reported in other publications concerning lasing from optically pumped polymer microcavities [22,40]. In several ultrafast spectroscopy studies, including one concerning Ooct-PPV [36,43] it was shown that the wavelength region of gain in polymer films is typically much broader, and on the basis of that one would anticipate a larger tuning range for laser emission in more optimized devices.

#### 4.4 Conclusions

In conclusion, we have observed mirrorless lasing in optically pumped, neat films of the copolymer SiPPV and the homopolymer Ooct-PPV. This mirrorless laser emission is the result of amplification of spontaneous emission (ASE) due to optically-induced net gain. Propagation of the emitted photons by waveguiding, inside the polymer film, is important, because it provides the necessary length of interaction of the emitted light to build up sufficient net gain. A threshold for spectral narrowing was observed above which coherent light emission appeared with a narrow spectral bandwidth of 6 – 7 nm (FWHM). The observed narrow emission band was located near the maximum of the low intensity fluorescence spectrum ( $\approx$ gain maximum) for both polymers. The possible involvement of superfluorescence (SF) in mirrorless lasing reported by several groups [35,44] cannot be ruled out, but until now there are no studies reported in which one was able to clearly identify SF over ASE based on ‘hard’ evidence obtained from time-resolved measurements.

We demonstrated ‘true’ lasing from an Ooct-PPV film with external optical feedback provided by a planar cavity consisting of two dielectric mirrors. This cavity construction enabled us to tune the wavelength of the laser emission within the same polymer film. A wavelength tuning range of approximately 20 nm was observed for the laser emission from Ooct-PPV, centred at the gain maximum located at 631 nm.

The observation of lasing in optically pumped polymer films with and without external feedback system gives hope for the possible development of an electrically pumped laser diode. The major limiting factor at this moment is the drive current necessary for electrically pumped lasing to be realized. One can make a rough estimation of the current threshold, based on the excitation density at which spectral narrowing occurs in optically pumped polymer films. It was estimated that current densities in excess of  $10^3$  A.cm<sup>-2</sup> [23] are needed to establish electrically induced lasing. The highest reported current density achieved in a polymer LED until now is  $\approx 25$  A.cm<sup>-2</sup> [45], which illustrates the barriers to be overcome concerning the development of a polymer laser diode. This was one of the reasons why we started to study the emission properties of PPV oligomers under pulsed laser excitation.

Oligomers have the ability to form well-ordered structures and due to this fact usually exhibit better charge transport properties. The results of this study are described in the next chapter.

#### 4.5 References

- [1] J.H. Burroughes, D.D.C. Bradley, A.R. Brown, R.N. Marks, K. Mackay, R.H. Friend, P.L. Burns, A.B. Holmes, *Nature (London)*, **347**, 539 (1990)
- [2] D. Braun, A.J. Heeger, *Appl. Phys. Lett.*, **58**, 1982 (1991)
- [3] N.C. Greenham, S.C. Moratti, D.D.C. Bradley, R.H. Friend, A.B. Holmes, *Nature (London)*, **365**, 628 (1993)
- [4] G. Grem, G. Leditky, B. Ulrich, G. Leising, *Adv. Mater.*, **4**, 36 (1992)
- [5] Y. Ohmori, M. Uchida, K. Muro, K. Yoshino, *Jpn. J. Appl. Phys.*, **30**, L1941 (1991)
- [6] Y. Ohmori, M. Uchida, K. Muro, K. Yoshino, *Jpn. J. Appl. Phys.*, **30**, L1938 (1991)
- [7] I. Sokolik, Z. Yang, F.E. Karasz, *J. Appl. Phys.*, **74**, 3584 (1993)
- [8] G.G. Malliaras, J.K. Herrema, J. Wildeman, R.H. Wieringa, R.E. Gill, S.S. Lampoura, G. Hadziioannou, *Adv. Mater.*, **5**, 721 (1993)
- [9] R.E. Gill, G.G. Malliaras, J. Wildeman, G. Hadziioannou, *Adv. Mater.*, **6**, 132 (1994)
- [10] H.J. Brouwer, A. Hilberer, V.V. Krasnikov, M. Werts, J. Wildeman, *Synth. Met.*, **84**, 881 (1997)
- [11] H.F. Wittmann, J. Grüner, R.H. Friend, G.W.C. Spencer, S.C. Moratti, A.B. Holmes, *Adv. Mater.*, **7**, 541 (1995)
- [12] T.A. Fisher, D.G. Lidzey, M.A. Pate, M.S. Weaver, D.M. Whittaker, M.S. Skolnick, D.D.C. Bradley, *Appl. Phys. Lett.*, **67**, 1355 (1995)
- [13] M. Berggren, O. Inganäs, T. Granlund, S. Guo, G. Gustafsson, M.R. Andersson, *Synth. Met.*, **76**, 121 (1996)
- [14] D. Moses, *Appl. Phys. Lett.*, **60**, 3215 (1992)
- [15] W. Holzer, A. Penzkofer, S-H. Gong, A. Bleyer, D.D.C. Bradley, *Adv. Mater.*, **8**, 974 (1996)
- [16] F. Hide, B.J. Schwartz, M.A. Díaz-García, A.J. Heeger, *Chem. Phys. Lett.*, **256**, 424 (1996)
- [17] M. Yan, L.J. Rothberg, E.W. Kwock, T.M. Miller, *Phys. Rev. Lett.*, **75**, 1992 (1995)
- [18] M. Yan, L.J. Rothberg, F. Papadimitrakopoulos, M.E. Galvin, T.M. Miller, *Phys. Rev. Lett.*, **72**, 1104 (1994)
- [19] M. Yan, L.J. Rothberg, B.R. Hsieh, R.R. Alfano, *Phys. Rev. B*, **49**, 9419 (1994)
- [20] W. Graupner, G. Leising, G. Lanzani, M. Nisoli, S. de Silvestri, U. Scherf, *Phys. Rev. Lett.*, **76**, 847 (1996)
- [21] T. Pauck, R. Henning, M. Perner, U. Lemmer, U. Siegner, R.F. Mahrt, U. Scherf, K. Müllen, H. Bässler, E.O. Göbel, *Chem. Phys. Lett.*, **244**, 171 (1995)
- [22] N. Tessler, G.J. Denton, R.H. Friend, *Nature*, **382**, 695 (1996)
- [23] F. Hide, M.A. Díaz-García, B.J. Schwartz, M.R. Andersson, Q. Pei, A.J. Heeger, *Science*, **273**, 1833 (1996)
- [24] H.J. Brouwer, V.V. Krasnikov, A. Hilberer, G. Hadziioannou, *Adv. Mater.*, **8**, 935 (1996)

- [25] G.H. Gelinck, J.M. Warman, M. Remmers, D. Neher, *Chem. Phys. Lett.*, **265**, 320 (1997)
- [26] S.V. Frolov, W. Gellermann, Z.V. Vardeny, M. Ozaki, K. Yoshino, *Synth. Met.*, **84**, 471 (1997)
- [27] G.J. Denton, N. Tessler, M.A. Stevens, R.H. Friend, *Adv. Mater.*, **9**, 547 (1997)
- [28] R.E. Gill, Design, synthesis and characterization of luminescent organic semiconductors (Ph.D. thesis, University of Groningen, 1996), chapter 3
- [29] A. Hilberer, J. Wildeman, H.J. Brouwer, F. Garten, G. Hadziioannou, *Spie Proceedings*, **2528**, 74 (1995)
- [30] P.W. Milonni, J.H. Eberly, *Lasers* (John Wiley & Sons, New York, 1988), 288 and 399
- [31] A.E. Siegman, *Lasers* (University Science book, Mill Valley CA, 1986), chapter 13
- [32] H. Kogelnik, Topics in applied optics: integrated optics (Springer-Verlag, Berlin, 1979), chapter 2
- [33] J.W. Swatos, B. Gordon III, *Polym. Prep.*, **31**, 505 (1990)
- [34] B.R. Hsieh, H. Antoniadis, D.C. Bland, W.A. Feld, *Adv. Mater.*, **7**, 36 (1995)
- [35] S.V. Frolov, W. Gellermann, M. Ozaki, K. Yoshino, Z.V. Vardeny, *Phys. Rev. Lett.*, **78**, 729 (1997)
- [36] S.V. Frolov, M. Ozaki, W. Gellermann, M. Shkunov, Z.V. Vardeny, K. Yoshino, *Synth. Met.*, **84**, 473 (1997)
- [37] R. Bonifacio, L.A. Lugatio, *Phys. Rev. A*, **11**, 1507 (1975)
- [38] R.G. Kepler, V.S. Valencia, S.J. Jacobs, J.J. McNamara, *Synth. Met.*, **78**, 227 (1996)
- [39] G.J. Denton, N. Tessler, N.T. Harrison, R.H. Friend, *Phys. Rev. Lett.*, **78**, 733 (1997)
- [40] M.A. García-Díaz, F. Hide, B.J. Schwartz, M.D. McGehee, M.R. Andersson, A.J. Heeger, *Appl. Phys. Lett.*, **70**, 3191 (1997)
- [41] N.C. Greenham, I.D.W. Samuels, G.R. Hayes, R.T. Phillips, Y.A.R.R. Kessner, S.C. Moratti, A.B. Holmes, R.H. Friend, *Chem. Phys. Lett.*, **241**, 89 (1995)
- [42] S.E. Burns, N.C. Greenham, R.H. Friend, *Synth. Met.*, **76**, 205 (1996)
- [43] B.J. Schwartz, F. Hide, M.R. Andersson, A.J. Heeger, *Chem. Phys. Lett.*, **265**, 327 (1997)
- [44] X. Long, A. Malinowski, D.D.C. Bradley, M. Inbasekaran, E.P. Woo, *Chem. Phys. Lett.*, **272**, 6 (1997)
- [45] D. Braun, D. Moses, C. Zhang, A.J. Heeger, *Appl. Phys. Lett.*, **61**, 3902 (1992)

## Chapter 5

# Stimulated emission from single crystals and vacuum-deposited thin films of a substituted oligo(*p*-phenylene vinylene)<sup>†</sup>

### Abstract

*Stimulated emission from both single crystals and vacuum-deposited polycrystalline thin films of a substituted 5-ring PPV oligomer has been demonstrated. In the case of the polycrystalline vacuum-deposited films, Amplified Spontaneous Emission ASE occurs within the individual crystalline domains and was only observed if the domain size was increased by annealing or recrystallization from the melt. The amplification length is restricted by the size of the crystalline domains due to high optical losses (scattering) from the crystallite boundaries. The threshold for mirrorless lasing for an individual crystalline domain is comparable to that for conjugated polymer films if the domain size is sufficiently large, as demonstrated in the recrystallized Oct-OPV5 films.*

---

<sup>†</sup> H.J. Brouwer, V.V. Krasnikov, T.-A. Pham, R.E. Gill, P.F. van Hutten, G. Hadziioannou, *Chem. Phys.* in press  
H.J. Brouwer, V.V. Krasnikov, T.-A. Pham, R.E. Gill, G. Hadziioannou, submitted to *Appl. Phys. Lett.*

## 5.1 Introduction

The generation of laser light under pulsed optical excitation, using conjugated polymers as active medium, has been demonstrated in solution [1,2], dilute blends [3] and more recently in neat thin films [4-8]. Our efforts concerning lasing from alternating PPV copolymers are described in chapter 3 (solution) and chapter 4 (thin films) of this thesis. The reported stimulated emission from photopumped neat polymer films is an important observation, which shows that singlet intrachain excitons, which are thought to be responsible for light emission (see [9] for a recent review), can be generated with high yields in the condensed phase. It is well-established that electroluminescence from polymer diodes originates from the same excited states as created by photoexcitations (PL and EL spectra are in the majority cases identical) and this makes one envisage the possible development of an electrically pumped polymer laser. The two proposed photophysical processes responsible for the observed net gain in photopumped neat polymer films without external feedback system are ordinary Amplified Spontaneous Emission (ASE) [7,10] and Superfluorescence (SF) [6] with its more subtle temporal characteristics. Also the combination of the two processes (co-existing in competition with each other) was suggested to explain the emission narrowing [11]. The structural complexity of polymers due to chemical and structural imperfections (conformational defects/mislinkages/saturated sites/molecular weight distributions/presence of end-groups) and the poorly defined microstructure in polymer films makes it difficult to identify the precise mechanism for the observed narrowing and to reconcile all reported studies. Detailed knowledge about the precise molecular structure of conjugated polymers and the structural organization of these polymers in thin films is of great importance for a better understanding of the underlying photophysics and structure/properties relationships.

An important question to be answered is whether or not it is possible to obtain electrically induced net gain. Based on the lasing threshold under optical excitation, it is estimated [4] that current densities in excess of  $10^3 \text{ A cm}^{-2}$  are needed to establish net gain in such devices, which is substantially higher than currently achieved in polymer LEDs. The low current densities in polymer LEDs, especially for electron transport, are the result of the low charge carrier mobilities, high trap densities and poor charge injection in conjugated polymers. However, electroluminescence (EL) of a 3 nm thick PPV film by tunnelling injection from a scanning tunnelling microscope (STM) tip with current densities of the order of  $10^4 \text{ A cm}^{-2}$  has been reported recently [12]. Despite the extreme circumstances, an ultrathin film (3 nm) in combination with a nanometer-sized cathode (end of the STM tip, area roughly  $1 \text{ nm}^2$ ), it indicates that light emission at high current densities is possible in polymer films.

Conjugated oligomers can be considered as an interesting alternative. They can serve as models for their parent polymers or chain segments thereof [13-17], due to the

precise control of conjugation length and chemical structure in combination with the ability of crystallization into well-ordered molecular crystals. This allows structural information to be obtained from X-ray diffraction data, which is useful as a guide for interpreting polymer diffraction data [18,19]. In the case of PPV oligomers, the optical properties (wavelength of absorbance, luminescence and photoconductivity maxima) as a function of the number of repeat units ( $n-1$ , where  $n$  is the number of phenyl rings in the backbone) are converging to that of the corresponding fully conjugated PPV polymer at the five ring level ( $n = 5$ ) [14-16]. Additionally, it is well-known that ordered conjugated organic materials exhibit low trap densities and high charge carrier mobilities, for both electrons and holes. As an example, in single crystals of anthracene [20] the hole and electron mobilities are approximately  $1 \text{ cm}^2\text{V}^{-1}\text{s}^{-1}$  and the crystal photoluminescence (PL) quantum yield at room temperature is almost unity. Both electroluminescence [20] and optically induced lasing [21] have been demonstrated in anthracene single crystals. From application point of view, organic single crystals are rather inconvenient, because perfect crystals are difficult to grow, hard to handle and have relatively large dimensions (typical thickness around 1 - 100  $\mu\text{m}$ ). The possibility to process oligomers into high-purity polycrystalline thin films by vacuum deposition allows the desired geometry for LED applications [22,23] to be realized. However, it is evident that the optical quality of polycrystalline films is rather poor due to scattering from grain boundaries, which is particularly disadvantageous for laser applications. Additionally, grain boundaries also have a negative impact on the electrical properties of such films. Hence, under any circumstances sufficiently large, crystalline domains are required.

In this chapter we describe the emission properties of both solution-grown single crystals and vacuum-deposited thin films of an all-*trans* 5-ring *n*-dioctyloxy-substituted oligo(*p*-phenylene vinylene)s under intense laser excitation. The morphology of the thin films was varied by annealing just below the first melting point and by recrystallization from the isotropic melt. In this way the crystalline domain size could be varied from a few microns up to several millimetres in the latter case. In both single crystals and thin films, mirrorless lasing has been observed. Stimulated emission in the polycrystalline thin films was only observed after the domain size was increased by thermal treatment.

## 5.2 Experimental

Optical microscopy pictures were taken on an Zeiss Photomicroscope. UV-vis spectra were obtained on a SLM Aminco 3000 Array spectrophotometer. Luminescence spectra were recorded on a Perkin Elmer LS50-B spectrofluorometer. Absolute luminescence quantum yields of the vacuum-deposited films and solution-grown single crystals were determined in a calibrated integrating sphere and luminescence

decay measurements were made by time-correlated single-photon counting as described in chapter 2. The lasing experiments were performed in an integrating sphere, with the third harmonic of a Nd:YAG laser (Quanta-Ray GRC 130-50,  $\lambda = 355$  nm, pulse width 15 ns, repetition rate 1 Hz) as photoexcitation source. Neutral density filters were used to attenuate the excitation energy. The vacuum-deposited films and single crystals were excited under normal incidence. The emitted light emerging from the sample was detected by an Optical Multichannel Analyzer (Chromex 250 SI polychromator with Chromcam I CCD detector). All optical measurements were performed under vacuum (glass cell, static vacuum better than  $10^{-4}$  mbar) unless otherwise stated.

### 5.3 Results and discussion

The synthesis and characterization of the all-*trans* 5-ring oligo(*p*-phenylene vinylene) (abbreviated as Ooct-OPV5) as well as the single-crystal structure [24] and the X-ray diffraction data of the thin-film morphologies are given in the Ph.D. thesis of R.E. Gill [25]. All solid-state optical properties of Ooct-OPV5 are described in more detail in chapter 2 of this thesis. For the sake of clarity a short description of the single-crystal structure and the thin-film morphologies is given in this section. The molecular structure of the oligomer is depicted in figure 5.1. The oligomer has a nematic liquid crystalline phase between 183 °C (crystal-mesophase transition, 77 J/mmol) and 204 °C (mesophase-isotropic transition, 0.98 J/mmol).

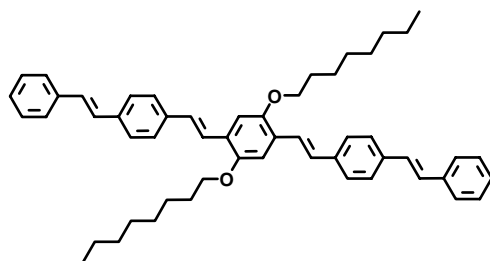


**Figure 5.1** Chemical structure of Ooct-OPV5.

The oligomer is soluble in common organic solvents like chloroform and tetrahydrofuran and yellow needle-shaped single crystals were obtained when the oligomer crystallized from a THF/methanol solution. The unit cell of the Ooct-OPV5 solution-grown single crystals is monoclinic, space group  $I2/a$ , and contains eight discrete molecules separated by normal van der Waals distances. Thin films were prepared by slow evaporation from a molybdenum boat just above the melting point (290 °C) and at a pressure of  $10^{-6}$  mbar, with the glass substrate positioned about 10 cm above the boat. Optical microscopy (crossed polarizers) and Atomic Force

Microscopy showed that the as-deposited oligomer films were pinhole-free and exhibited a granular structure, indicating some extent of crystallinity. Optical micrographs (crossed polarizers) of all different thin-film morphologies are shown in chapter 2 of this thesis. Annealing the film at a temperature of 120 °C resulted in a morphological change, which was irreversible. This morphological change occurred below the first melting point of the oligomer and manifested itself in an increase of the crystal domain size from approximately 4  $\mu\text{m}$  to 20  $\mu\text{m}$ . X-ray diffraction studies on the as-deposited and annealed films confirmed the enhanced molecular order and the increase in crystal domain size upon annealing. The crystalline domains were found to be oriented with the *ab*-axis standing up on the substrate. The crystalline structures of the single crystal, the as-deposited and the annealed film differ slightly from each other. The existence of different crystalline forms is attributed to the compressibility of the aliphatic layer (side chains) between the conjugated backbone, resulting in a deformability of the unit cell [25].

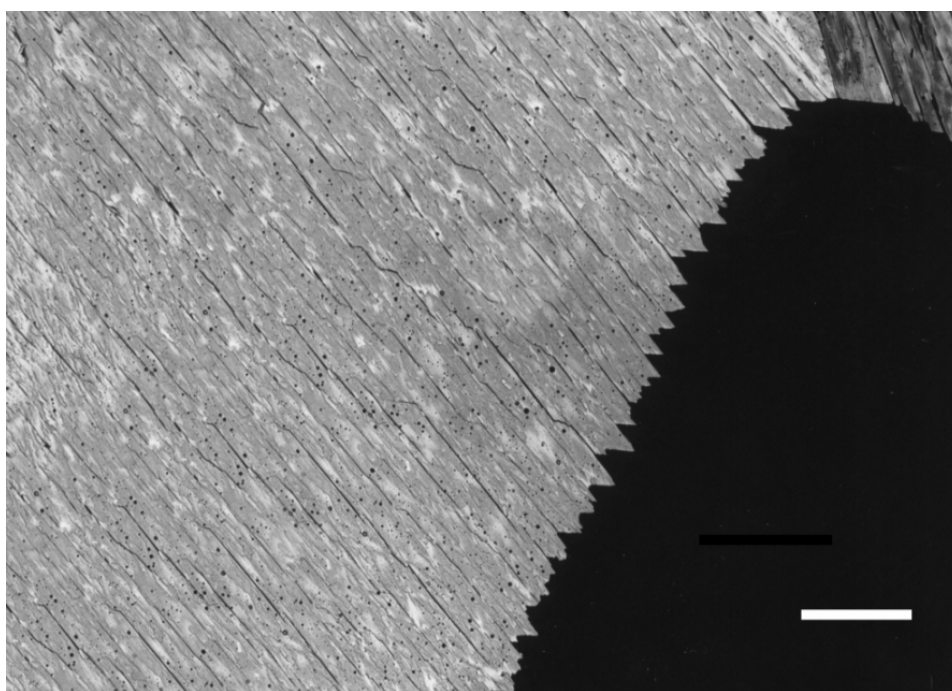


**Figure 5.2** Optical micrograph (crossed polarizers) of a thin film of Ooct-OPV5, obtained after slow cooling from the isotropic melt. Scale bar: 250  $\mu\text{m}$ .

Heating the film to the isotropic melt (210 °C) and subsequent slow cooling resulted in a different morphology. Large domains were formed with dimensions up to several millimeters. In figure 5.2 an optical micrograph (crossed polarizers) of a recrystallized

Ooct-OPV5 film is shown. The highly birefringent domains consisted of small bundles running parallel to the substrate. An in-plane dichroic ratio of approximately  $D = A_{\parallel}/A_{\perp} \approx 30$  was determined from polarized absorption spectra recorded within one domain. Additionally a dichroic ratio in luminescence emission of  $I_{\parallel}/I_{\perp} = 20 \pm 10$  was measured, both ratios indicate a high degree of orientation of the conjugated backbones. The exact microstructure of this morphology has not yet been revealed.

### *Single crystals*

We have recorded emission spectra as a function of excitation energy from single crystals and thin films of Ooct-OPV5 photoexcited with ns pulses from a frequency tripled Nd:YAG laser ( $\lambda = 355$  nm). Our efforts were mainly focused on thin films, because of the possibility to make light emitting diodes out of them eventually in a later stage. The solution-grown single crystals were tried in first instance to check whether or not it was possible to generate stimulated emission in crystalline Ooct-OPV5, because of their large dimensions (millimeter-sized) and reasonable optical quality.

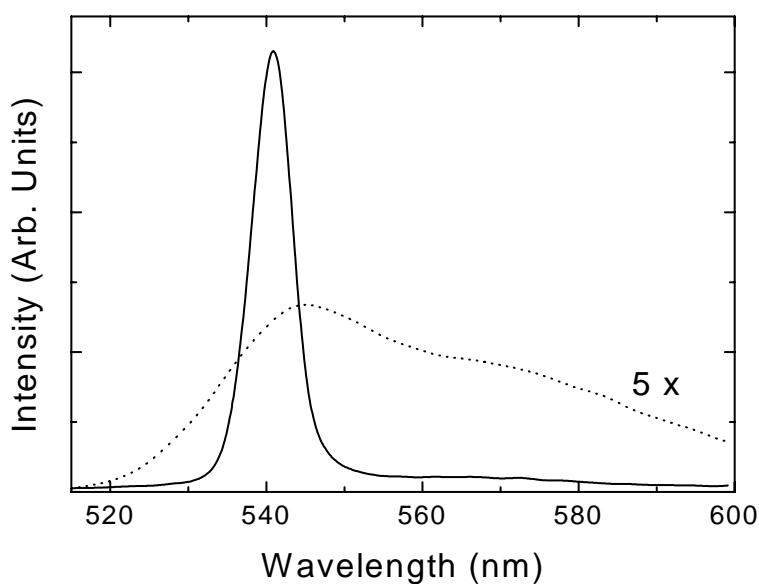


**Figure 5.3** Emission spectra of a solution-grown single crystal of Ooct-OPV5. Excitation energy: 0.2 mJ (dotted line, scaled for clarity) and 0.5 mJ (solid line). Excitation spotsize  $\approx 0.5$  mm.

The emission spectra of a 30  $\mu\text{m}$  thick solution-grown single crystal at low and high excitation energy are shown in figure 5.3. The solution-grown single crystals showed spectral behaviour similar to that of SiPPV and Ooct-PPV as described in the preceding chapter. Above an excitation threshold, which depended on the illumination spot size, ASE with a spectral bandwidth of 6 nm (FWHM) was observed, centred at 540 nm, in close proximity of the fluorescence maximum. The broad luminescence tails were almost fully suppressed at high excitation energy ( $I_{(\text{ASE}, 540 \text{ nm})}/I_{(\text{luminescence}, 560 \text{ nm})} > 100$  at  $E_{\text{ex}} = 0.5 \text{ mJ}$ ). The intense emission was mainly emerging from the edge faces of the crystal. The observed behaviour is typical for organic single crystals with high PL quantum yield and was already reported a long time ago for anthracene [19]. It should be stated that the threshold and intensity dependence for optical pumping is highly dependent on the quality of the crystals, the perfection of the facets, and the crystal thickness, which resulted in reasonably large crystal-to-crystal variations. The solution-grown Ooct-OPV5 single crystals on the average were far from perfect, due to thickness variations, defects and damage (small cracks) resulting from handling. Especially the larger crystals had a larger quantity of growth defects. Attempts to cleave the Ooct-OPV5 single crystals in a controlled way, to obtain thinner crystals with improved optical quality failed, due to the relative softness of the crystals resulting from the presence of long aliphatic side chains.

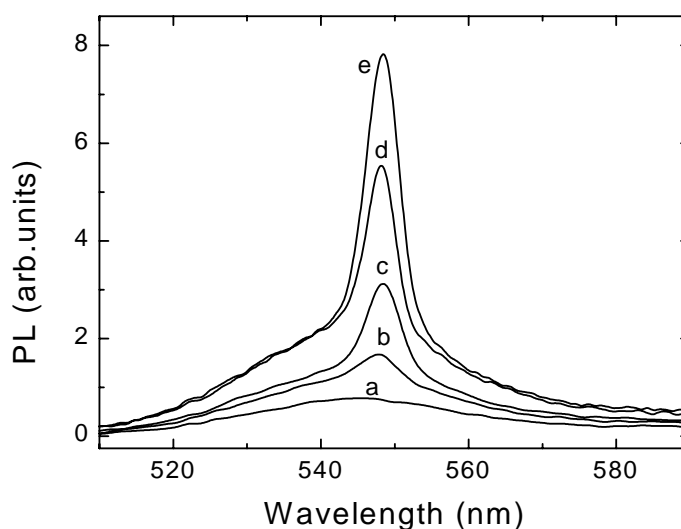


**Figure 5.4** Emission spectra of an annealed thin (300 nm) film of Ooct-OPV5. Excitation energy: (a) 0.9, (b) 1.6, (c) 2.1, (d) 3.1 and (e) 3.9 mJ, excitation beam diameter  $\approx 1.8 \text{ mm}$ .

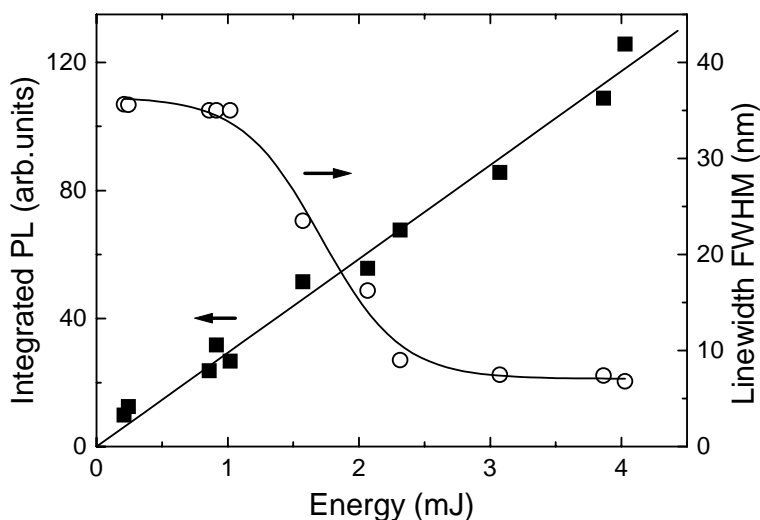


**Figure 5.5** Integrated PL ( $\circ$ ) and linewidth ( $\bullet$ ) as a function of excitation energy for an annealed thin (300 nm) film of Ooct-OPV5.

#### *Vacuum-deposited films*

For the study of the different thin-film morphologies, films with a thickness of 300 nm were prepared by vacuum deposition onto glass substrates. The as-deposited films showed no spectral narrowing at any pump energy up to the damage threshold. After annealing the film at 120 °C for 5 minutes under vacuum, ASE was observed in the same film. A set of emission spectra as a function of excitation energy collected from this annealed Ooct-OPV5 film is shown in figure 5.4. The integrated intensity of all light emerging from the film (measured in an integrated sphere) and the emission linewidth (FWHM) as a function of excitation energy are plotted in figure 5.4. At low excitation energy only the ordinary luminescence spectrum was observed. Above an energy threshold of approximately 1.6 mJ, a sharp emission peak appeared with a bandwidth of  $\approx 7$  nm centred around 548 nm (0-1 transition). The amplitude of the peak intensity scaled superlinear with excitation energy and the linear dependence of the integrated intensity depicted in figure 5.5 strongly supports that there is energy redistribution within the emitted light. The shift in emission wavelength compared to the Ooct-OPV5 single crystals can be attributed to the difference in crystal packing, which alter the emission properties (see chapter 2). It is evident from figure 5.4 that the suppression of the broad luminescence tails (ratio  $I_{\text{ASE}}/I_{\text{Lum}} \approx 5$ ) is substantially weaker than that observed with the solution-grown single crystals. The spot-to-spot

reproducibility of the measured characteristics was good, and we could measure up to excitation energies of 4 mJ without visual damage of the illuminated spot. Lasing was not observed in annealed films of 100 nm thickness, which indicated that waveguiding inside the domains is crucial.

The energy threshold for linewidth collapse is approximately 1.6 mJ with a round excitation spot size of  $\approx 1.8$  mm, which corresponds to a threshold pump fluence of  $63 \text{ mJ.cm}^{-2}$  and a pump intensity of  $7.10^{24} \text{ photons.cm}^{-1}.\text{s}^{-1}$ . This threshold value is three orders of magnitude higher than that reported for PPV's [4,6-8,11]. This can be attributed to the polycrystalline structure of the thin films. We believe that laser generation in the annealed films occurs only within the individual single crystal domains, which on the average have dimensions of approximately  $20 \mu\text{m}$ . Scattering at grain boundaries likely results in high optical losses, which prevents sufficient net gain to be realized over multiple domains. Hence, the amplification length is restricted by the size of the individual crystalline domains. The domain size in as-deposited films, approximately  $4 \mu\text{m}$ , is too small to achieve significant gain at all. Based on this argument one should expect that the threshold fluence for linewidth collapse in the case of the annealed Oct-OPV5 films remains constant if the excitation spot size is decreased (up to a diameter comparable to the crystalline domain size  $\approx 20 \mu\text{m}$ ). This was checked experimentally by putting an adjustable iris before the focusing lens to vary the excitation spot size, while maintaining approximately the same excitation fluence. A reduction of the excitation spot size from 1.8 mm (pump energy 3 mJ) to 1 mm did not alter the shape of the emission spectrum significantly and the same magnitude of amplification was observed. This confirmed that the interaction length was significantly smaller than the diameter of the excited area. This behaviour differed significantly from that observed for neat copolymer films (chapter 4). In that case a reduction of the spot size resulted in a large decrease of the magnitude of amplification, indicating that the interaction length was equal to the diameter of the excited area.

Additionally, a much smaller area of the films was excited by focussing the pump beam to a spot size with a diameter of approximately  $30 \mu\text{m}$ . With such a beam size only a few single crystal domains are excited, at the most. Sample alignment was found to be crucial with such a small spot size. Mirrorless laser generation was not observed at each spot excited on the sample and the magnitude of spectral narrowing varied highly from spot to spot, indicating that the excitation beam should be well aligned above a crystalline domain. The best results obtained from these experiments at low and high excitation energy (6 and 180  $\mu\text{J}$ , respectively) are shown in figure 5.6. Note that both spectra are recorded at excitation energies above the threshold for spectral narrowing. Furthermore, restricting the excitation area to only a few domains appears to result in a more pronounced suppression of the broad luminescence tail. The threshold fluence estimated from these experiments is roughly  $100\text{-}200 \text{ mJ.cm}^{-2}$ , which is a few times higher than obtained with an excitation spot size of 1.8 mm. The

excitation threshold observed in the experiments using a spot diameter of 1.8 mm is an average value over roughly 8000 crystal domains. Also the shape of the time-averaged emission spectra is determined by this. It is obvious that with a spot diameter of roughly the size of a crystalline domain, the chance to locate the most optimum domain is extremely small, which explains the discrepancy between the threshold values.

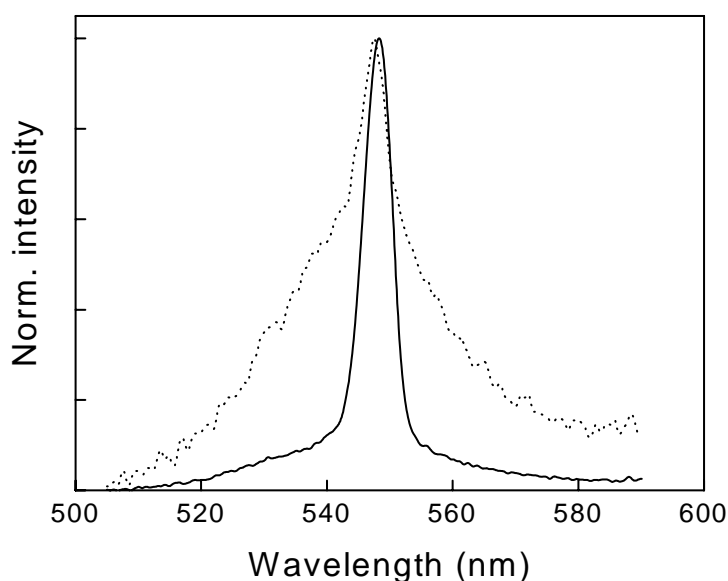


**Figure 5.6** Emission spectra recorded from an annealed Ooct-OPV5 film using a smaller excitation spot size (diameter  $\approx 30 \mu\text{m}$ ). Excitation energy:  $6 \mu\text{J}$  (dotted line) and  $180 \mu\text{J}$  (solid line).

It is evident from all these experiments that it is possible to generate ASE in thin films of the model oligomer Ooct-OPV5, but that the amplification length is restricted by the size of the crystalline domains. Increasing the domain size will likely result in excitation thresholds for ASE comparable to that reported for conjugated polymer films [4,6-8,11], which are typically in the range of  $10 \mu\text{J}\cdot\text{cm}^{-2}$  to a few hundred  $\mu\text{J}\cdot\text{cm}^{-2}$ , using ns pulses. This was checked experimentally with Ooct-OPV5 films recrystallized from the isotropic melt. Recrystallization of the films resulted in the formation of large domains with dimensions up to several millimeters. The normalized emission spectra for different excitation energies for a recrystallized film are shown in figure 5.7. The excitation spot diameter was 1 mm in these experiments and the beam was focused within one domain. The domains were excited with the pump light

polarized parallel to the molecular axis. The O.D. at 355 nm for the recrystallized films was approximately twice as high of that for the annealed film. The lowest measured energy threshold for linewidth collapse was approximately  $4 \mu\text{J}$  corresponding to a threshold fluence of  $\approx 500 \mu\text{J}\cdot\text{cm}^{-2}$ , which is substantially lower than that measured for the annealed films and cannot be explained only on the basis of the difference in optical density with respect to the annealed film.

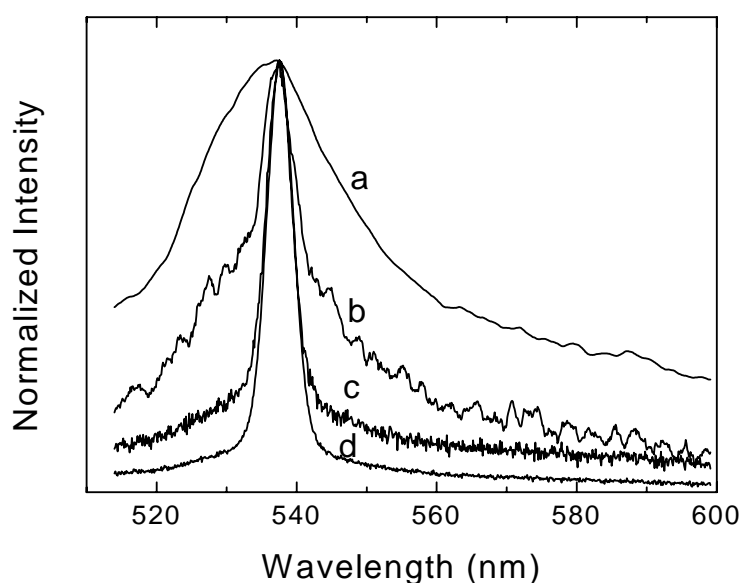


**Figure 5.7** Normalized emission spectra of a recrystallized thin (300 nm) film of Oct-OPV5. Excitation energy: (a) 1, (b) 10, (c) 50 and (d) 70  $\mu\text{J}$ , excitation beam diameter  $\approx 1 \text{ mm}$ .

The energy threshold was dependent on the excitation spot size at constant pump intensity, which indicated that amplification occurred over the whole illuminated area. It should be stated that despite the large domains, the optical quality within the domains is less than that of the annealed films. This gives rise to additional scattering losses which decreases the magnitude of the amplification.

#### 5.4 Conclusions and outlook

In conclusion, stimulated emission from both single crystals and vacuum-deposited polycrystalline thin films of a substituted 5-ring PPV oligomer has been demonstrated.

In the case of the polycrystalline vacuum-deposited films, ASE occurs within the individual crystalline domains and was only observed if the domain size was increased by annealing or recrystallization from the melt. The amplification length is restricted by the size of the crystalline domains due to high optical losses (scattering) from the crystallite boundaries. The threshold for mirrorless lasing for an individual crystalline domain is comparable to that for conjugated polymer films if the domain size is sufficiently large, as demonstrated in the recrystallized Ooct-OPV5 films ( $\approx 500 \mu\text{J}\cdot\text{cm}^2$ ). Current research efforts are directed towards the preparation of Ooct-OPV5 thin films consisting of large domains with a higher degree of perfection.

## 5.5 References

- [1] D. Moses, *Appl. Phys. Lett.*, **60**, 3215 (1992)
- [2] H.J. Brouwer, V.V. Krasnikov, A. Hilberer, J. Wildeman, G. Hadziioannou, *Appl. Phys. Lett.*, **66**, 3404 (1995)
- [3] F. Hide, B.J. Schwartz, M.A. Díaz-García, A.J. Heeger, *Chem. Phys. Lett.*, **256**, 424 (1996)
- [4] F. Hide, M.A. Díaz-García, B.J. Schwartz, M.R. Andersson, Q. Pei, A.J. Heeger, *Science*, **273**, 1833 (1996)
- [5] N. Tessler, G.J. Denton, R.H. Friend, *Nature*, **382**, 695 (1996)
- [6] S.V. Frolov, W. Gellermann, M. Ozaki, K. Yoshino, Z.V. Vardeny, *Phys. Rev. Lett.*, **78**, 729 (1997)
- [7] H.J. Brouwer, V.V. Krasnikov, A. Hilberer, G. Hadziioannou, *Adv. Mater.*, **8**, 935 (1996)
- [8] G.H. Gelinck, J.M. Warman, M. Remmers, D. Neher, *Chem. Phys. Lett.*, **265**, 320 (1997)
- [9] R.H. Friend, G.J. Denton, J.J.M. Halls, N.T. Harrison, A.B. Holmes, A. Köhler, A. Lux, S.C. Moratti, K. Pichler, N. Tessler, K. Towns, H.F. Wittmann, *Solid State Commun.*, **102**, 249 (1997)
- [10] G.J. Denton, N. Tessler, M.A. Stevens, R.H. Friend, *Adv. Mater.*, **9**, 547 (1997)
- [11] X. Long, A. Malinowski, D.D.C. Bradley, M. Inbasekaran, E.P. Woo, *Chem. Phys. Lett.*, **272**, 6 (1997)
- [12] D.G. Lidzey, D.D.C. Bradley, S.F. Alvarado, P.F. Seidler, *Nature*, **386**, 135 (1997)
- [13] Z. Yang, H.J. Geise, M. Mehdod, G. Debrue, J.W. Visser, E.J. Sonneveld, L. van't Dack, R. Gijbels, *Synth. Met.*, **39**, 137 (1990)
- [14] A. Ohlemacher, R. Schenk, H.P. Weitzel, N. Tyutyulkov, M. Tasseva, K. Müllen, *Makromol. Chem.*, **193**, 81 (1992)
- [15] H.S. Woo, O. Lhost, S.C. Graham, D.D.C. Bradley, R.H. Friend, C. Quattrocchi, J.L. Brédas, R. Schenk, K. Müllen, *Synth. Met.*, **59**, 13 (1993)
- [16] H.E. Katz, S.F. Bent, W.L. Wilson, M.L. Schilling, S.B. Ungashe, *J. Am. Chem. Soc.*, **116**, 6631 (1994)
- [17] H. Kretzschmann, H. Meier, *J. Prakt. Chem.*, **336**, 247 (1994)

- [18] J.K. Herrema, J. Wildeman, F. van Bolhuis, G. Hadziioannou, *Synth. Met.*, **60**, 239 (1993)
- [19] A. Yassar, F. Garnier, F. Deloffre, G. Horowitz, L. Ricard, *Adv. Mater.*, **6**, 661 (1994)
- [20] M. Pope, C.E. Swenberg, *Electronic processes in organic crystals* (Clarendon press, Oxford, 1982)
- [21] O.S. Avanesjan, V.A. Benderskii, V. Brikenstein, V.L. Broude, L.I. Korshunov, A.G. Lavrushko, I.I. Tartakovskii, *Mol. Cryst. Liq. Cryst.*, **29**, 165 (1973)
- [22] G. Gustafson, C.M. Treacy, Y. Cao, F. Klavetter, N. Colameri, A.J. Heeger, *Synth. Met.*, **55**, 4123 (1993)
- [23] G. Horowitz, P. Delannoy, H. Bouchriha, F. Deloffre, J.L. Fave, F. Garnier, R. Hajlaoui, M. Heyman, F. Kouki, P. Valat, V. Wintgens, A. Yassar, *Adv. Mat.*, **6**, 752 (1994)
- [24] R.E. Gill, A. Meetsma, G. Hadziioannou, *Adv. Mater.*, **8**, 212 (1996)
- [25] R.E. Gill, *Design, synthesis and characterization of luminescent organic semiconductors* (Ph.D. thesis, University of Groningen, 1996), chapter 3



## Chapter 6

# Light-Emitting Diodes based on alternating PPV copolymers and oligo(*p*-phenylene vinylene)s

### Abstract

*In this chapter the performance of several novel alternating PPV copolymers and 5-ring oligo(*p*-phenylene vinylene)s as active layer in LEDs are presented. The colour of emission of the copolymers and oligomers is varied by means of different substituents (cyano groups, alkyl/alkoxy side-chains), attached to the conjugated backbone, which alter the electronic structure of the molecules. Electroluminescence in the blue, green and orange wavelength region was achieved in single-layer devices with air-stable Al cathodes. The external electroluminescence efficiencies of all single-layer devices were found to be in the range of 0.01 to 0.03 % photons/electron, values comparable to those reported for fully conjugated PPVs. The influence of the thin-film morphology on LED performance has been investigated for the 5-ring oligomers. For Ooct-OPV5 a more than tenfold increase in efficiency was observed for devices consisting of an annealed active layer, which has been attributed to enhanced electron transport upon annealing.*

*Device optimization by means of additional charge-transport layers has been applied to enhance the electroluminescence efficiency. A novel polymer with oxadiazole-based side-chains has been used successfully as an electron-transport/hole-blocking layer. In combination with a PPV copolymer as the emissive layer, external EL efficiencies up to 0.1 % were obtained. The best-performing double-layer LEDs were based on the cyano-substituted copolymers and oligomers as the electron-transport/emissive layer. In this case, external electroluminescence efficiencies up to 0.4 % are reached.*

---

H.J. Brouwer, A. Hilberer, V.V. Krasnikov, M.P.L. Werts, G. Hadziioannou, *Synth. Met.*, **84**, 881 (1997)

## 6.1 Introduction

The most widely used semi-conducting polymers for application in light-emitting diodes are poly(*p*-phenylene vinylene) (PPV) and its derivatives, which have the highest luminescence efficiencies of all conjugated polymers. Their excellent emissive properties already have been demonstrated in chapter 3 in 4, where photopumped lasing of PPV polymers in solution and solid state has been described. After the introduction of Light-Emitting Diodes (LEDs) based on PPV in 1990 by Friend *et al.* [1], a lot of research in the field of semi-conducting polymers has been directed towards the development of new efficient polymeric emitters (for a recent review see [2,3]). A whole range of polymeric LEDs, emitting over the whole visible wavelength region from blue to red, has been reported [4,5]. Furthermore, the LED performance was greatly improved by means of additional charge-transport layers, which effectively balance the injection and transport of charges and move the e-h recombination zone away from the metal cathode [6]. Double-layer LEDs with high peak brightness and internal electroluminescence efficiencies up to 4 % [7] have been reported. Nevertheless, no commercial polymer LEDs has been manufactured yet. The long-term device stability and device efficiencies of polymer LEDs are rapidly increasing, but improvements are still desired, especially for polymers emitting in the blue wavelength region.

In conjugated polymers and oligomers, the overlap of  $\pi$ -orbitals provides a continuous system of electron density along the molecular backbone. The extent of this overlap (the so-called conjugation length) determines the HOMO-LUMO energy gap, which is, in general, found to be within the visible wavelength region. In conjugated homopolymers, the actual conjugation length is an average value determined principally by random conformational or chemical defects in the polymer backbone and is difficult to control. Our approach to controlling the conjugation length (described in chapter 1) and making the link between the luminescence properties of oligomers and those of polymers, is through alternating copolymers containing well-defined conjugated sequences with non-conjugated spacer units. This approach is particularly suitable for the design of blue-light emitters, which have a large HOMO-LUMO gap. This demands a high degree of control over the conjugation length. Furthermore, this approach can enhance the photo- and electroluminescence efficiency through confinement of the excitons to the conjugated blocks, which hinders the migration to quenching sites [8]. Braun *et al.* [9] showed that the PL efficiency increased with increasing fraction of the non-conjugated blocks in the backbone. Blue-light emitting devices with external efficiencies up to 0.7 % [10] were reported by our group with alternating SiPPV copolymers made according this concept.

PPV oligomers gained considerable interest, both as model compounds [11] and for application as active layer in LEDs [12,13]. They are highly fluorescent, have

a well-defined chemical structure and conjugation length and the ability to crystallize into well-ordered molecular crystals, which allows structural information to be obtained. Furthermore, they can be processed by vacuum deposition from the vapour phase into high-purity thin films. The morphology of the thin films can be controlled by means of adjustment of the substrate temperature during evaporation, or like in our case an annealing treatment after deposition. At low temperature the molecules stick where they collide, but at a substrate temperature close to the melting point of the oligomer, the molecules have sufficient thermal energy to diffuse and to minimize their structural energy, resulting in a more ordered packing. For example, in the case of  $\alpha$ -sexithiophene, this led to improved transport properties [14]. Furthermore, the control of molecular order allows the systematic investigation of the influence of thin-film morphology on LED performance.

In this chapter we evaluate the electrical and optical characteristics of light-emitting diodes based on alternating PPV copolymers and 5-ring oligo(*p*-phenylene vinylene)s. The colour of emission of the copolymers and oligomers is varied by means of different substituents (cyano, alkoxy), attached to the conjugated backbone, which alter the electronic structure of the molecules. Electroluminescence was achieved in the blue, green and orange wavelength region with single-layer devices consisting of transparent indium-tin-oxide anodes and air-stable Al cathodes. The efficiencies of the single-layer copolymer/oligomer LEDs are comparable to those reported for fully conjugated PPVs. Fowler-Nordheim tunnelling theory was used to analyse the current-voltage characteristics in order to determine the barriers for hole-injection in the single-layer devices. In combination with cyclic voltammetry and optical absorption measurements it was possible to estimate energy diagrams for all copolymers and oligomers, which could be used to describe the results obtained in a qualitative way. Furthermore, the influence of the thin-film morphology on LED performance has been investigated for the octyloxy-substituted oligo(*p*-phenylene vinylene).

Device optimization by means of additional charge-transport layers was applied to enhance the electroluminescence efficiency. A novel polymer with oxadiazole-based side-chains was used successfully as an electron-transport/hole-blocking layer, in a double-layer configuration with an orange-light-emitting PPV copolymer as the emissive layer. Also single-layer devices based on blends of the transport polymer and the PPV copolymer were studied.

The best-performing copolymer and oligomer double-layer devices were obtained by using an electronegative cyano-substituted PPV copolymer/oligomer as the electron-transport/emissive layer in combination with a hole-transport layer.

## 6.2. Experimental

### *Sample preparation*

Polymer light-emitting diodes (PLEDs) were fabricated by spincoating the copolymers from filtered (0.2  $\mu\text{m}$ -filters) chloroform solutions (3% w/w) onto 20  $\text{mm}^2$  ITO-covered glass slides (Merck Balzers AG, sheet resistance  $\leq 200\Omega/\square$ ). The ITO plates were ultrasonically cleaned in a series of nonpolar and polar solvents (*p*-xylene/2-propanol/ethanol) and rinsed in de-ionized water prior to use. By varying the rotation speed in the range of 700-2500 rpm, film thicknesses of 50-175 nm were obtained. The polymer films were dried for one hour at 40°C in a vacuum oven. Oligomer light-emitting diodes (OLEDs) were prepared by slow evaporation (pressure  $\approx 10^{-6}$  mbar, evaporation rate 2-4  $\text{\AA}/\text{s}$ ) of the compounds from a molybdenum boat just above their melting point, with the ITO plates positioned about 10 cm above the boat. The home-built evaporator was equipped with two separate sources, which enabled us to prepare double-layer devices in one run. Al or Au top electrodes (area:  $1 \times 9 \text{ mm}^2$ ) were deposited by evaporation (pressure  $< 2 \times 10^{-6}$  mbar, evaporation rate  $< 5 \text{ \AA}/\text{s}$ , thickness  $\approx 80 \text{ nm}$ ) through a shadow mask. The active area of the device  $1 \times 8 \text{ mm}^2$  is defined by the overlap of the ITO and the top metal electrode. Atomic Force Microscopy was used to monitor the quality of the copolymer and oligomer films. A Dektak 3030ST surface profiler was used to determine the layer thickness.

### *LED characterization*

Photo- and electroluminescence spectra of the thin-film devices were recorded on a SLM-Aminco SPF500C spectrofluorometer or Perkin-Elmer LS-50B. Absorbance spectra of the thin films were measured on a SLM-Aminco 3000 Array spectrophotometer.

Current-voltage (I-V) and luminance-voltage (L-V) measurements were performed in a dry-nitrogen atmosphere glove box to avoid exposure to ambient oxygen and water. I-V-measurements were taken with a Keithley 236 SMU operated in pulsed mode (low duty cycle,  $t_{\text{on}} = 100 \text{ ms}$  and  $t_{\text{off}} = 500 \text{ ms}$ ) to minimize heating effects. The external quantum efficiencies (number of emitted photons per injected electron) of the devices were determined by measuring the light output of the diodes vs. current with a calibrated photodiode mounted on an integrated sphere (LabSphere). A photon counter (Stanford Research SR400) was used to measure the photodiode output.

*Cyclic voltammetry*

Cyclic voltammetry was used to determine the oxidation potentials of the copolymers. The cyclic voltammetry measurements were performed on a Parc EG&G galvanometer using platinum working and counter electrodes and silver as the reference electrode in dichloromethane with tetrabutylammonium hexafluorophosphate as the electrolyte. The cyclovoltammograms were calibrated towards the normal hydrogen electrode (NHE) using the ferrocene/ferrocenium-ion couple as an internal standard [15,16].

*Electroabsorption measurements*

It is known that the work function of ITO is a poorly defined quantity, and that its value varies significantly (4.5–5.3 eV) [17,18] depending on the fabrication conditions and supplier. The built-in electric field in our metal/polymer(oligomer)/ITO diodes was determined via electroabsorption measurements [19], in order to obtain the work function of our ITO electrodes (Balzer A.G. Austria).

The electroabsorption response is proportional to the imaginary part of the third order susceptibility  $\text{Im}\chi^{(3)}(h\nu)$  and the square of the electric field.

$$\Delta\alpha(h\nu) \propto -\frac{\Delta T}{T}(h\nu) \propto \text{Im}\chi^{(3)}(h\nu)E^2 \quad (6.1)$$

where  $\alpha$  is the absorption coefficient,  $h\nu$  is the photon energy,  $T$  the transmission and  $E$  the electric field. The electroabsorption response to an applied AC bias is:

$$E = E_0 + E_{AC} \cos(\Omega t), \quad \Omega \cong 1 \text{kHz},$$

$$-\frac{\Delta T}{T}(h\nu) \propto \text{Im}\chi^{(3)}(h\nu)\{E_{AC}^2[1 + \cos(2\Omega t)]/2 + 2E_{AC}E_0 \cos(\Omega t) + E_0^2\} \quad (6.2)$$

where  $E_0$  is the static electric field and  $E_{AC}$  is the amplitude of the AC electric field. In the presence of a static electric field the, electroabsorption is modulated at both the fundamental and the second harmonic frequency of the applied AC voltage. The built-in electric field is measured by applying an external DC bias and finding the external potential at which the electroabsorption signal at the fundamental frequency vanishes. The built-in electric field, in a diode with a constant electric field throughout the device, will be equal to the difference in work function of the metal electrodes, if the work function of the metals lies within the HOMO-LUMO gap of the polymer/oligomer.

For these experiments single-layer diodes were prepared following the procedure described in the *sample preparation* section. The oligomer Ooct-OPV5 was used as active layer. Electrical measurements on several Al/Ooct-OPV5/ITO diodes with different Ooct-OPV5 layer thickness showed that the I-V-dependence scaled with the Ooct-OPV5 layer thickness (see section 6.3.2), which indicated that there is a constant electric field throughout the bulk. In figure 6.1 the electroabsorption response at  $\lambda = 510$  nm is shown for 200 nm thick Ooct-OPV5 films sandwiched between Al/ITO, Au/ITO and Al/Au electrodes. The Al/Ooct-OPV5/Au device was prepared by successive evaporation of the oligomer and Al counter electrodes onto a 40 nm thick semi-transparent Au layer on glass. The DC bias was referenced to the high work function contacts (ITO or Au). The DC bias of 1.0 Volts required to null the electroabsorption signal in the Al/Au diode corresponded closely to the difference in work function between the two metals ( $\phi_{\text{Al}} = 4.2\text{-}4.3$  eV and  $\phi_{\text{Au}} = 5.1\text{-}5.2$  eV) [20].

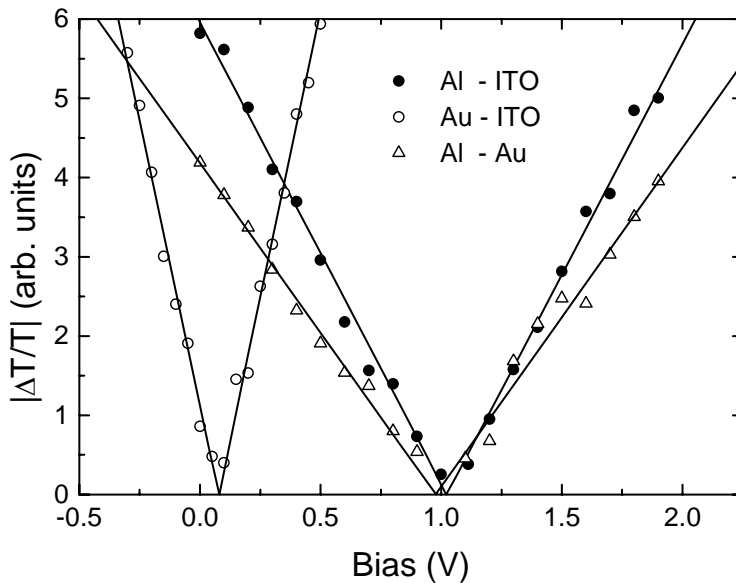


**Figure 6.1** Electroabsorption response at  $\lambda=510$  nm for 200 nm thick Ooct-OPV5 films sandwiched between Al/ITO, Au/ITO and Al/Au electrodes.

The DC biases to null the electroabsorption signal in the Al/ITO and Au/ITO devices were 1.0 and 0.1 Volts, respectively. From these measurements we determined a work function of  $\phi_{\text{ITO}} = 5.2 \pm 0.1$  eV for our ITO electrodes. The reproducibility of the electroabsorption measurements was good, and the same values for the ITO work

function were obtained from measurements with single-layer diodes made from the PPV based copolymers.

## 6.3 Results and discussion

### 6.3.1 Alternating PPV copolymers

A series of three alternating PPV copolymers containing substituted distyrylbenzene units as the light-emitting chromophores were used as active layer in LEDs. The chemical structures of the copolymers are depicted in figure 6.2. The substitution pattern (octyl/octyloxy side-chains and cyano groups on the vinylene linkages) in the copolymers was varied in order to tune the wavelength of emission. In such a way light emission from the blue to orange/red wavelength region was established. The synthesis and full characterization of the PPV copolymers are described in the references [21,22].

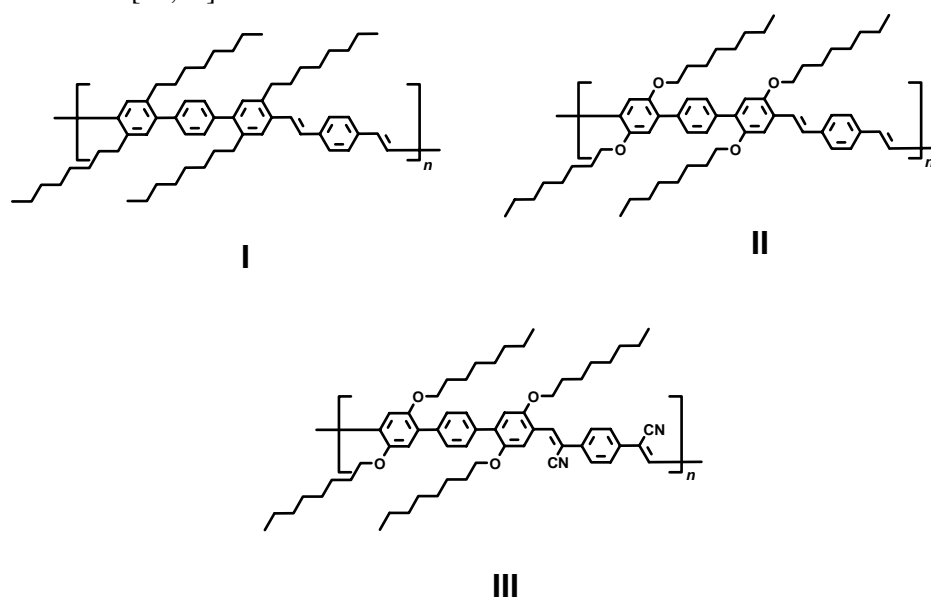


**Figure 6.2** Chemical structure of the copolymers.

The molar masses and the solid-state optical properties are summarized in table 6.1 (see also chapter two for more detail). The copolymers have a well-defined conjugated backbone consisting of regularly alternating terphenylene and *p*-phenylenebisvinylene blocks. The desired control of conjugation length was achieved through steric interactions between the side-chains and the rings within the terphenyl part of the copolymer. The octyl and octyloxy side chains in these polymers serve a

dual role: (1) interrupting the conjugation and (2) providing solubility. The middle rings in the terphenyl units are twisted out of plane, disabling the possibility of conjugation through the three consecutive phenyl rings. Thus, the conjugation of the fully unsaturated backbone is regularly interrupted, resulting in well-defined distyrylbenzene chromophores connected by non-coplanar phenylene groups. The copolymers show intense fluorescence in solution (0.4-0.9) as well as in the solid state. The films cast from copolymer **I** and **III** have photoluminescence efficiencies in the range of 30 – 40 %, whereas that from copolymer **II** has a substantially lower efficiency of  $\approx 9\%$  (see chapter 2 for more details).

**Table 6.1** Molar masses of the copolymers and absorption, emission and PL efficiency in solid state.

Copolymer	$M_w$ (g.mol <sup>-1</sup> ) <sup>a</sup>	$M_n$ (g.mol <sup>-1</sup> ) <sup>a</sup>	$\lambda_{Abs,max}$ (nm)	$\lambda_{Flu,max}$ (nm)	$\Phi_{Flu}$
<b>I</b>	5000	3000	355	445	0.4
<b>II</b>	39000	22000	418	485	0.09
<b>III</b>	7200	6500	450	592	0.4

a) Molecular weights obtained from reference [21,22]

LED devices were prepared as described in the experimental section. Analysis with Atomic Force Microscopy showed that the film surfaces were homogeneous and pinhole-free, with a surface roughness of a few percent of the total layer thickness. The electroluminescence spectra obtained from Al/copolymer/ITO devices are shown in figure 6.3. Copolymer **I**, in which the chromophore is an alkyl-substituted distyrylbenzene unit, emits in the blue (445 nm). The change of the type of side chains from alkyl to alkoxy (copolymer **II**) shifts the emission wavelength to the green (485 nm), due to the increased electron density of the  $\pi$ -system induced by the electron-donating alkoxy group. Alkoxy side chains in combination with cyano substituents (copolymer **III**) results in a red shift to the orange part of the spectrum (592 nm). It has been demonstrated that cyano groups on the vinylene linkage lower both the HOMO and LUMO level, but that the LUMO level is stabilized more, resulting in a red shift [7,23]. The HOMO-LUMO gaps for the copolymers **I** to **III** determined by the onset of absorption are 3.0, 2.6 and 2.3 eV, respectively.

All electroluminescence spectra of the copolymers coincided with the solid-state photoluminescence spectra. The photoluminescence spectrum of copolymer **III** is shown in figure 6.3 as an example. This implies that the excited states (created by charge injection) responsible for light emission in a PLED, are the same as those produced by photoexcitation.

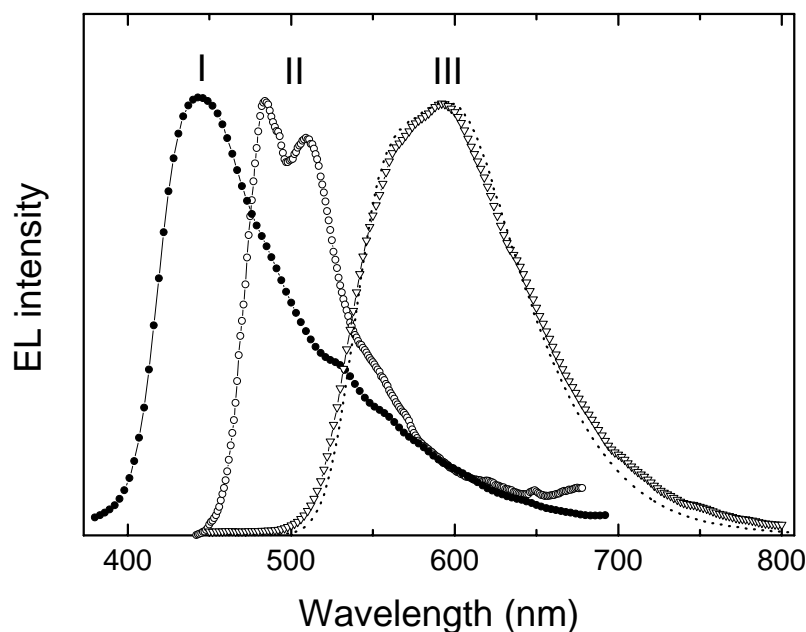


**Figure 6.3** Electroluminescence spectra of the copolymers (solid lines + symbols) and photoluminescence spectrum of copolymer III (dotted line).

In figure 6.4 the current density and luminance as a function of drive voltage in forward bias are shown for a single-layer ITO/copolymer I/Al device with a layer thickness of 80 nm (in table 6.2 the electrical characteristics and EL efficiencies of all single-layer devices are summarized). Forward bias is defined as the positive voltage on the hole-injecting ITO contact. Electron-injecting Al contacts were chosen for reasons of stability but have the disadvantage that they limit the electron-injection rates. This is due to the relatively large difference between the molecular LUMO-levels of the polymers and the work function of Al [17,24], resulting in a high injection barrier for electrons. Additionally, there is good evidence that holes are considerably more mobile than electrons in PPV polymers due to severe trapping of electrons [25] at electron-accepting impurities, related to oxygen (molecular oxygen, carbonyl moieties, etc.). This makes these polymers preferentially hole transporters. The unbalanced electron and hole currents, due to the low injection rate and poor transport of electrons in comparison with holes, has as a consequence that there is a large (hole) loss current. In addition, since the electrons are not able to move far into the bulk due to trapping, the electron-hole recombination zone is located close to the metal cathode of the device, which has the effect of quenching the emission. Single-

layer devices therefore have low EL efficiencies. The use of the low work function metal Ca [17,26] as electron-injecting contact will result in more balanced injection, higher efficiencies and lower operating voltages but has the drawback of being highly reactive under ambient conditions.

The LEDs with copolymer I as active layer (80 nm) started emitting light at a turn-on voltage of 15 Volts. This corresponds to an electric field strength ( $E=V/d$ ,  $d$  is the layer thickness) at turn-on of  $1.9 \times 10^8$  V/m (see top x-axis in figure 6.4). Turn-on voltage is defined here as the voltage at which the electroluminescence starts exceeding the background signal. It should be stated that the sensitivity for the detection of light of our set-up is low, due to the use of an integrating sphere. Only a small fraction of the photons emitted into the integrating sphere will reach the photodiode. So the turn-on voltage measured by our set-up is significantly higher as the voltage required to reach 'flat-band' conditions, which is the correct definition of the turn-on voltage [17]. The 'real' turn-on voltage is essentially independent of the layer thickness. In our case, we see a slight dependence of the turn-on voltage on the thickness of the active layer. This is due to the fact that we need to create a sufficiently large flux of photons to reach the lower detection limit of our set-up. So, the turn-on voltage obtained by our set-up also depends on the EL-efficiency of the LEDs and the quantum yield of the photodiode in the spectral region of emission.

Blue light, visible to the eye, was observed at drive voltages above 25 V. The emission was homogeneous over the whole active area at high drive voltages. The electroluminescence intensity increased linearly with drive current, and a maximum external EL-efficiency of  $2.3 \times 10^{-2}$  % ph/el was reached at a drive current of  $8 \times 10^{-2}$  A/cm<sup>2</sup>. The current-voltage characteristics of the devices scaled with layer thickness over the range of 50–175 nm, indicating that the electric field is uniformly distributed throughout the bulk and that significant band bending is absent at both metallic interfaces. The dependence of the device current on the electric field rather than the drive voltage is considered as evidence for field-emission tunnelling of charge carriers across an interfacial barrier [17].

A change of the electron-injecting metal from Al ( $\phi_{Al} = 4.3$  eV) to Au ( $\phi_{Au} = 5.2$  eV), resulted in light emission in forward bias at a much higher turn-on voltage of 24 Volts ( $E = 3.0 \times 10^8$  V/m). The external EL quantum efficiency of the diodes was  $\approx 3 \times 10^{-3}$  % ph/el. The I-V characteristics in forward and reverse bias were nearly symmetrical in the ITO/Au diodes, due to the small difference in work function between the opposite contacts. In reverse bias, light emission started at a turn-on voltage of -25 Volts. This observation supports the conclusion that field-driven electron injection determines the emissive properties of a polymer LED.

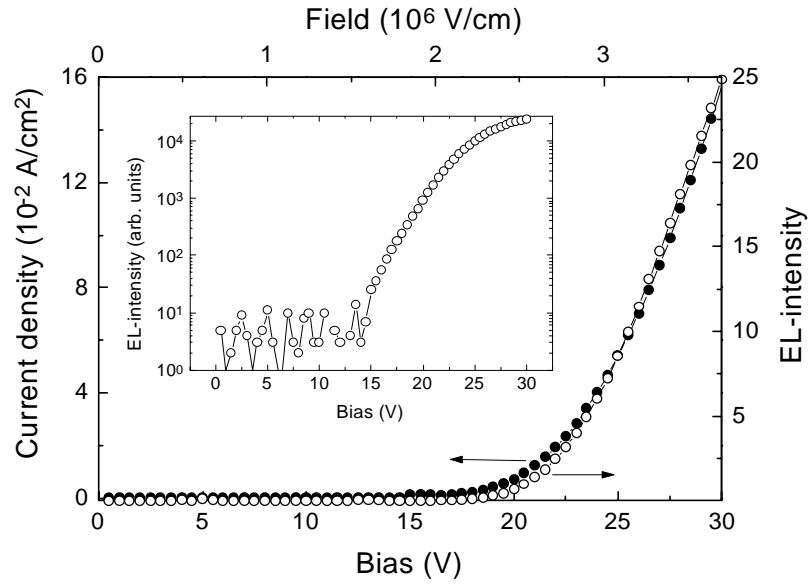


**Figure 6.4** Current density (closed circles) and luminance (open circles) of a single-layer ITO/copolymer I/Al device as a function of bias voltage. Layer thickness 80 nm. Inset: semilog plot of the luminance as a function of bias voltage.

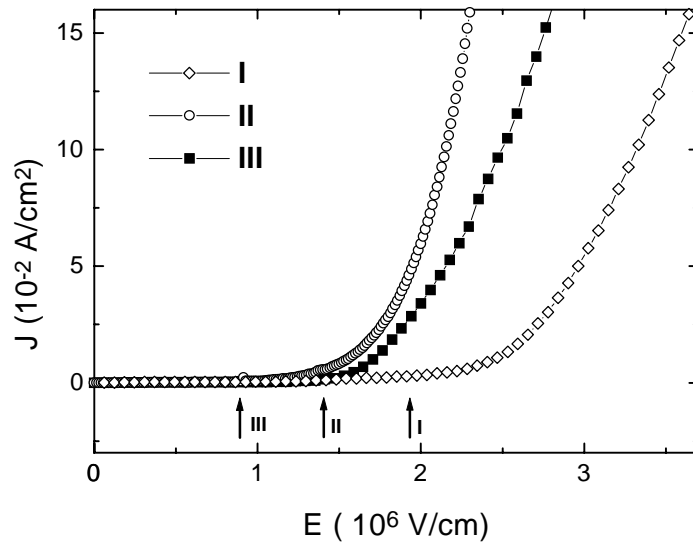


**Figure 6.5** Current density as a function of electric field for single layer ITO/Copolymer/Al devices. Arrows: the electric field strength at onset of emission.

In figure 6.5 the I-V dependencies for all copolymer devices are plotted. The electric field strength at the onset of light emission for polymers **I** to **III** are equal to  $1.9 \times 10^8$ ,  $1.4 \times 10^8$  and  $0.8 \times 10^8$  V/m, respectively. The consecutive lowering of the electric field is the result of the reduced HOMO-LUMO gaps, due to the substitution by octyloxy side-chains and cyano-groups onto the copolymer backbone, which decreases the barrier for electron injection.

**Table 6.2** Electrical properties and efficiencies of single-layer copolymer LEDs with ITO hole-injecting contacts in forward bias operation.

Copolymer	Layer Thickness (nm)	Electrode	Bias voltage at turn-on (V)	Field at turn-on ( $10^8$ V/m)	Ext.EL efficiency ( $10^{-2}$ ph/el)
<b>I</b>	80	Al	15	1.9	2.3
	80	Au	24	3.0	0.3
<b>II</b>	90	Al	13	1.4	0.9
<b>III</b>	140	Al	11.7	0.8	3.0

#### The hole-injection barrier

The injection of holes at the ITO anode into the polymer is controlled by a superposition of tunnelling and thermionic emission, the important parameter being the magnitude of the injection barrier [17,27]. At high fields, charge injection is dominated by tunnelling. The field dependence of the I-V characteristics were analysed using Fowler-Nordheim (FN) tunnelling theory in order to estimate the barrier heights for charge injection into the copolymer films. On the basis of this analysis we are able to roughly estimate the ionization potential or HOMO-level of the copolymers in an indirect way. In combination with the HOMO-LUMO gaps determined from the absorption spectra it is possible to derive an energy diagram for the copolymers. Fowler-Nordheim field emission tunnelling of electrons and holes through a triangular barrier gives [17,28]:

$$I \propto E^2 \exp\left(\frac{-\kappa}{E}\right), \quad (6.3)$$

$$\kappa = \frac{8\pi(2m^*)^{1/2}\phi^{3/2}}{3qh} \quad (6.4)$$

where  $I$  is the current,  $E$  is the electric field,  $\phi$  is the barrier height,  $m^*$  is the effective mass of the charge carriers ( $m^*$  is taken to be the free electron mass) and  $\kappa$  is a

parameter that depends on the barrier shape [29]. If  $\ln(I/E^2)$  versus  $1/E$  is plotted, a linear dependence is obtained with a slope representing  $\kappa$ . In our ITO/copolymer/Al devices, the majority carriers are holes, due to the high work function of the electron injecting Al contacts. For this reason, they can be considered as “hole-only” devices. Therefore, FN analysis of the I-V curves in forward bias will yield the barrier heights between the hole-injecting ITO-contact and the molecular HOMO-level (Ionisation Potential, IP) of the copolymers. The FN analysis has been performed on at least three samples with different layer thickness, each consisting of four separate diodes. An example of a Fowler-Nordheim plot of a 95 nm thick ITO/Copolymer I/Al device is shown in figure 6.6.

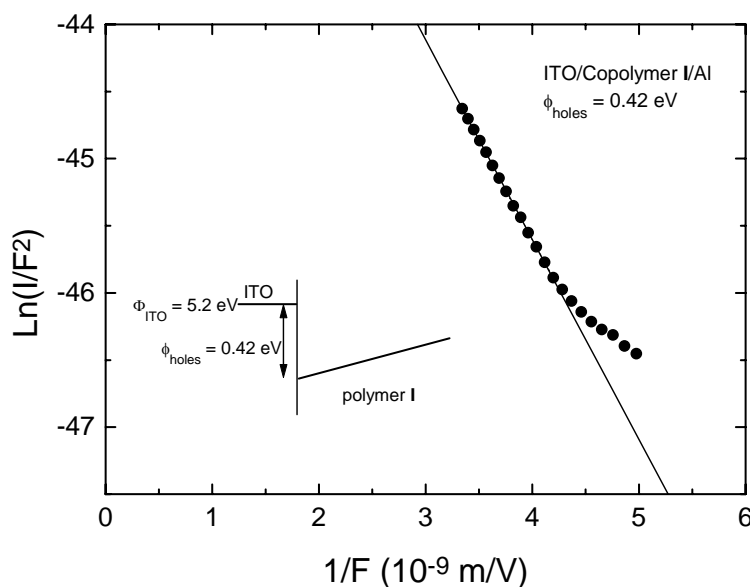


**Figure 6.6** Fowler-Nordheim plot for a 95 nm thick ITO/Copolymer I/Al device.

The results of the FN-analysis of all four copolymers are summarized in table 6.3. The diode-to-diode and sample-to-sample reproducibility of the obtained barrier heights was reasonably good ( $\pm 0.05$  eV). Additionally, several devices were made with Au contacts to check the validity of the analysis for ITO/Al devices. The obtained barrier heights in ITO/Al and ITO/Au diodes were identical. This indicates that we indeed obtained the barrier for hole injection in ITO/Al diodes and that the contribution of the electron current to the total cell current can be neglected in such devices. The calculated hole injection barriers and ionization potentials (taking the work function of ITO to be  $\phi_{\text{ITO}} = 5.2$  eV) are listed in table 6.3. It should be explicitly stated that although the good reproducibility of the obtained barrier height, the absolute value for

the ionisation potential of the copolymers will be a rough estimate. This is caused by the influence of impurities, interface defects, bandbending, image force effects [29,30], and the uncertainty in the value of the work function of ITO, which will lead to errors of the value of the barrier height and the ionization potential.

For this reason, cyclic voltammetry was used to determine the ionization potentials of the copolymers in solution as additional check to the Fowler-Nordheim analysis. With this electrochemical technique one can measure the oxidation potential of a molecule. The obtained oxidation potential can be converted to the ionization potential using an internal reference. Cyclovoltammograms were recorded in dichloromethane solution with tetrabutyl ammonium hexafluorophosphate as the electrolyte. The ferrocene/ferrocenium couple was used as internal reference to calibrate the cyclovoltammograms towards the Normal Hydrogen Electrode [16,31]. An ionization potential of 4.8 eV with respect to zero vacuum energy level was taken for ferrocene [32].

**Table 6.3** Ionization potentials and hole-injection barriers obtained by cyclic voltammetry and Fowler-Nordheim analysis.

Copolymer	IP (eV) cyclic voltammetry	$\phi_{\text{holes}}$ (eV) FN-analysis	IP (eV) FN-analysis
<b>I</b>	>5.8	0.4	5.6
<b>II</b>	5.7	0.2	5.4
<b>III</b>	5.8	0.3	5.5

The measured oxidation potentials were 0.9 and 1 Volts for the copolymers **II** and **III**, respectively. This corresponds to ionization potentials of 5.7 and 5.8 eV. The observed redox processes were reversible for both copolymers. For the copolymer **I**, no oxidation potential could be measured, due to oxidation of the electrolyte solution. This indicates that the oxidation potential of copolymer **I** is probably located beyond the measurement range. The trend in ionization potentials obtained with cyclic voltammetry corresponded with the trend obtained from Fowler-Nordheim analysis; only the absolute values are higher in the case of cyclic voltammetry.

In the copolymer LEDs the (hole) cell-current is determined by the injection barriers for holes in combination with the hole mobility in the copolymer. The trend in hole-injection barrier found for the copolymers corresponds with the observed electrical characteristics depicted in figure 6.5. The importance of the mobility for the cell current is reflected by the fact that the actual device current is usually several orders of magnitude smaller than the calculated Fowler-Nordheim tunnelling current. An explanation for this discrepancy was reported by Davids *et al.*[33]. They found that the low mobility in the polymer leads to a large backflow of injected carriers into the injecting contact, which decreases the injection rate of charges.

It is obvious that for the copolymers under discussion, the intrachain conductivity and hence the mobility, is affected by the steric interactions in the terphenyl parts of the backbone. It is known [34] that isolated non-substituted oligophenylenes are non-planar, because steric hindrance between protons on adjacent phenyl rings induces a twist between the rings. Molecular modelling calculations showed that this twist is about  $40^\circ$  [35]. In such a situation some overlap of the  $\pi$ -orbitals is still possible, which allows conjugation. When substituents on the rings are present the twist angle will be larger. Hilberer *et al.* [21] performed supplementary calculations on substituted terphenylenes by means of the AM1 semi-empirical quantum chemical method. They found that alkyl-substituted terphenylenes have twist angles between adjacent rings which are significantly shifted to  $90^\circ$ . In the case of the sterically less demanding alkoxy side-chains, the twist angle was less ( $\approx 50^\circ$ ). These findings suggest that overlap in  $\pi$ -orbitals is significantly diminished in the case of alkoxy substitution and effectively cancelled for alkyl substituents. Hence the barrier for carriers to move (hopping/tunnelling) between adjacent chromophores is smaller in the octyloxy-substituted copolymers.

#### Energy diagrams

Based on the ionization potentials obtained by FN-analysis and the HOMO-LUMO gaps derived from the onset of absorption, an energy diagram for the copolymers can be estimated, which is depicted in figure 6.7.

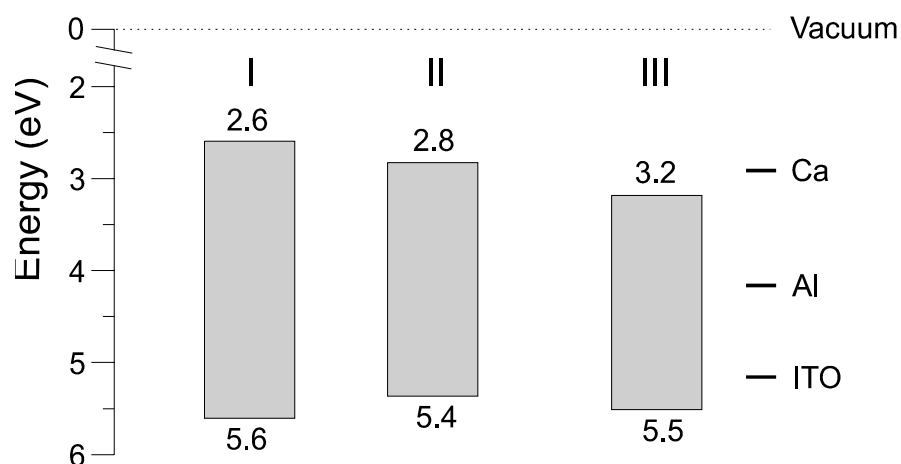


**Figure 6.7** Schematic energy diagram for the PPV-based copolymers.

With the value of  $\phi_{Al}$  at 4.3 eV, the electron-injection barriers derived from the energy diagram for the copolymers **I** to **III** are  $\phi_{electrons} = 1.7, 1.5$  and  $1.1$  eV, respectively.

The copolymer diodes have external EL efficiencies of approximately  $\approx 2 \times 10^{-2}\%$  ph/el, except for copolymer **II**, which has an efficiency of  $9 \times 10^{-3}\%$  ph/el (see table 6.2). A rough estimate of the maximum external quantum efficiency achievable in an organic LED can be obtained from equation (6.5), which contains all factors governing the EL efficiency (Rothberg *et al.* [2]):

$$\Phi_{EL} = \chi \Phi_F \eta_R \eta_E \leq \left(\frac{1}{4}\right) \times 1 \times 1 \times \left(\frac{1}{2n^2}\right) \quad (6.5)$$

where  $\chi$  is the fraction of recombinations that result in a singlet exciton,  $\Phi_F$  is the fraction of excitons that emit (PL quantum yield),  $\eta_R$  is the fraction of electrons and holes that recombine in the emissive layer and  $\eta_E$  the fraction of emitted photons that escape the emissive layer, which acts as a planar waveguide ( $n$  is the refractive index). According to a simple spin statistics argument of recombining e-h pairs (singlet:triplet generation rate is  $\approx 1:3$ ),  $\chi$  is limited to 0.25. The PL quantum efficiency  $\Phi_F$  can be as high as unity. The fraction of e-h recombination  $\eta_R$  can also be close to unity if deep trapping is negligible and unipolar current flow is completely blocked. So the EL efficiency of an LED reflects the PL efficiency of the emissive layer. Based on equation (6.5) the upper limit of the external EL efficiency  $\Phi_{EL}$  for copolymer **I**, for example, should be approximately 1.9 % (with  $n \approx 1.6$  and  $\Phi_F \approx 0.4$ ). The difference with the actual efficiency ( $2 \times 10^{-2}\%$ ) illustrates the large imbalance of the electron and hole currents in our single-layer ITO/copolymer/Al diodes.

The trend found in EL efficiencies for our copolymers is in reasonable agreement with the trend in solid-state PL efficiencies (for PL efficiencies see table 6.1). However, if we compare copolymer **I** and **III**, we would expect a higher efficiency for copolymer **III**. From the energy diagrams depicted in figure 6.7, it is obvious that the electron and hole currents in a copolymer **III** device should be more balanced in comparison with copolymer **I**, and hence a larger value for  $\eta_R$  and a higher EL-efficiency would be anticipated.

#### *Device optimization*

From the preceding section it has become clear that the efficiency of single-layer devices is rather low due to unbalanced injection and transport of charge carriers. Electrons are not able to move far into the bulk due to trapping, resulting in an e-h recombination zone close to the metal electrode in a single-layer device, which has the effect of quenching the emission. Furthermore, the large unipolar loss current of holes, which do not recombine but are captured by the counter electrode, is significant in a single-layer device, reducing the efficiency greatly.

One way to optimize the efficiency of a device is by blending of the active material in a polymeric binder, which does not contribute to the emission. Bässler *et al.* [36] reported that blending of PPV in polystyrene (1:1 w/w) increased the efficiency approximately two orders of magnitude in comparison to a conventional PPV LED. Dilution of the polymer in a host matrix can have a two-fold effect. (1) An enhanced PL-efficiency due to the reduction of intermolecular exciton transfer to quenching sites, and (2) a reduction of the unipolar loss current (if the emitting polymer acts as a trap for holes).

Device optimization by means of electron transport molecules in a double-layer configuration has proven to be the most important approach to the enhancement of the quantum efficiency by well-balanced injection and transport [37,6]. The introduction of an electron-transport/hole-blocking layer (ETL) will move the recombination zone away from the interface. This is due to the introduction of an energy offset (hole-injection barrier) at the polymer/ETL interface, which prevents holes to cross the ETL layer, which results in a positive space-charge interfacial zone in the emissive layer. The space-charge zone will increase the field over the ETL layer, resulting in enhanced electron-injection from the cathode. Hence, e-h recombination takes place in a small region of the PPV layer near the heterojunction. The difference in EL efficiencies using Ca or Al as electron-injecting electrode in double-layer devices is smaller in comparison to single-layer devices. This is caused by the fact that the redistribution of the internal electric field by hole blocking has a larger effect on electron injection than the difference in the barrier height. A few examples of electron transport molecules are molecular acceptors with oxadiazole [37,38] and triazole [39,40] moieties. The most widely used transport molecule is 2-(4-*t*-butyl-phenyl)-5-(4-biphenyl)-1,3,4-oxadiazole (PBD). However, the main drawback of this molecule is its crystallinity. For this reason PBD is usually blended with an amorphous transparent host polymer, e.g. poly(methyl methacrylate) [38,6], to suppress crystallization. Loading of the host polymer is limited to 3:1 w/w PBD:PMMA. The disadvantage of this method is the reduced conductivity upon dilution resulting in higher operating voltages and device failure due to phase separation (recrystallization) of the blend under applied bias (device heating).

In our group, a novel PBD side-chain polymer (pPBD) was synthesized via a TEMPO-mediated “living” free-radical polymerization [41,42], which is used as electron transport layer in this study. The chemical structure is depicted in figure 6.8. The pPBD polymer has a molecular weight of  $M_w = 18,000 \text{ g.mol}^{-1}$  (polydispersity 1.2), which corresponds to approximately 50 repeat units per chain. The polymer was soluble in toluene, and uniform layers could be prepared by spincoating. A rough estimate of the HOMO and LUMO levels for pPBD can be obtained by taking the values for vacuum-deposited PBD determined by photoemission and optical absorption measurements by Kido *et al.* [43]. PBD has its HOMO and LUMO at 5.9 and 2.4 eV. The HOMO-LUMO gap of pPBD determined by the onset of absorption

(see figure 6.8) was approximately 3.4 eV, which is close to the HOMO-LUMO gap value found by Kido for PBD.

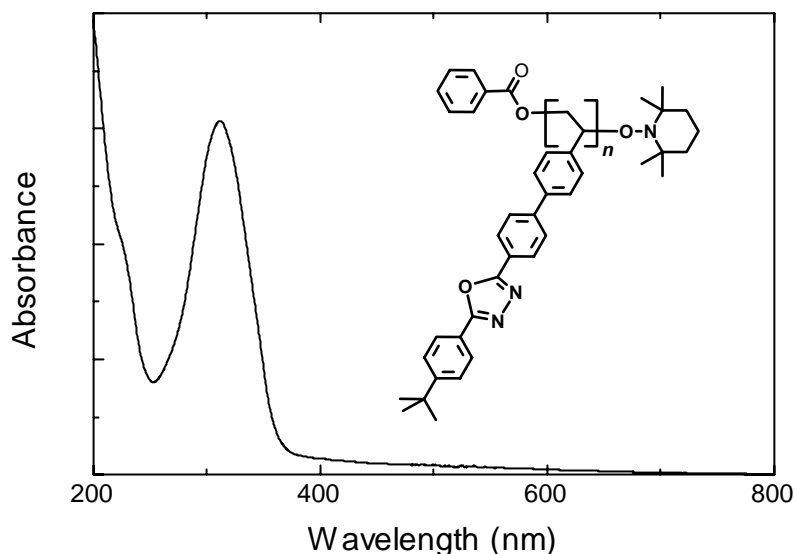


**Figure 6.8** Chemical structure and absorption spectrum (film) of pPBD.

Double-layer devices were prepared with copolymer **III** as emissive layer. The total layer thickness of the devices was  $\approx 110$  nm. It was impossible to determine the thickness of the individual layers in an accurate way, due to the good solubility of the two polymers, which will make the pPBD solution wash a fraction of the initial copolymer **III** away. Spincoating of the pPBD polymer on glass with the same rotation speed used for the preparation of the heterojunction gave a layer thickness of 40 nm. The maximum external efficiency measured in the double-layer devices was approximately 0.12 % ph/el, with a maximum brightness of approximately 250 cd/m<sup>2</sup>. However, the reproducibility between different diodes and samples was poor.

In addition, blends of copolymer **III** and pPBD were made. Single-layer devices consisting of blends with 38 w% and 63 w% pPBD were prepared. Based on the HOMO and LUMO-levels of both compounds, copolymer **III** should act as a trap for both electrons and holes. Furthermore, it is expected that the loss current of the majority carriers will decrease and that exciton diffusion to quenching sites is further diminished due to dilution. Indeed the efficiency increased to 0.04 and 0.08 % (at low drive-current) for the blend with 38 w% and 63 w% pPBD, respectively, but the I-V-curves shifted to higher fields with increasing content of pPBD (see figure 6.9). This

is the result of the higher barrier for injection in pPBD, which limits the injection of both holes and electrons. The maximum luminance reached is highest for the blend with 38 w% pPBD, because the blend with 63 w % pPBD sustains lower current before device breakdown occurred. The PL and EL spectra were blue-shifted (yellow emission) compared to that of pure copolymer **III** due to dilution in pPBD, indicating that copolymer **III** is molecularly dispersed in pPBD. So blending increased the efficiency to 0.08 %, but has as drawback that higher operating voltages have to be applied.

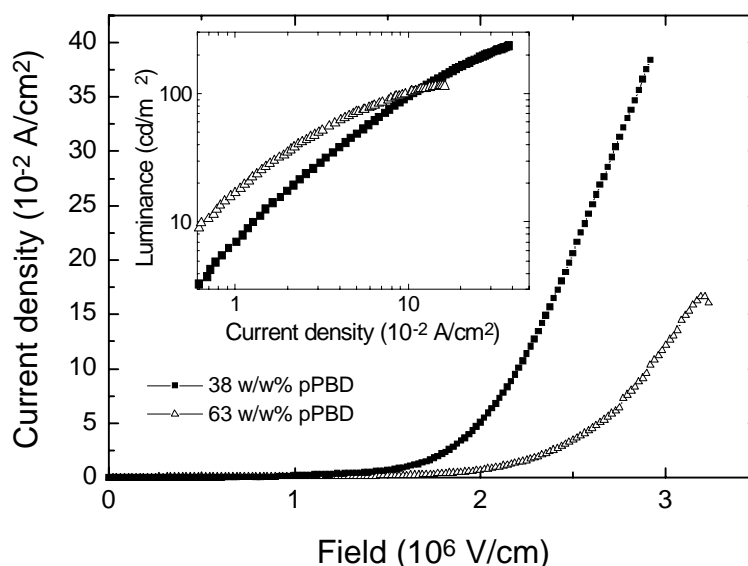


**Figure 6.9** *I-V characteristics of single-layer LEDs containing blends of copolymer **III** with pPBD (38 and 63 w%). Inset: luminance as a function of drive current.*

The most efficient polymer LEDs up to date are based on double-layer devices made from PPV and cyano-substituted PPV derivatives. Internal efficiencies up to 4% are reported for such heterojunction polymer LEDs [7,44]. The cyano-substituted PPV derivatives are highly fluorescent and the strong electron-accepting cyano groups on the vinylene linkages lower the LUMO-level (and HOMO-level to a lesser extent) of the polymer, which makes them useful as both electron transport and emissive layer. The offset in HOMO and LUMO level at the polymer/polymer interface will block both holes and electrons, resulting in balanced transport, which is schematically depicted in figure 6.10.

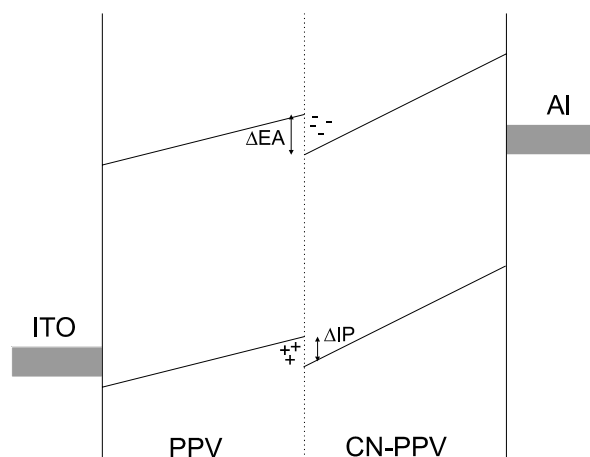


**Figure 6.10** Schematic energy level diagram for a two-layer LED under forward bias (from reference [7]).

By confining the charges in the interface region, a large field is built up, which promotes tunnelling through the heterojunction. Emission is established when a hole tunnels through the barrier and recombines in the CN-PPV layer or when an electron tunnels through the barrier and forms an exciton in the PPV layer, which then migrates into the lower-energy CN-PPV polymer and radiatively decays. Thus, emission is almost solely produced in the CN-PPV layer.

We applied this concept to obtain enhanced device efficiencies for the cyano-substituted copolymer **III**. Double-layer devices were prepared by spin-casting copolymer **II** from a chloroform solution onto ITO substrates. After drying of the layer under vacuum, copolymer **III** was spin-cast on top of the copolymer **II** layer and Al-electrodes were deposited as electron-injecting contacts. The highest measured external efficiency obtained from a 190 nm thick double-layer device was  $7 \times 10^{-2}\%$  ph/el, which is twice as high in comparison with the single layer copolymer **III** devices. The EL-emission spectrum corresponded with the PL spectrum of copolymer **III**, as expected. The diode-to-diode (on the same device) and device-to-device reproducibility of the double-layer devices was poor. This is mainly caused by the good solubility of both copolymers in the solvents used for processing, as mentioned in the preceding section. A large part of the copolymer **II** layer was washed away upon casting of copolymer **III** and substantial mixing of the two copolymers resulted in an ill-defined interface. We were unable to determine the individual layer thickness of the two copolymers in the devices in an accurate way. The efficiency enhancement was rather poor in comparison with that reported in literature. The most plausible reasons for the poor enhancement are the ill-defined interface region and the fact that

the offset between the HOMO-levels of the two polymers,  $\approx 0.1$  eV, was most probably too small to achieve significant hole blocking.

A second set of devices was made with a hole-transport layer of PPV prepared via the so-called sulphonium precursor route [45]. This polymer has a molecular weight of  $M_w \approx 1 \times 10^6$  g.mol<sup>-1</sup> as determined by GPC. The precursor was spincoated from methanol solution onto the ITO substrates and thermally converted to PPV at 220 °C for 6 hours. The thickness of the PPV layer was approximately 50 nm as determined with a profilometer. The major advantage of this polymer is that it is fully insoluble after conversion, which assures the formation of a well-defined heterojunction. A 70 nm thick layer of copolymer **III** was spin-coated on top. In this case external efficiencies up to 0.4 %ph/el and brightness's up to approximately 600 cd/m<sup>2</sup> were achieved, which is substantially higher than in the previous case. These values correspond to an internal efficiency of  $\approx 2$  %, approaching the maximum achievable efficiency of 10 % based on theoretical considerations. The exact ionization potential (IP) and electron affinity (EA) values of PPV are unknown. Values for IP and EA of 5.05 and 2.32 eV, based on quantum chemical calculations by Brédas [46], would imply to barriers of roughly 0.3 – 0.4 eV for both holes and electrons at the heterojunction.

### 6.3.2 Oligo(*p*-phenylene vinylene)s

A series of three different five-ring oligo(*p*-phenylene vinylene)s (OPVs) has been studied as active layer in Light-Emitting Diodes. The chemical structures of the OPVs employed for this study are depicted in figure 6.11. The synthesis and characterization of the model compounds can be found in reference [47] and the optical properties in chapter 2 of this thesis.

In first instance, non-optimized single-layer LEDs were prepared by vacuum sublimation following the procedure described in the experimental section. All thin layers of the different OPVs showed similar morphologies in the optical microscope after deposition onto the ITO substrates. The electrical properties and efficiencies for the series of ITO/OPV/Al and Ca (for Ooct-OPV5) single-layer devices are summarized in table 6.4. From all OPVs working LEDs could be prepared. It should be stated that the minimum thickness of the active layer must be of the order of 150 nm and thicker to obtain reproducible diode characteristics. Thinner devices all suffered from shorts and non-uniform light emission over the active area of the diodes. In figure 6.12 the current-voltage characteristics are shown for all OPVs in a single-layer configuration with electron-injecting Al contacts. The arrows indicate the electric field strength at which light emission was detectable. All ITO/OPV/Al diodes showed rectifying behaviour and we were not able to observe electroluminescence in reverse bias for any of the OPV-based devices.

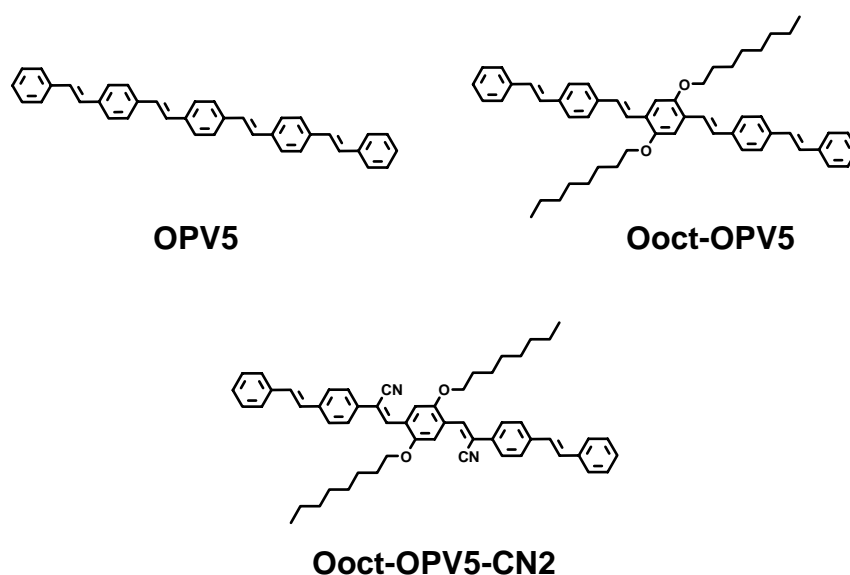


**Figure 6.11** Chemical structure of the oligo(*p*-phenylene vinylene)s.

**Table 6.4** Electrical properties and efficiencies of the single-layer and double-layer oligomer LEDs with ITO hole-injecting contacts in forward bias operation.

Oligomer <sup>a</sup>		Cathode	Layer thickness (nm)	$V_{\text{turn-on}}^{\text{(b)}}$ (V)	$E_{\text{turn-on}}$ ( $10^8$ V/m)	Ext. eff. ( $10^{-2}$ %)
OPV5	As	Al	380	18.1	0.5	1.1
Oct-OPV5	As	Al	193	24.4	1.3	0.1
	An			20.4	1.1	1.2
	As	Ca	183	11.8	0.6	10.0
Oct-OPV5-CN2	As	Al	150	20	1.3	1.5
Oct-OPV5/ Oct-OPV5-CN2	As	Al	150/45	8.7	0.5	31

a) As: as-deposited, An: annealed. b) turn-on is defined here as the point at which the emission is detectable.

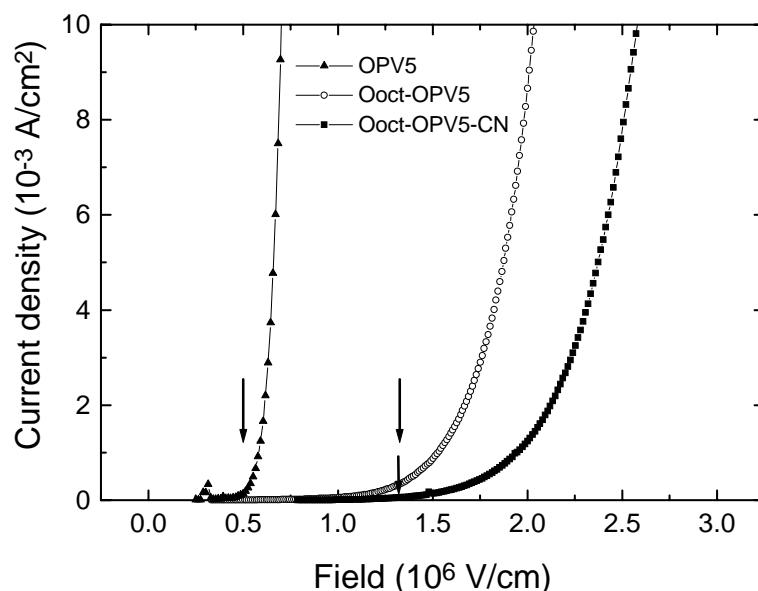


**Figure 6.12** Electrical characteristics (current density versus electric field) of the ITO/OPV/Al devices. The arrows indicate the onset of light emission.

Electrical measurements on devices with different layer thickness showed that the diode current depends on the applied field rather than the drive voltage. The same behavior as was observed with the alternating PPV copolymers. This indicates that field-driven injection determines the electrical characteristics. From figure 6.12 it is evident that OPV5 has the lowest onset for both current and emission. By means of Fowler-Nordheim analysis of the I-V characteristics and optical absorption measurements we estimated the injection barrier for holes and the HOMO-LUMO bandgap, respectively. The results of this analysis are given in table 6.5. The difference between the onset of current and light, for OPV5 and Ooct-OPV5, is significant and contradicts to the band offsets derived from table 6.5:

- (a) The onset for light emission for OPV5 appears at half the electric field strength of Ooct-OPV5, while the barrier for electron-injection is approximately 0.3 eV higher.
- (b) The IV-characteristics are determined by the majority carriers in these devices, which are holes. On the basis of the similar hole-injection barrier for both OPVs, one would expect approximately the same electrical characteristics.

A possible explanation for this discrepancy could be that the charge-carrier mobilities (holes and electrons) in the case of OPV5 are much higher, resulting in a higher injection rate of charge carriers [33]. If we now compare the electrical characteristics of Ooct-OPV5 and Ooct-OPV5-CN2 it is obvious that the onset of current appears at higher drive field in the case of Ooct-OPV5-CN2. This is consistent with the value found for the hole-injection barrier, which is 0.2 eV higher. However, the onset of emission appears at the same field as for Ooct-OPV5, which reflects the lowering of the LUMO-level due to the presence of cyano groups (approximately 0.5 eV lower than that of Ooct-OPV5). The external EL efficiencies of the single-layer OPV devices were typically in the range of 0.01–0.02 %ph/el. Only the EL efficiency of the Ooct-OPV5 devices was an order of magnitude lower. On the basis of the PL efficiencies, which were all in the same range (40-50 %), one would expect similar values for Ooct-OPV5.

**Table 6.5** *Estimated HOMO-LUMO gaps and hole-injection barriers.*

Oligomer	HOMO-LUMO gap (eV) <sup>(a)</sup>	$\phi_{\text{holes}}$ (eV) <sup>(b)</sup>
OPV5	2.7	0.2
Ooct-OPV5	2.4	0.2
Ooct-OPV5-CN2	2.1	0.4

a) Optical absorption measurements b) Fowler-Nordheim analysis

To optimize the performance of single-layer Ooct-OPV5 devices, Ca instead of Al was used as cathode, which lowers the injection barrier for electrons with approximately 1.3 eV. The change of cathode resulted in a more than twofold reduction of the drive field at turn-on ( $6 \times 10^7$  V/m) and two orders of magnitude enhancement in EL efficiency (0.1 %), due to improved electron-injection.

The electroluminescence spectra of the single-layer devices are depicted in figure 6.13. All EL spectra coincided with the solid-state photoluminescence spectra, indicating that the same excited states are involved in both PL and EL. The broad luminescence spectrum for Ooct-OPV5-CN2 is attributed to excimer emission (see chapter 2).

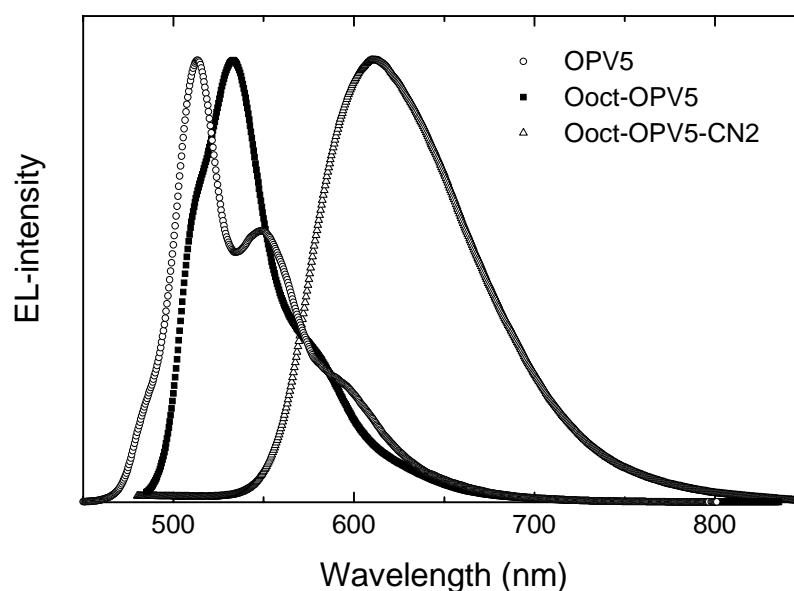


**Figure 6.13** Electroluminescence spectra of the ITO/OPV/AI devices.

*The influence of morphology on the device performance*

The influence of the thin-film morphology on the device performance was investigated for Ooct-OPV5 by means of annealing (as described in chapter 2 and 5). For Ooct-OPV5 annealing leads to an increase of the single-crystal domain size and an enhanced molecular orientation (see chapter 2). The external efficiency of the annealed Ooct-OPV5 films was more than one order of magnitude higher than that of the as-deposited film (inset figure 6.14). The photoluminescence quantum yield as measured under laser illumination in an integrating sphere was approximately 20 % larger for the annealed film. If we assume that photoexcitation and charge injection give rise to the same excited state (the singlet exciton), the 20 % rise in PL efficiency alone, cannot account for the 10-15 fold increase in EL efficiency. As can be seen from figure 6.14 there is no significant difference in cell current upon annealing. The majority charge carriers in these devices are holes, so we may infer that the hole current is the same for both morphologies. Fowler-Nordheim analysis of the IV-characteristics revealed that the barrier for hole-injection is the same for both morphologies, and from the similar absorbance spectra of both morphologies we can conclude that the bandgap doesn't change upon annealing.

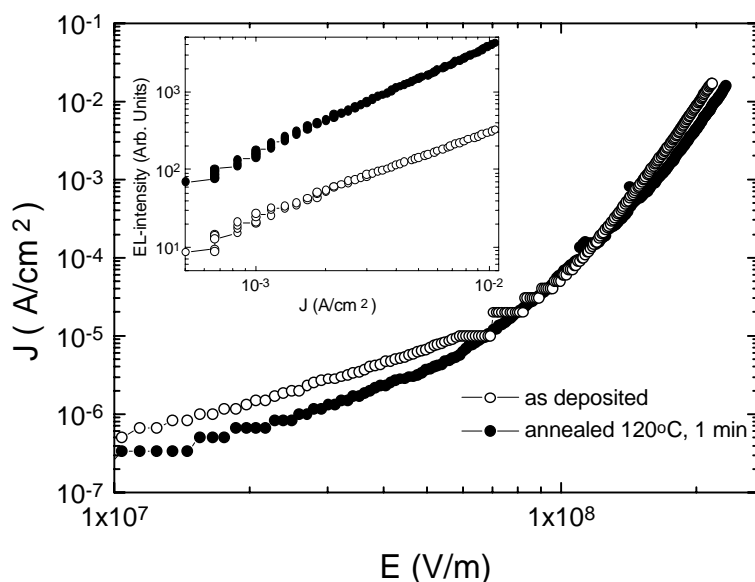


**Figure 6.14** *J-E characteristics for a single-layer ITO/Ooct-OPV5/Al devices with an as-deposited and an annealed active layer, respectively. Inset: Luminance as a function of cell current for both thin-film morphologies.*

The electron current in such devices is much smaller and is fully masked by the current of the majority carriers. For this reason Al/Ooct-OPV5/Ca devices were prepared, which can be considered as “electron-only” devices. In the annealed “electron-only” devices the current was approximately one order of magnitude higher. Hence, it seems that the increase in efficiency upon annealing can be attributed to an increase of electron mobility. The improvement of molecular orientation and the reduction of the density of grain boundaries upon annealing may be considered as possible explanations for the improved electron mobility. For Ooct-OPV-CN2 and OPV5 it was not possible to prepare working devices with annealed layers. Annealing resulted in the formation of small holes in the evaporated films causing short-circuited devices.

#### *Double-layer devices*

Double-layer devices were prepared, consisting of an Ooct-OPV5 hole-transport layer and an Ooct-OPV5-CN2 electron-transport/emissive layer to balance charge transport and injection. The device characteristics are summarized in table 6.4 and depicted in figure 6.15. The voltage at which EL was detectable was also significantly reduced to

8.7 Volts ( $4.5 \times 10^7$  V/m). External efficiencies up to 0.31 % were reached in an ITO/Ooct-OPV5(150 nm)/Ooct-OPV5-CN2(45 nm)/Al device, which corresponds to an internal efficiency of  $\approx 1.5$  %. A more than one order of magnitude enhancement of the efficiency in comparison to single-layer Ooct-OPV5-CN2 devices. Despite the high EL efficiency, only low current levels were reached before critical device failure, which resulted in a maximum brightness of only  $\approx 30$  cd/m<sup>2</sup>. Orange/red emission was observed above turn-on in the double-layer device indicating that Ooct-OPV5-CN2 is the emissive species in the device. However, the electroluminescence spectrum (inset figure 6.15) revealed that there is a small contribution of EL emission originating from Ooct-OPV5 (see arrow in the inset).

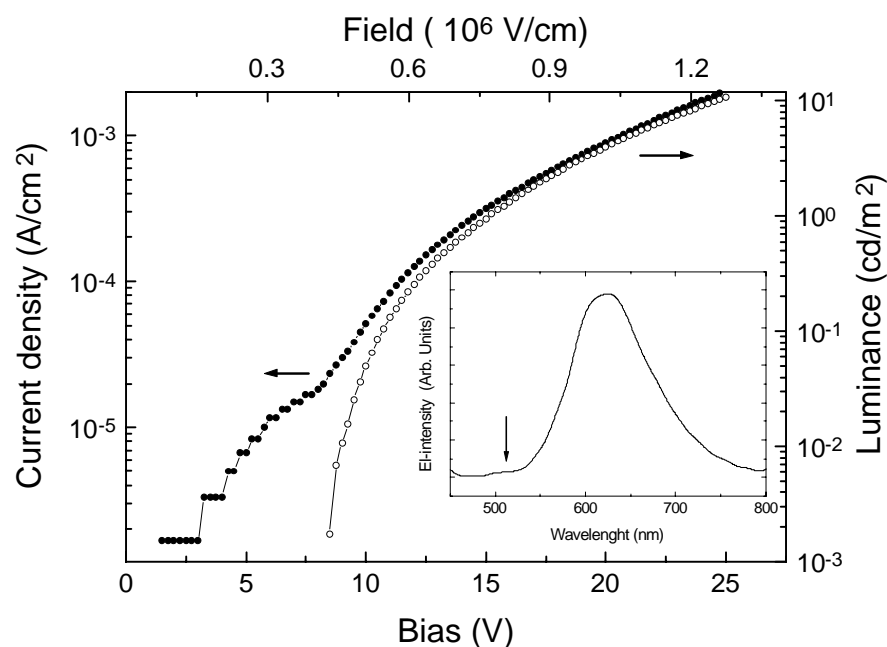


**Figure 6.15** Semilog plot of current density (closed circles) and luminance (open circles) of an ITO/Ooct-OPV5(150 nm)/Ooct-OPV5-CN2(45 nm)/Al double-layer device as a function of bias voltage. Inset: double-layer electroluminescence spectrum.

## 6.4 Conclusions

Electroluminescence was achieved in the blue, green and orange wavelength region with single-layer devices consisting of transparent indium-tin-oxide anodes and air-stable Al cathodes. The efficiencies of the single-layer copolymer/oligomer LEDs are comparable to those reported for fully conjugated PPVs. Fowler-Nordheim tunnelling theory was used to analyse the current-voltage characteristics in order to determine the barriers for hole injection in the single-layer devices. In combination with cyclic

voltammetry and optical absorption measurements it was possible to estimate energy diagrams for all copolymers and oligomers, which could be used to describe the results obtained in a qualitative way. Furthermore, the influence of the thin-film morphology on LED performance has been investigated for the octyloxy-substituted oligo(*p*-phenylene vinylene). The EL efficiency is drastically increased for Oct-OPV5 films with improved molecular orientation and larger crystalline domains sizes, which is attributed to enhanced electron transport.

Device optimization by means of additional charge-transport layers to enhance the electroluminescence efficiency has been applied successfully. Balanced hole and electron currents, and e-h recombination distant from the metal cathode are probably achieved in such devices, resulting in improved device performance. A novel polymer with oxadiazole-based side-chains has been used successfully as an electron-transport/hole-blocking layer. In combination with a cyano-substituted PPV copolymer as the emissive layer, external EL efficiencies up to 0.1 % were obtained. The best-performing double-layer LEDs were based on the electronegative cyano-substituted copolymers and oligomers as the electron-transport/emissive layer. In this case, external electroluminescence efficiencies up to 0.3-0.4 % are reached.

## 6.5 References

- [1] J.H. Burroughes, D.D.C. Bradley, A.R. Brown, R.N. Marks, K. Mackay, R.H. Friend, P.L. Burns and A.B. Holmes, *Nature*, **347**, 537 (1990)
- [2] L.J. Rothberg, A.J. Lovinger, *J. Mater. Res.*, **11**, 3174 (1996)
- [3] R. H. Friend, G.J. Denton, J.J.M. Halls, N.T. Harrison, A.B. Holmes, A. Köhler, A. Lux, S.C. Moratti, K. Pichler, N. Tessler, K. Towns, H.F. Wittmann, *Solid State Commun.*, **102**, 249 (1997)
- [4] D. Braun and A.J. Heeger, *Appl. Phys. Lett.*, **58**, 1982 (1991)
- [5] C. Zhang, H. von Seggern, K. Pakbaz, B. Kraabel, H.-W. Schmidt, A.J. Heeger, *Synth. Met.*, **62**, 35 (1994); J.K. Herrema, J. Wildeman, R.H. Wieringa, R.E. Gill, G.G. Malliaras, S.S. Lampoura, G. Hadziioannou, *Polym. Preprints*, **34**, 282 (1993)
- [6] D.D.C. Bradley, *Synth. Met.*, **54**, 401 (1993)
- [7] N.C. Greenham, S.C. Moratti, D.D.C. Bradley, R.H. Friend and A.B. Holmes, *Nature*, **365**, 628 (1993)
- [8] C. Zhang, D. Braun, A.J. Heeger, *J. Appl. Phys.*, **73**, 5177 (1993)
- [9] D. Braun, E.G.J. Staring, R.C.J.E. Demandt, G.L.J. Rikken, Y.A.R.R. Kessener, A.H.J. Venhuizen, *Synth. Met.*, **66**, 75 (1994)
- [10] F. Garten, A. Hilberer, F. Cacialli, Y. ten Dam, E. Esselink, R.H. Friend, T.M. Klapwijk and G. Hadziioannou, *Adv. Mater.*, **9**, 127 (1997)
- [11] R. Schenk, H. Gregorius, K. Meerholz, J. Heinze, K. Müllen, *J. Am. Chem. Soc.*, **113**, 2634 (1991)
- [12] C. Adachi, A. Tsutsui, S. Saito, *Appl. Phys. Lett.*, **56**, 799 (1990)

- [13] M.D. Joswick, I.H. Campbell, N.N. Barashkov, J.P. Ferraris, *J. Appl. Phys.*, **80**, 883 (1996); T. Goodson III, L. Wenjie, A. Gharavi, L. Yu, *Adv. Mater.*, **9**, 639 (1997)
- [14] J. Servet, G. Horowitz, S. Ries, O. Lagorsse, P. Alnot, A. Yassar, F. Deloffre, R. Srivastava, R. Hajlaoui, P. Lang, F. Garnier, *Chem. Mater.*, **6**, 1809 (1994)
- [15] G.A. Mabbot, *J. Chem. Ed.*, **60**, 697 (1983)
- [16] R.R. Gagné, C.A. Koval, G.C. Lisensky, *Inorg. Chem.*, **56**, 462 (1984)
- [17] I.D. Parker, *J. Appl. Phys.*, **75**, 1656 (1994)
- [18] D.V. Morgan, Y. Aliyu, R.W. Bunce, *Phys. Status Solidi A*, **133**, 77 (1992)
- [19] I.H. Campbell, T.W. Hagler, D.L. Smith, J.P. Ferraris, *Phys. Rev. Lett.*, **76**, 1900 (1996)
- [20] Handbook of Chemistry and Physics (CRC press, Boca Raton, Florida, 1986)
- [21] A. Hilberer, P.F. van Hutten, J. Wildeman, G. Hadziioannou, *Macromol. Chem. Phys.*, **198**, 2211 (1997)
- [22] M.P.L. Werts, Synthesis of cyano-substituted PPV-polymers for LEDs (undergraduate report, University of Groningen, 1996)
- [23] J.L. Brédas, *Adv. Mater.*, **7**, 264 (1995)
- [24] J. Grüner, R.H. Friend, J. Huber, U. Scherf, *Chem. Phys. Lett.*, **251**, 204 (1996)
- [25] H. Antoniadis, M.A. Abkowitz, B.R. Hsieh, *Appl. Phys. Lett.*, **65**, 2030 (1994)
- [26] D. Braun, A.J. Heeger, *Appl. Phys. Lett.*, **58**, 1982 (1991)
- [27] S. Karg, W. Riess, V. Dyakonov, M. Schwoerer, *Synth. Met.*, **54**, 427 (1993)
- [28] R.H. Fowler, L. Nordheim, *Proc. R. Soc., London Ser. A.*, **119**, 173 (1928)
- [29] M. Lampert, Current injection in solids (Academic Press, New York, 1970), 189
- [30] Y. Yang, Q. Pei, A.J. Heeger, *J. Appl. Phys.*, **79**, 934 (1996)
- [31] G. Gritzmer, J. Kuta, *Pure Appl. Chem.*, **56**, 462 (1984)
- [32] H.M. Koeppe, H. Wendt, H. Strehlow, *Z. Electro Chem.*, **64**, 483 (1960)
- [33] P.S. Davids, Sh.M. Kogan, I.D. Parker, D.L. Smith, *Appl. Phys. Lett.*, **69**, 2270 (1996)
- [34] K.N. Backer, A.V. Vratini, T. Resch, H.C. Knachel, W.W. Adams, E.P. Socci, B.L. Farmer, *Polymer*, **34**, 1571 (1993)
- [35] B. Champagne, D.H. Mosley, J.G. Fripiat, J.-M. André, *Phys. Rev. B*, **54**, 2381 (1996)
- [36] H. Vestweber, J. Oberski, A. Greiner, W. Heitz, R.F. Mahrt, H. Bässler, *Adv. Mat. Optics Elect.*, **2**, 197 (1993)
- [37] C. Adachi, T. Tsutsui, S. Saito, *Appl. Phys. Lett.*, **57**, 531 (1990)
- [38] A.R. Brown, D.D.C. Bradley, P.L. Burns, J.H. Burroughes, R.H. Friend, N.C. Greenham, A.B. Holmes, A. Kraft, *Appl. Phys. Lett.*, **61**, 2793 (1992)
- [39] J. Kido, C. Ohtaki, K. Hongawa, K. Okuyama, K. Nagai, *Jpn. J. Appl. Phys.*, **32**, L917 (1993)
- [40] M. Strukelj, F. Papadimitrakopoulos, T.M. Miller, L.J. Rothberg, *Science*, **267**, 1969 (1995).
- [41] M. Moroni, A. Hilberer, G. Hadziioannou, *Macromol. Rapid. Commun.*, **17**, 693 (1996)
- [42] M. Moroni, A. Hilberer, G. Hadziioannou, *Macromolecules* (1997) submitted
- [43] J. Kido, *Appl. Phys. Lett.*, **67**, 2281 (1995)
- [44] D.R. Baigent, N.C. Greenham, J. Grüner, R.N. Marks, R.H. Friend, S.C. Moratti, A.B. Holmes, *Synth. Met.*, **67**, 3 (1994)

- [45] A. Delmotte, M. Biesman, H. Rahier, M. Gielen, E.W. Meyer, *Synth. Met.*, **58**, 325 (1993)
- [46] J.L. Brédas, *Adv. Mater.*, **7**, 263 (1995)
- [47] R.E. Gill, Design, synthesis and characterization of luminescent organic semiconductors (Ph.D. thesis, University of Groningen, 1996), chapter 3

# Summary

$\pi$ -conjugated polymers attract much interest nowadays for use as active component in electronic, optical and optoelectronic applications, like light-emitting diodes, light-emitting electrochemical cells, photodiodes, photovoltaic cells, field-effect transistors, optocouplers and optically pumped lasers.  $\pi$ -conjugated polymers combine the properties of classical macromolecules, such as low weight, good mechanical behaviour (strength and flexibility) and processability with semiconductor properties, arising from their particular electronic structure. Conjugated polymers like poly(*p*-phenylene vinylene) and poly(*p*-phenylene) have a backbone consisting of alternating single and double carbon-carbon bonds. The overlap of  $\pi$  orbitals forms a continuous system of electron density along the backbone. The extent of this overlap (the conjugation length) together with the bond alternation determines the HOMO-LUMO bandgap. These materials are often strongly fluorescent and emit in the range from near infrared to the ultraviolet (1-4 eV). Especially PPV and soluble derivatives thereof, are of great interest, due to the combination of emission in the visible wavelength region and high luminescence quantum yields.

The wavelength of emission depends on the extent of conjugation, and can be controlled by modification of the chemical structure. This can be achieved by the attachment of functional groups, which alter the electronic structure of the polymer or by making copolymers with non- $\pi$ -conjugated sequences, which interrupt the  $\pi$ -orbital overlap. So, light emission is possible over the entire visible range of the visible spectrum, by “chemical” tuning of the HOMO-LUMO energy gap of the polymer. Their tuneable emissive properties are particularly attractive for lighting and display applications, especially in combination with (relatively) low material cost and the possibility of large-area device fabrication by means of simple casting techniques.

The primary interest of this study has been the solid-state photophysical characterization of a series of novel well-defined alternating PPV copolymers and crystalline 5-ring oligo(*p*-phenylene vinylene)s, and their application as emissive medium in light-emitting diodes and photopumped lasers. The chemical structure of the compounds used in this study, are shown in figure 1 on the next page. In the copolymers **I** to **III** the PPV blocks are linked through an aromatic phenyl ring within a fully rigid-rod chain. The desired control of the conjugation length is achieved through steric interactions between the side chains and the rings within the terphenylene parts of the copolymer. The middle ring in the terphenylene unit is twisted out of coplanarity, effectively interrupting the  $\pi$ -orbital overlap along the backbone. In copolymer **IV**, abbreviated as SiPPV, PPV oligomers (distyrylbenzene) are linked through dimethylsilylene units. The dimethylsilylene units provide flexibility to the polymer backbone. The choice of this interrupting block is based on previous studies carried out in our group on poly[(silanylene)thiophene]s. In this study it has been shown that the presence of only one silicon atom in the backbone effectively interrupts the conjugation.

In both types of copolymers the chromophores are distyrylbenzene units. By the introduction of electron-accepting cyano-substituents on the vinylene linkage and by changing the side-chains from alkyl to alkoxy (an electron-donating moiety), the emission could be tuned from the blue to the red part of the spectrum.

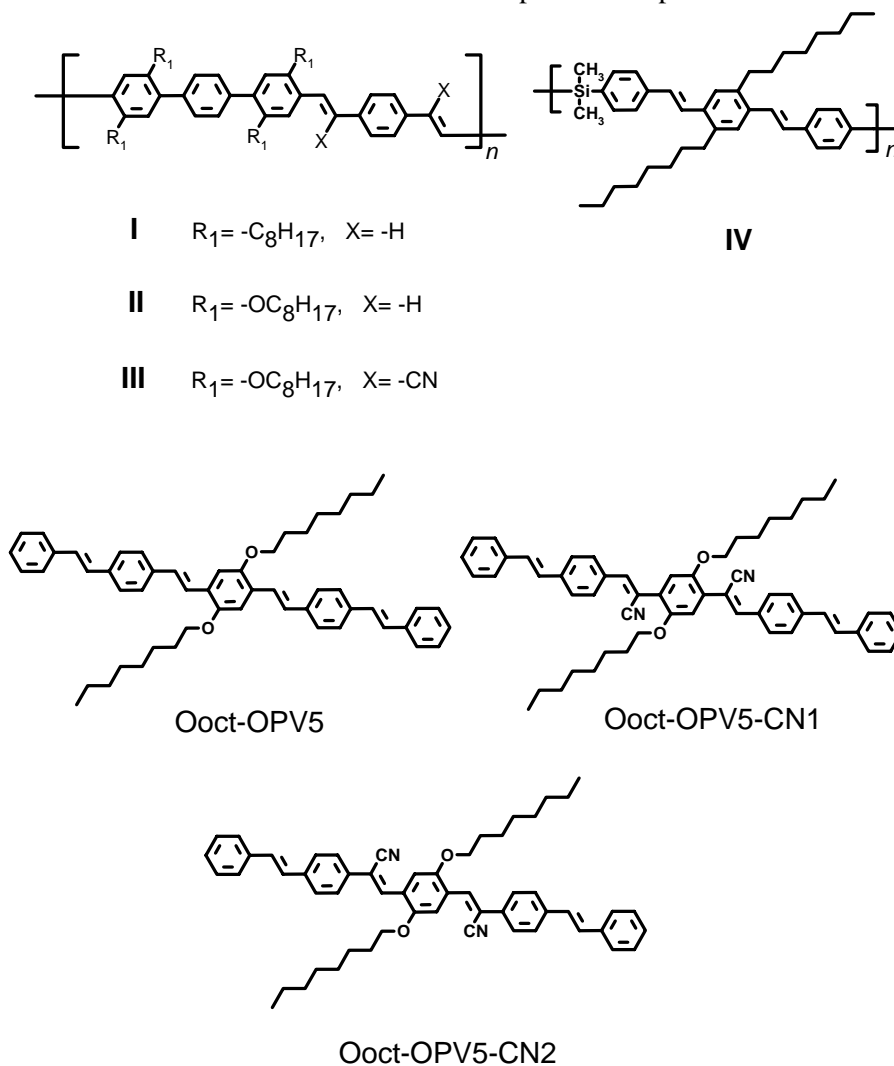


**Figure 1** chemical structure of the alternating PPV-based copolymers (I to IV) and oligo(*p*-phenylene vinylene)s.

In chapter 2, the optical properties in solution and solid state for the series of well-defined alternating PPV copolymers and all-*trans* 5-ring oligo(*p*-phenylene vinylene)s are described. The optical properties of the copolymers in dilute solution were

compared to those of substituted distyrylbenzene model oligomers representing the chromophores in the polymer backbone. The optical characteristics of the copolymers were similar to that of the models, indicating that the conjugation is effectively interrupted in the copolymers. For the blue-light-emitting alternating copolymers the photoluminescence (PL) efficiency and lifetime did not significantly change going from solution to the solid-state, indicating that the contribution from additional non-radiative decay channels due to interchain interactions in the condensed state is negligible, resulting in efficient solid-state PL ( $\eta_{\text{PL}} \approx 0.4$ ).

For both the cyano-substituted copolymer and Ooct-OPV5-CN1, a fast double-exponential PL decay was measured in dilute solution, which is the result of a fast non-radiative relaxation pathway associated with the cyano substituents on the vinylene linkages. Restricting the molecular motion (twisting/bending) by dispersing the oligomer in a solid polysulfone matrix resulted in an effective inhibition of the non-radiative decay channel and a much longer single-exponential PL decay with a time constant of 1.7 ns. Remarkably, for Ooct-OPV5-CN2 in solution this effect was not so strong. A reasonably long PL-decay with a PL lifetime of 1.4 ns was measured, which indicates that the position of the cyano moieties on the vinylene bonds is an important parameter, governing this fast non-radiative decay pathway.

For the Ooct-OPV5-CN2 single crystals, the PL spectrum was broad and featureless and a long PL lifetime of 8 ns was measured. The long-lived luminescence is attributed to excimer emission. This is positively confirmed by X-ray diffraction data of the single crystal. On the basis of the packing of the molecules in the crystal lattice, significant  $\pi$ - $\pi$  interactions between adjacent (face-to-face) molecules are to be expected. Also in the case of the cyano-substituted copolymer there is evidence that the luminescence originates from eximers, but though the characteristic features are less pronounced as observed for Ooct-OPV5-CN2 and that reported for cyano-PPV homopolymers.

In *chapter 3*, we have demonstrated efficient laser action of a novel blue-light-emitting PPV copolymer in solution, photoexcited by ns pulses from the frequency-tripled output of a Nd:YAG laser. The energy conversion efficiency and wavelength tuning range of TOP-PPV in *n*-hexane exceeded that of both reference coumarin dyes. This study clearly demonstrates the potential of conjugated PPV polymers for dye laser applications. The prospects for PPV polymers as active lasing medium in optically pumped solid state dye lasers and amplifiers based on dilute blends seem good, based on the above mentioned observations in solution. The superior mechanical properties and thermal stability of conjugated polymers over conventional laser dyes in combination with efficient emission will likely result in an overall improvement of the performance of such solid-state dye lasers.

In *chapter 4*, mirrorless lasing in optically pumped, neat films of the copolymer SiPPV and the homopolymer Ooct-PPV. This mirrorless laser emission is the result of amplification of spontaneous emission (ASE) due to optically-induced net gain. Propagation of the emitted photons by waveguiding, inside the polymer film, is

important, because it provides the necessary length of interaction of the emitted light to build up sufficient net gain. A threshold for spectral narrowing was observed above which coherent light emission appeared with a narrow spectral bandwidth of 6–7 nm (FWHM). The observed narrow emission band was located near the maximum of the low intensity fluorescence spectrum for both polymers. Furthermore, we demonstrated ‘true’ lasing from an Ooct-PPV film with external optical feedback provided by a planar cavity consisting of two dielectric mirrors and a compressible transparent spacer layer. This cavity construction enabled us to tune the wavelength of the laser emission. A wavelength tuning range of approximately 20 nm was observed for the laser emission from Ooct-PPV, centred at the gain maximum located at 631 nm.

The observation of lasing in optically pumped polymer films with and without external feedback system gives hope for the possible development of an electrically pumped laser diode. The major limiting factor at this moment is the drive current necessary for electrically pumped lasing to be realized. This was one of the reasons why we started to study the emission properties of PPV oligomers under pulsed laser excitation. Oligomers have the ability to form well-ordered structures and due to this fact usually exhibit better charge transport properties.

In *chapter 5*, stimulated emission from both single crystals and vacuum-deposited polycrystalline thin films of a substituted 5-ring PPV oligomer has been demonstrated. In the case of the polycrystalline vacuum-deposited films, ASE occurs within the individual crystalline domains and was only observed if the domain size was increased, above a critical minimum size, by annealing or recrystallization from the melt. The amplification length is restricted by the size of the crystalline domains due to high optical losses (scattering) from the crystallite boundaries. The threshold for mirrorless lasing for an individual crystalline domain is comparable to that for conjugated polymer films if the domain size is sufficiently large, as demonstrated in the recrystallized Ooct-OPV5 films ( $\approx 500 \mu\text{J}\cdot\text{cm}^2$ ).

*Chapter 6* describes the performance of single and double layer light-emitting diodes based on the alternating PPV copolymers and oligo(*p*-phenylene vinylene)s. Electroluminescence was achieved in the blue, green and orange wavelength region with single-layer devices consisting of transparent indium-tin-oxide anodes and air-stable Al cathodes. The efficiencies of the single-layer copolymer/oligomer LEDs are comparable to those reported for fully conjugated PPVs. Fowler-Nordheim tunnelling theory was used to analyse the current-voltage characteristics in order to determine the barriers for hole-injection in the single-layer devices. In combination with cyclic voltammetry and optical absorption measurements it was possible to estimate energy diagrams for all copolymers and oligomers, which could be used to describe the obtained results in a qualitative way. Furthermore, the influence of the thin-film morphology on LED performance has been investigated for the octyloxy-substituted oligo(*p*-phenylene vinylene). For Ooct-OPV5 a more than ten-fold increase in efficiency was observed for devices consisting of an annealed active layer, which has been assigned to enhanced electron transport upon annealing.

Device optimization by means of additional charge-transport layers to enhance the electroluminescence efficiency has been applied successfully. Balanced hole and electron currents, and electron-hole recombination distant from the metal cathode are probably achieved in such devices, resulting in improved device performance. A novel polymer with oxadiazole-based side-chains has been used successfully as an electron-transport/hole-blocking layer. In combination with a cyano-substituted PPV copolymer as the emissive layer, external EL efficiencies up to 0.1 % were obtained. The best performing double-layer LEDs were based on the electronegative cyano-substituted copolymer as the electron-transport/emissive layer and a PPV hole-transport layer. In this case, external electroluminescence efficiencies up to 0.3-0.4 % are reached. Similar results were obtained with Ooct-OPV5/Ooct-OPV5-CN2 double-layer LEDs.

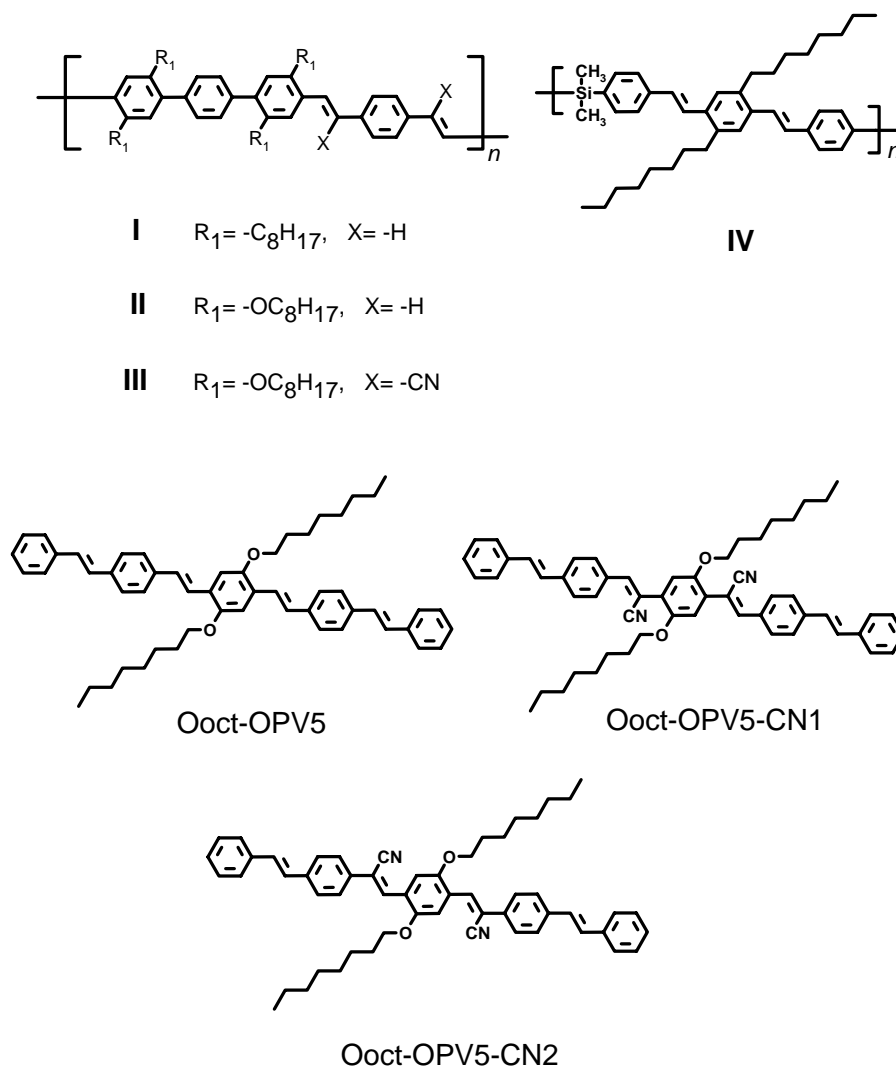


# Samenvatting

$\pi$ -geconjugeerde polymeren staan heden ten dage sterk in de belangstelling voor de potentiële toepassing als actieve componenten in elektronische, optische en opto-elektronische devices zoals lichtemitterende diodes, licht emitterende electrochemische cellen, veld-effect transistoren, fotodiodes, fotovoltaïsche cellen en optisch gepompte lasers.  $\pi$ -geconjugeerde polymeren combineren halfgeleidereigenschappen met die van conventionele polymeren, zoals laag soortelijk gewicht, goede mechanische eigenschappen en de goede verwerkbaarheid. Vooral poly(*para*-fenyleenvinyleen) (PPV) en derivaten zijn erg interessant voor verlichting en display doeleinden, omdat deze polymeren licht uitzenden in het zichtbare gedeelte van het spectrum en vaak een hoge fotoluminescentie-efficiëntie hebben. De emissiegolflengte van deze polymeren wordt bepaald door de mate van conjugatie ( $\pi$ -orbitaal overlap) en de electronendichtheid van de geconjugeerde segmenten in het polymeer skelet. Deze kan beïnvloed worden door de chemische structuur van het polymeer te modificeren. Dit kan op twee manieren bewerkstelligd worden: (a) door substitutie van functionele groepen aan het polymeerskelet die de elektronische structuur beïnvloeden (zoals bijvoorbeeld alkoxyzijstaarten die elektronenstuwende zuurstofatomen bevatten) of (b) door het gecontroleerd onderbreken van de conjugatie door het inbouwen van (i) niet- $\pi$ -geconjugeerde spacergroepen of (ii) stereochemisch geïnduceerde conjugatie-onderbrekingen. Op deze manier kan de kleur van uitgezonden licht gevarieerd worden van blauw naar rood.

Dit proefschrift beschrijft voornamelijk de fotofysische karakterisering van een serie goed gedefinieerde alternerende PPV-copolymeren en all-trans vijfkring PPV-oligomeren (OPV's) en hun toepassing als lichtgevende component in lichtemitterende diodes en optisch gepompte lasers. De chemische structuur van de copolymeren en oligomeren is weergegeven in figuur 1 op de volgende bladzijde. Voor de copolymeren I t/m III wordt de golflengte van het uitgezonden licht bepaald door stereochemische conjugatie-onderbrekingen (de middelste ring in de terfenyl groepen uit het vlak gedraaid) in combinatie met de elektronische invloed van de aanwezige substituenten (alkyl/alkoxyzijstaarten en cyanogroepen op de vinyleen bindingen). De kleur van het uitgezonden licht varieert van blauw voor copolymeer I tot oranje/rood voor copolymeer III. In het blauw licht emitterende copolymeer IV (SiPPV) zijn niet- $\pi$ -geconjugeerde dimethylsilyleengroepen gebruikt om de conjugatie te onderbreken. Voor alle copolymeren geldt dat de effectieve luminescerende segmenten gesubstitueerde distyrylbenzeen-eenheden zijn. Het grote verschil tussen de copolymeren I t/m III en copolymeer IV is de ketenstijfheid. In het geval van copolymeer IV zijn de ketensegmenten redelijk flexibel door toedoen van de silyleengroepen wat resulteert in een meer amorfe structuur. De copolymeren I t/m III daarentegen zijn redelijk star (rigid rod) door toedoen van het volledig aromatische skelet. In figuur 1 zijn ook de chemische structuren van drie 5-ring OPV's

weergegeven. Alle OPV's hebben alkoxyzijstaarten ( $C_8$ ) aan de centrale fenyling, om de oplosbaarheid te verhogen. Twee daarvan (Ooct-OPV5-CN1 en CN2) hebben cyanosubstituenten op verschillende posities aan de vinyleenbindingen rondom de centrale fenyling.



**Figuur 1** Chemische structuur van de alternerende copolymeren (I t/m IV) and vijf-ring oligomeren.

Het voordeel van oligomeren is dat ze een precies gedefinieerde chemische structuur hebben en een hoge fotoluminescentie-efficiëntie. Vanwege het lage molecuulgewicht en de precieze chemische structuur kunnen eenkristallen verkregen worden, wat bij polymeren niet mogelijk is. De zo verkregen structuurinformatie kan zo in relatie gebracht worden met optische eigenschappen in de vaste fase. Oligomeren worden daarom ook vaak als modelverbindingen gebruikt voor de overeenkomstige polymeren of polymeersegmenten. Tevens kunnen dunne oligomeerfilms worden gefabriceerd via depositie in de dampfase die als actieve luminescerende laag gebruikt kunnen worden in LED's.

In *hoofdstuk 2* worden de optische eigenschappen in oplossing en vaste stof beschreven van een serie goed gedefinieerde alternerende PPV-copolymeren en vijftring oligo(*para*-fenyleenvinyleen)en (OPV's). De optische eigenschappen van de copolymeren in oplossing zijn vergeleken met die van gesubstitueerde distyrylbenzeen modeloligomeren, die de lichtgevende OPV-segmenten van het copolymeer vertegenwoordigen. De optische eigenschappen van de copolymeren komen overeen met dat van de modelverbindingen, wat aangeeft dat de conjugatie effectief onderbroken wordt in de copolymeren. De fotoluminescentie-efficiëntie en levensduur veranderden niet significant gaande van oplossing naar de vaste stof voor de blauw licht emitterende copolymeren (I en IV), wat aangeeft dat de bijdrage van niet-radiatief verval door intermoleculaire interacties verwaarloosbaar is, wat resulteert in efficiënte vaste stof fotoluminescentie ( $\eta_{PL} \approx 0.4$ ).

Voor zowel het cyano-gesubstitueerde copolymer als Ooct-OPV5-CN1 in oplossing, werd een snel, dubbelexponentieel fotoluminescentieverval gemeten. Dit snelle niet-radiatieve vervalmechanisme is waarschijnlijk gerelateerd aan de cyanosubstituenten op de vinyleenbindingen. Door de oligomeren te dispergeren in een transparante polysulfonmatrix, kan de moleculaire bewegingsvrijheid (twisting/bending) sterk worden beperkt. Dit resulteerde in een effectieve remming van het niet-radiatieve vervalkanaal. In dit geval werd een PL levensduur van 1.7 ns gemeten, i.p.v. 70 ps. Opmerkelijk is het feit dat voor Ooct-OPV5-CN2 in oplossing dit effect veel minder sterk was. Voor dit oligomeer werd in oplossing een redelijk lange fotoluminescentielevensduur van 1.4 ns gemeten, wat impliceert dat de positie van de cyanogroepen op het OPV-segment een belangrijke parameter is met betrekking tot het snelle niet-radiatieve vervalmechanisme.

Ook zijn de optische eigenschappen van de oligomeer-éenkristallen bestudeerd. Voor de Ooct-OPV5-CN2 éenkristallen, werd een sterk roodverschoven, breed PL-spectrum waargenomen, zonder vibrationele fijnstructuur. Tevens werd een redelijk lange PL-levensduur gemeten van 8 ns. Dit komt overeen met een natuurlijke radiatieve levensduur van 16 ns. Dit wordt toegeschreven aan excimeeremissie. Dat er in dit geval sprake is van excimeeremissie wordt verder ondersteund door de röntgen structuurdata van het betreffende éenkristal. Dit cyanogesubstitueerde oligomeer heeft een dichte intermoleculaire kristalpakking waarbij het  $\pi$ -systeem van de individuele

moleculen een vlakke geometrie heeft. Deze dichte pakking wordt toegeschreven aan een effectieve Coulombinteractie tussen naburige moleculen, door de aanwezigheid van cyanosubstituenten. De afstand tussen de aangrenzende oligomeren in het rooster is ongeveer 3.5 Å en er is een redelijke mate van overlap tussen de vlakke aromatische systemen. Op basis hiervan kan men concluderen dat er sterke  $\pi$ - $\pi$  interacties kunnen plaatsvinden. Ook voor het cyanogesubstitueerde copolymeer (III) zijn er aanwijzingen dat de emissie afkomstig is van excimeren, alleen zijn de karakteristieke kenmerken minder sterk als in het geval van Ooct-OPV5-CN2 en dat gerapporteerd voor cyano-PPV homopolymeren.

In *hoofdstuk 3* wordt aangetoond dat het mogelijk is om laserlicht te genereren uit oplossingen van een blauw licht emitterend PPV-copolymeer, door fotoexcitatie met ns pulsen van de derde harmonische van een Nd:YAG-laser. De laserperformance van het copolymeer is vergeleken met die van twee commercieel verkrijgbare coumarin kleurstoffen (dyes) die in hetzelfde golflengtegebied licht uitzenden. Voor het copolymeer in hexaan was de energie-omzettingsefficiëntie (ratio tussen de uitree-energie van de dye-laser en de Nd:YAG pompenergie) meer dan twee keer zo hoog als voor de coumarine laser kleurstoffen. Tevens kon voor het copolymeer laserlicht opgewekt worden in een veel groter golflengtegebied. Deze studie laat duidelijk zien dat polymeren potentieel interessant kunnen zijn voor toepassing in een dye-laser. Het nadeel van dye-lasers is dat er meestal vluchtige oplosmiddelen worden gebruikt, die schadelijk voor de gezondheid zijn. Er wordt daarom ook veel onderzoek verricht op het gebied van vaste stof dye-lasers. Dit zijn meestal gebaseerd op blends waarin de laserkleurstof gedispergeerd is (lage concentratie) in een transparant matrixpolymeer, bijvoorbeeld PMMA. De vooruitzichten voor PPV-polymeren als actief lasermedium voor (optisch gepompte) vaste stof dye-lasers en versterkers gebaseerd op blends lijken goed. De superieure mechanische eigenschappen en thermische stabiliteit van geconjugeerde polymeren in vergelijking met conventionele laag-moleculaire laserkleurstoffen, in combinatie met een hoge energieconversie -efficiëntie zal mogelijk resulteren in een langere levensduur van de vaste stof dye-laser en een verbetering van de dye laser performance.

In *hoofdstuk 4* wordt aangetoond dat het mogelijk is om laserlicht op te wekken in dunne (pure) polymeerfilms via foto-excitatie, zonder gebruik te maken van een extern optisch feedbacksysteem (spiegelloos). Twee polymeren zijn hiervoor gebruikt, namelijk het copolymeer SiPPV (IV) en het homopolymeer Ooct-PPV. Deze spiegellose laseremissie is het gevolg van versterking van spontane emissie (Amplified Spontaneous Emission, ASE). ASE werd waargenomen als de excitatieenergie hoger was dan een specifieke drempelwaarde. Deze drempelwaarde is afhankelijk van het type polymeer, de optische kwaliteit van de film en de diameter van de excitatiebundel. Boven deze drempelwaarde werd een scherpe ASE-piek waargenomen, met een bandbreedte van 6-7 nm (breedte op halve hoogte). De

golflengte van het uitgezonden laserlicht kwam overeen met het maximum in het fluorescentiespectrum voor beide polymeren. De propagatie van de uitgezonden fotonen via golfgeleiding (waveguiding) in de polymeerfilm is een belangrijk aspect, omdat hierdoor de noodzakelijke interactielengte van de uitgezonden fotonen met de populatie aan aangeslagen toestanden wordt bereikt en er zodoende netto versterking (gain) bewerkstelligd kan worden. Verder wordt in dit hoofdstuk aangetoond dat het ook mogelijk is om 'echt' laserlicht op te wekken met behulp van een optisch feedbacksysteem. Hiervoor werd een vlakke resonator gebruikt bestaande uit twee diëlectrische spiegels, waartussen een Ooct-PPV-film was aangebracht samen met een samendrukbare transparante spacerlaag. Met dit type resonator was het mogelijk om de golflengte van het uitgezonden licht te regelen, door de afstand tussen de twee spiegels te veranderen. Het bleek dat de golflengte van het laserlicht te variëren was in een spectraal gebied van ongeveer 20 nm, gecentreerd rond het golflengtemaximum van het fluorescentiespectrum.

De in hoofdstuk 4 beschreven resultaten bieden perspectieven voor de mogelijke toekomstige ontwikkeling van een elektrisch gestuurde polymeer-diodelaser, daar hiervoor eenzelfde constructie gebruikt kan worden als in een polymeer LED. De beperkende factor op dit moment is de extreem hoge stroom die noodzakelijk is om een populatieinversie te creëren in de polymeerlaag. Op basis van de energiedrempelwaarde voor ASE, verkregen door de foto-excitatie-experimenten, kan men een ruwe schatting maken van de dichtheid aan aangeslagen toestanden die vereist is om ASE te genereren. Op basis hiervan kan men de ladingsdichtheid afschatten die nodig is om eenzelfde dichtheid aan aangeslagen toestanden te creëren via injectie van ladingsdragers. De minimale stroomdichtheid noodzakelijk voor ASE is meer dan drie ordes van grootte hoger dan de maximale stroomdichtheid die tot nu toe gerapporteerd is voor conventionele polymeer-LED's. Dit was voor ons een van de redenen om oligomeren te gaan gebruiken als alternatief. Oligomeren hebben een hoge fotoluminescentie-efficiëntie, hebben een precies gedefinieerde chemische structuur en kunnen verkregen worden als macroscopische éénkristallen. Het is bekend dat de mobiliteiten van ladingsdragers (gaten en elektronen) over het algemeen veel hoger zijn in goed gedefinieerde microscopische structuren (kristallen) dan in wanordelijke materialen. Uitzonderingen daargelaten. Vanwege door de betere transporteigenschappen, zou men verwachten dat in zulke materialen een hogere ladingsdichtheid gecreëerd kan worden van zowel gaten als elektronen.

Deze studie wordt beschreven in *hoofdstuk 5* van dit proefschrift. Hier wordt aangetoond dat het ook mogelijk is om ASE te genereren in éénkristallen en dunne films van Ooct-OPV5. In het geval van de polykristallijne films die verkregen zijn door depositie uit de dampfase, is alleen ASE waargenomen na herkristallisatie van de films d.m.v. verwarmen (annealen) bij een temperatuur net onder de eerste overgangstemperatuur (kristal-mesofase overgang) van het oligomeer, of na afkoelen

van de film uit de isotrope smelt. Deze herkristallisatie leidt tot een betere moleculaire oriëntatie en grotere kristallijne domeinen. De domeingrootte van de kristallieten is een belangrijke parameter met betrekking tot ASE. De interactie lengte van de uitgezonden fotonen met de populatie aan aangeslagen toestanden wordt beperkt door de grootte van de kristallijne domeinen, doordat het licht verstrooid wordt aan de grensvlakken, wat leidt tot hoge optische verliezen. De reden dat geen ASE is waargenomen in de niet-geannealde films is derhalve dat de domeingrootte te klein is en hier geen netto versterking (gain) optreedt. De drempelwaarde in excitatie-energie waarboven ASE plaatsvindt voor Ooct-OPV5, is vergelijkbaar met die gerapporteerd voor polymeerfilms, mits de kristallijne domeinen voldoende groot zijn zoals in het geval van de Ooct-OPV5-films na herkristallisatie uit de isotrope smelt.

In *hoofdstuk 6* worden de optische en elektrische eigenschappen beschreven van enkel- en dubbellaags LED's gebaseerd op PPV-copolymeren en vijfkring OPV's. Electroluminescentie in het blauwe tot oranje/rode golflengtegebied kon worden gegenereerd met enkellaags copolymeer/oligomeer-LED's met transparante indiumtinoxide anodes (gateninjectie) en aluminium cathodes (electroneninjectie). De electroluminescentie-efficiënties van de enkellaags copolymeer/oligomeer-LED's zijn vergelijkbaar met die gerapporteerd voor enkellaags PPV LED's met aluminium cathodes. Fowler-Nordheim tunnellingtheorie is gebruikt om de elektrische karakteristieken (voltage-stroom curves) te analyseren en zo de barrièrehoogtes voor gateninjectie te bepalen. Hiermee kan men een schatting maken van de ionisatiepotentiaal ( $\approx$ HOMO niveau) van de betreffende materialen. De zo verkregen ionisatiepotentialen (IP) komen redelijk overeen met de IP's verkregen met cyclische voltammetrie. In combinatie met de HOMO-LUMO gaps bepaald via absorptiemetingen was het mogelijk voor alle verbindingen een energiediagram (bandenplaatje) te schetsen, wat gebruikt kon worden om de diodekarakteristieken op een kwalitatieve wijze te beschrijven. Tevens is de invloed van de dunne laag morfologie op de electroluminescentie-efficiëntie van een enkellaags oligomeer-LED onderzocht. Voor een Ooct-OPV5-LED werd een tienvoudige verhoging van de efficiëntie waargenomen na annealen van de Ooct-OPV-laag. Deze efficiëntieverhoging is toegeschreven aan een verhoging van de electronenstroom in een geannealde Ooct-OPV5-laag, waardoor er een meer gebalanceerd ladingtransport plaatsvindt. Optimalisatie van de electroluminescentie-efficiëntie van de LED's is bewerkstelligd door het gebruik van transportlagen. De transportlagen zorgen voor een meer gebalanceerde injectie en transport van de ladingdragers en bewerkstelligen dat electron-gat recombinatie niet plaatsvindt in de buurt van de metaalelectrodes, wat resulteert in een hogere electroluminescentie-efficiëntie. Een nieuw polymeer met oxadiazoolzijketens gesynthetiseerd via een 'levende' (TEMPO) radicaalpolymerisatie is met succes toegepast als electronentransport/gatenblokkeer laag. In combinatie met het cyanogesubstitueerd copolymeer (III) als de luminescerende laag werden efficiënties tot 0.1% behaald. De hoogste efficiënties zijn verkregen met dubbellaags-

LED's bestaande uit een cyanogesubstitueerd copolymeer-laag als de electrontransport/lichtemitterende laag en een PPV gattransportlaag. In dit geval werden electroluminescentie-efficiënties behaald van 0.3 – 0.4 %. Eenzelfde resultaat werd verkregen met een dubbellaags-LED gebaseerd op overeenkomstige oligomeren (Ooct-OPV5-CN2/Ooct-OPV5-LED's).



# List of publications

P.C.M. Grim, H.J. Brouwer, R.M. Seyger, G.T. Oostergetel, W.G. Bergsma-Schutter, A.C. Arnberg, P. Guenther, K. Dransfeld, G. Hadziioannou, "Investigation of polymer surfaces using Scanning Force Microscopy (SFM)", *Macromol. Chem. Macromol. Symp.*, **62**, 141 (1992)

A. Hilberer, H.J. Brouwer, J. Wildeman, B.J. van der Scheer, G. Hadziioannou, "Synthesis and characterization of a new efficient blue-emitting copolymer", *Macromolecules*, **28**, 4525 (1995)

A. Hilberer, H.J. Brouwer, F. Garten, J. Wildeman, G. Hadziioannou, "Conjugated block copolymers for light-emitting diodes", *Spie Proceedings San Diego*, **2528**, 74 (1995)

H.J. Brouwer, V.V. Krasnikov, A. Hilberer, J. Wildeman, G. Hadziioannou, "Novel high efficiency copolymer laser dye in the blue wavelength region", *Appl. Phys. Lett.*, **66(25)**, 3404 (1995)

J. Wildeman, A. Hilberer, H.J. Brouwer, V.V. Krasnikov, G. Hadziioannou, "Light-emitting copolymers", *Eur. Patent. 95201681.4-2102* (1995)

H.J. Brouwer, A. Hilberer, M. Werts, J. Wildeman, G. Hadziioannou, **Invited paper**, "LEDs based on conjugated PPV block copolymers", *Spie Proceedings Denver*, **2852**, 170 (1996)

S.C. Veenstra, G.M. Malliaras, H.J. Brouwer, F.J. Esselink, V.V. Krasnikov, P.F. van Hutten, Wildeman, H.T. Jonkman, G.A. Sawatsky, G. Hadziioannou, "Sexithiophene-C60 blends as model systems for photovoltaic devices", *SPIE Proceedings Denver*, **2852**, 277 (1996)

H.J. Brouwer, V.V. Krasnikov, A. Hilberer, G. Hadziioannou, "Blue laser emission from neat semi-conducting alternating copolymer films", *Adv. Mater.*, **8(11)**, 935 (1996)

H.J. Brouwer, A. Hilberer, M. Werts, J. Wildeman, G. Hadziioannou, "LEDs based on conjugated block copolymers", *Synth. Met.*, **84**, 881 (1997)

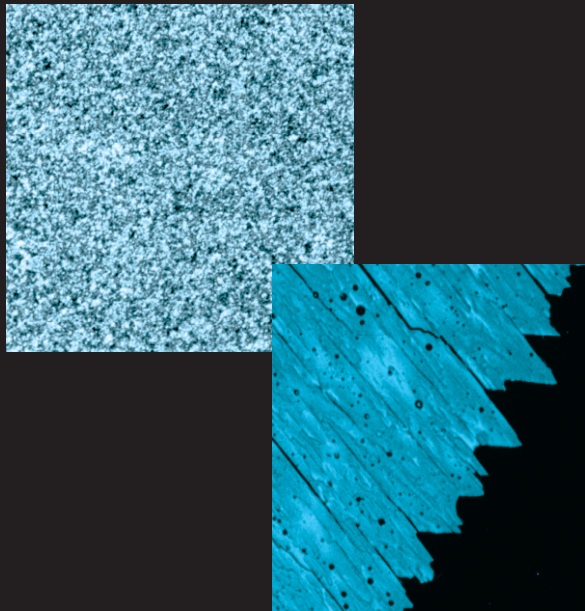
S.C. Veenstra, G.M. Malliaras, H.J. Brouwer, F.J. Esselink, V.V. Krasnikov, P.F. van Hutten, J. Wildeman, H.T. Jonkman, G.A. Sawatzky, G. Hadziioannou, "Sexithiophene-C<sub>60</sub> blends as model systems for photovoltaic devices", *Synth. Met.*, **84**, 971 (1997)

A. Hilberer, M. Moroni, R.E. Gill, H.J. Brouwer, V.V. Krasnikov, T.A. Pham, G.G. Malliaras, S.C. Veenstra, M.P.L. Werts, P.F. van Hutten, G. Hadziioannou, "Photonic materials for electroluminescent, laser and photovoltaic devices", *Macromol. Symp.*, **125**, 99 (1997)

P.F. van Hutten, H.J. Brouwer, V.V. Krasnikov, T.A. Pham, R.E. Gill, G. Hadziioannou, "Stimulated emission from films of conjugated polymers and oligomers", *SPIE Proceedings San Diego*, 1997, in press

H.J. Brouwer, V.V. Krasnikov, T.A. Pham, R.E. Gill, P.F. van Hutten, G. Hadziioannou, "Optical properties of single crystals and vacuum-deposited thin films of a substituted oligo(*p*-phenylene vinylene), to be published in *Chemical Physics*

H.J. Brouwer, V.V. Krasnikov, T.A. Pham, R.E. Gill, G. Hadziioannou, "Stimulated emission from vacuum-deposited thin films of a substituted oligo(*p*-phenylene vinylene)", *submitted to Appl. Phys. Lett.*



ISBN-90-367-0878-8